Measurements from the Prompt and Delayed Radiation of Fission Fragments: Deformation Properties of Neutron Rich Nuclei

By

Nathan T. Brewer

Dissertation

Submitted to the Faculty of the

Graduate School of Vanderbilt University

in partial fulfillment of the requirements

for the degree of

DOCTOR OF PHILOSOPHY

in

Physics

May, 2013

Nashville, Tennessee

Approved:

Professor Joseph Hamilton

Professor Akunuri Ramayya

Professor Sait Umar

Professor Volker Oberacker

Professor Michael Stabin

To my family,

especially my wife Laura

and

a large community of friends and mentors

ACKNOWLEDGMENTS

There are many people that is appropriate to acknowledge in this work, including the friends, family, and mentors that prepared me to enter into graduate school that are truly appreciated, but are too numerous to name.

It has been my extreme pleasure to have worked along side of great scholars and leaders in their field. I am especially grateful to Dr. Hamilton and Dr. Ramayya for their advice and hard work to prepare in advance good work for me to do. I also would also like to thank the other members of my committee, Dr. Stabin, Dr. Oberacker and Dr. Umar for their advice, instruction and constructive questioning of my thoughts and methodologies. It has been my pleasure to work in collaboration with J.K. Hwang, Y.X. Luo, J.O. Rasmussen, S.J. Zhu, and A.V. Daniel in their expertise in the analysis of ^{252}Cf data. As well as many people at ORNL with the LeRIBSS and UNISOR and RMS experiments: J.C. Batchelder, R. Grzywacz, C.J. Gross, and K.P. Rykaczewski among many other scholars. At Vanderbilt it has been my pleasure to work with graduate students S.H. Liu (who was a great friend and mentor in my early years as a graduate student) and E.H. Wang. It has also been a fantastic part of my experience to see how undergraduates and high school students can be drawn into productive and cutting edge research and some of this work was done in conjunction with W.A. Yzaguirre (Vanderbilt University) and B. Doll (NBPHS). The work at Vanderbilt University was supported by the U.S. Department of Energy under Grant No. DE-FG05-88ER40407.

I cannot express enough how much the support of friends and family have meant to me during this time. I am very grateful to my wife, Laura and the sacrificies that have made been made by her and her unwaivering support.

To anyone who reads this work: thank you.

TABLE OF CONTENTS

LIST OF FIGURES

LIST OF TABLES

CHAPTER 1

INTRODUCTION

The intent of this thesis is to demonstrate several things. It is not only a presentation of the cutting edge research that has been accomplished in this work, but also a presentation of how these things have been learned. The thesis, especially the introductory material, is intended to be understood by the advanced undergraduate or a graduate student unfamiliar with nuclear physics. This approach was chosen because it could be used by other students who wish to learn about nuclear deformation or spectroscopy techniques.

1.1 Physics of Neutron Rich Nuclei

Human beings throughout history have continually developed tools to test the structure and consistency of the world around us. Our curiosity fuels our innovations, and as questions are asked and answers are discovered, it fuels more questions. When a theory is hypothesized in science, it is tested repeatedly and it is only valid within the context for which it has been tested. The general relativistic theory of gravity is perhaps the most famous example of this. Within our context on earth, Newtonian gravity that varies as $1/r^2$ works very well. Observations had to be made on stellar and planetary systems at much larger scales to begin to test the theory of relativity. In order to further this theory, and fully understand quantum gravity, scientists need a way to probe sources of large gravity at small scale. In the same way the theories of nuclear physics, which were developed at and near the line of stability, are tested in the context of nucleon excess. In this work, the focus is on neutron-rich nuclei.

The intent is to show how theories of nuclear deformation and structure have been developed, and in this present context if and to what extent they are valid. The framework for discussing

deformation is the multipole expansion of Electromagnetic Moments. The electric moments arise because of charge distributions in the nucleus and the magnetic moments arise from charged currents in the nucleus. When structure is discussed, what is meant are things like the nuclear shape, modes of rotation, vibration, and the quantum mechanical properties associated with the states in the nucleus. The nucleus is a complex, energetically degenerate, strongly bound, fermionic many-body system and structures can be associated with few, or many nucleons. This is shown in Fig. 1.1[1]. This figure shows how the observed structure of the nucleus may depend on the energy scale involved. At low energy, in the range of a few tens of keV's, collectivity dominates the description and as energy increases, more of the intrinsic structure of nucleons and sub-nucleonic matter becomes evident. Because of this level of complexity, there is at present no single theory that can explain the many and different structures that can be seen in nuclei. Therefore, a few simple models are selected and their validity is tested, with the understanding that these models have known limitations and may be expected to fail.

1.2 Outline of the Thesis

This thesis comes in five basic sections and eight chapters. Chapter 2 describes the details of the necessary building blocks for discussing nuclear physics. Chapter 3 presents the theoretical physics of deformation that are being tested. These theories are older theories that were developed near stability and at low spin. Namely, the shell model, the Interacting Boson Model, the collective model, and a geometric model for reflection asymmetric nuclei. These are theoretical constructs that are most easily associated with experiment. Deviations from these models are data that may reveal new physics. This section is followed by some details on modern and microscopic theoretical approaches. These are better approaches and modern techniques are an attempt toward a universal and microscopic theory as opposed to qualitative phenomenology. In chapter 4 are the details of the experimental setups used to access the nuclei of interest. Both production of fission fragments and measurement techniques associated with prompt and beta-delayed gamma emmission are presented. The experimental results are then shown in the last three chapters. In

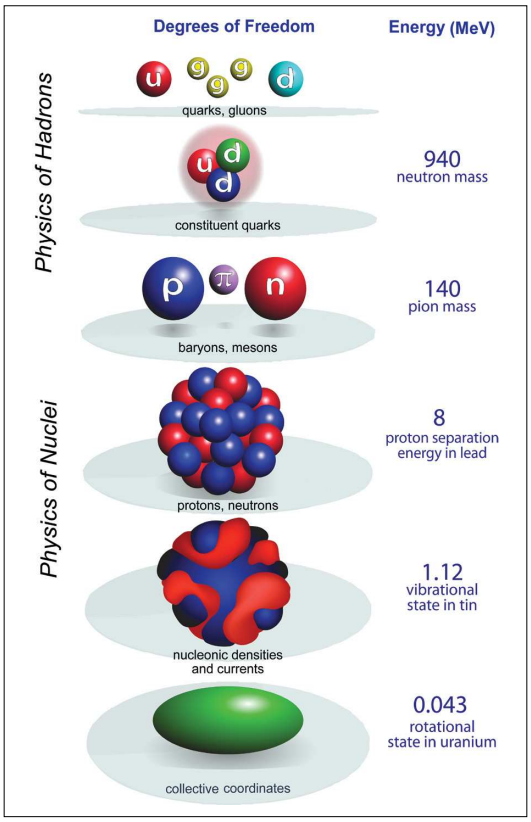

Figure 1.1: The energy scales that can help delineate the structures able to be seen in the nucleus [1].

chapter 5, the structure of ^{122}Ag near the Z=50 shell is explored, and it is shown in comparison to the anharmonic vibrational model. In chapter 6, nuclei that are quadrupole deformed are examined in the framework of the collective model of Bohr and Mottelson. Finally, in chapter 7 octupole deformation and reflection asymmetric shapes are discussed.

1.3 Broader Impact

It is also important to highlight the significance of the work presented. Not only do the experiments probe basic nuclear structure, but in general, it can be emphasized that these studies of basic science have an impact on other fields and have real world applications. The connection between nuclear physics and astrophysics is especially rich and has real needs for nuclear data. Astrophysical processes thought to be responsible for stellar nucleo-synthesis are shown in Fig. 1.2. Nuclear astrophysics needs inputs of capture cross sections and rates, masses, decay branching ratios, and lifetimes. Our collaboration has recently published such data [2–7]. The decay spectroscopy with which our collaboration has been involved has had applications to the measurement of total decay heat and branching ratios for reactor physics [8, 9] and accurate dose measurements for isotopes used in PET scans [10]. Specifically, the study of nuclear shapes and moments has application to tests of fundamental symmetries [11, 12], spintronic decoherence [13], the fission and fusion processes [11, 14] and the production of super-heavy elements [15, 16].

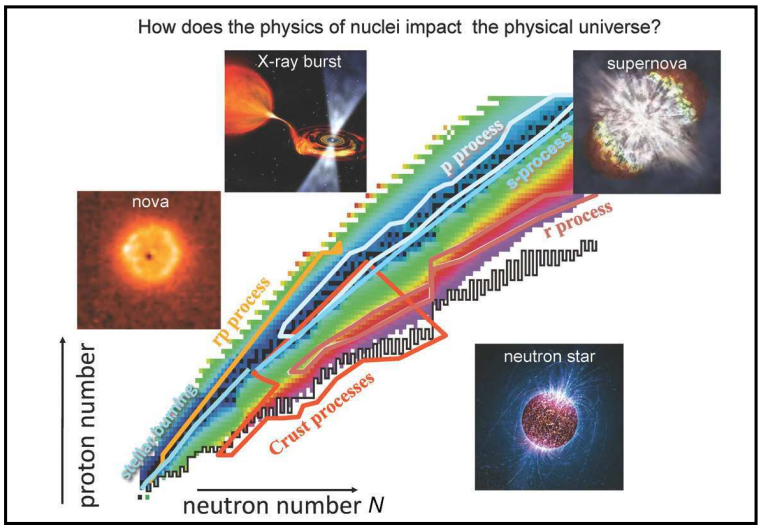

Figure 1.2: The chart of nuclides, showing astrophysical processes where there is a need for nuclear physics input [1]

CHAPTER 2

NUCLEAR DECAY

Our primary method of determining structures depends on trustworthy experimental data and its comparison to theoretical interpretations. A good theory recommends observables that are testable. The primary method used in this study to access observables is to measure the gamma rays emitted from excited states in a nucleus populated from beta decay or spontaneous fission. Coincidence information is gathered, and with that information inferences are made regarding the quantized energy levels present in a nucleus. A level scheme is built and this picture can lend itself to a structure interpretation. It is also possible to measure the quantum mechanical character of the radiation emitted from a nucleus. The gamma radiation can be classified as electric or magnetic and carries angular momentum away from the nucleus. Measurement of these properties can also help identify the spins and parities of nuclear states. These techniques will be discussed in chapter 4.

2.1 Introductory Material for Nuclear Physics

It is important to first discuss basic nuclear radiative processes and useful mathematical structures and tools for analyses of radiative processes which are essential concepts for the analyses of nuclear decay. Notice that the Chart of Nuclides [17] can be organized in terms of decay processes. This is shown in Fig. 2.1. It shows that by far the most common process is β decay. When a nucleus has excess nucleons of one type it can become more stable via beta decay by converting a proton to a neutron or vice-versa. If the imbalance is too great,one or more nucleons are emitted and at a certain point the last neutron cannot be bound to the nucleus. These limits are called the proton and neutron drip lines, respectively. As the nuclei become heavy, and Z^2/A becomes large, α particle emission dominates. Then, as Z^2/A becomes even larger, spontaneous fission becomes

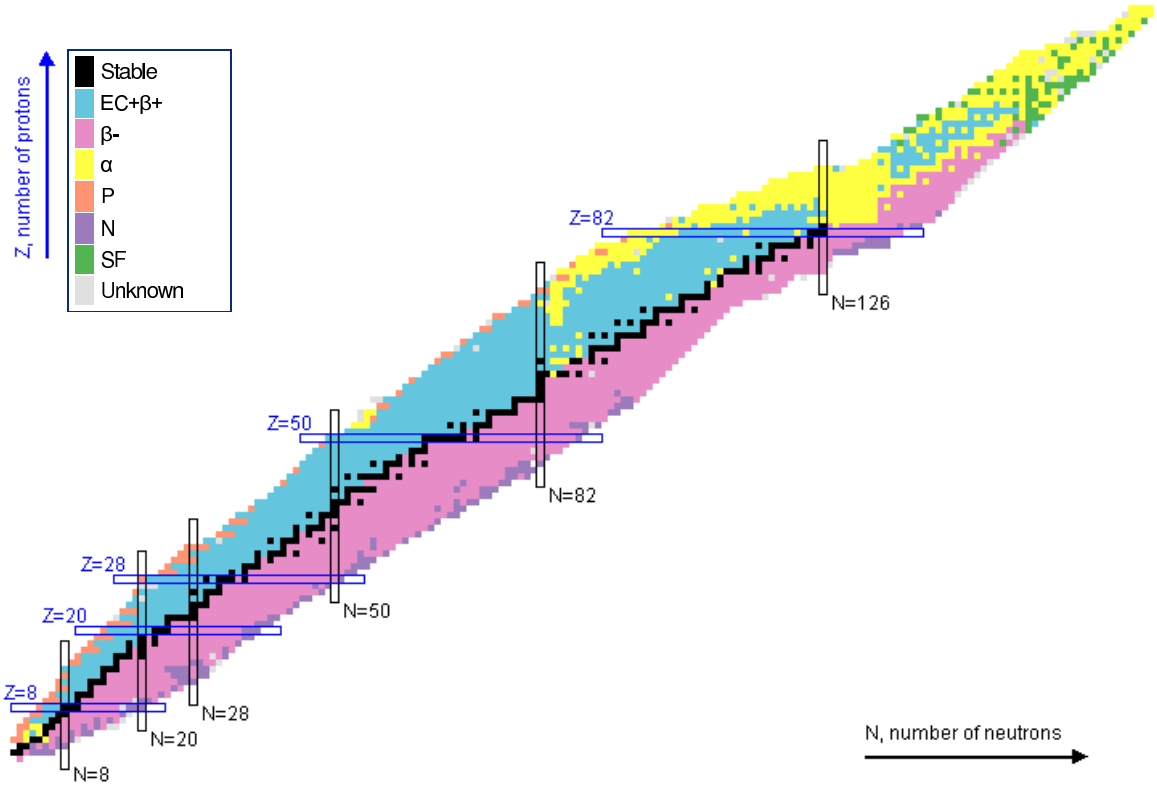

Figure 2.1: A map of the Chart of Nuclides showing decay modes [17]

more likely. Eventually, there may be a limit of how heavy a nucleus can be before it ceases to bind at the fission limit.

2.1.1 Building Blocks

There is some commonality between nuclear processes, and there is some necessary language that is required to explain decay or radiative processes. This material can be found in many places but, unless otherwise noted, is compiled from the following books [18–20] and references therein. Radioactive decay is a statistical process that is energetically motivated. The representation of a transition from one energy level to another is shown as an energy level diagram. An example is shown in Fig. 2.2. In this figure, X represents the higher energy level and is therefore the energy of the transition to the level at 0.0 which is labeled next to the arrow. Most often, when 0.0 is used it means that the ground state (i.e. the rest mass, $E=mc^2$) has been used to define the relative energy scale to be used. For low-energy nuclear structure physics, the typical energy scale is keV

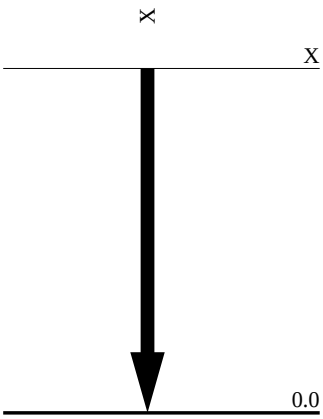

Figure 2.2: An example diagram for the transition between two energy states

(kilo-electron volt).

All nuclear levels, unless they are the ground state of a stable nuclide, undergo radioactive decay. When that happens, they follow the exponential decay law. It is easy to construct this law assuming only that the random process and therefore, the change in the number of states is proportional to a decay constant, the current number of particles and the change in time. That is:

$$dN(t) = -\lambda N(t)dt \tag{2.1a}$$

$$\int_0^t \frac{dN(t')}{N(t')} = -\int_0^t \lambda\, dt' \tag{2.1b}$$

$$ln(\frac{N(0)}{N(t)}) = \lambda t \tag{2.1c}$$

$$N(t) = N(0)e^{-\lambda t} \tag{2.1d}$$

So then the decay constant λ is in units of inverse time, with the mean life of a nuclear state defined as $\tau = \frac{1}{\lambda}$ and the half-life $T_{1/2} = ln(2)\tau = \frac{ln(2)}{\lambda}$ in units of time. This is governed in practice by the laws of statistics and measurement. In reality, a large initial population and sufficient time is required to make an accurate measurement of the half-life.

Any nuclear state also has quantized (in units of $\hbar$) intrinsic angular momentum called spin.

It also has an associated symmetry parameter called parity, called + or -, odd or even. Though there are many other parameters that may be associated with a nuclear state, these are the only ones that are physically measurable. Any other properties are inferred or are model dependent.

Because of the statistical nature of nuclear decay there is also a probability of a given transition occurring. If there are multiple pathways from a state there will be some probability for each pathway. But in order to to discuss that in more detail for the radiation of electromagnetic waves it is necessary to discuss the classical approach to the laws of electromagnetism [21].

The four laws called Maxwell's equations, began to be derived in ≈1830. They were developed and tested by a host of scientists including Carl Friederich Gauss, André-Marie Ampère, and Michael Faraday. James Clerk Maxwell's contribution was a correction to Ampere's Law and a coherent electromagnetic theory of light [22]. When placed together, the set is referred to as Maxwell's equations. They are shown in equations 2.2a-d in microscopic, differential form.

$$\nabla \bullet E = \frac{\rho}{\varepsilon_0} \tag{2.2a}$$

$$\nabla \bullet B = 0 \tag{2.2b}$$

$$\nabla \times E = -\frac{\partial B}{\partial t} \tag{2.2c}$$

$$\nabla \times B = \mu_0 J + \mu_0 \varepsilon_0 \frac{\partial E}{\partial t} \tag{2.2d}$$

The four Maxwell's equations, where E is the electric field, B the magnetic field, ρ is the charge density, J is the current density, the permeability of free space $\mu_0 \equiv 4\pi * 10^{-7}$ N*A^{-2}, and the permitivity of free space $\varepsilon_0 \equiv \frac{1}{\mu_0 c^2} \approx 8.854 * 10^{-12} F m^{-1}$ and is defined relative to μ_0 and c the speed of light in vacuum.

One of the solutions to these equations (which exists in vacuum) is a free, self-propagating electro-magnetic wave traveling at the speed c=$\frac{1}{\sqrt{\mu_0 \varepsilon_0}}$, the speed of light. The amazing thing is that

there is no reference frame specified to define this speed. This lead Einstein to form his relativistic theories, and scientists are still trying to understand fully the ramifications of the absolute speed of light and general relativity. In order to derive this solution, one sets ρ and J to zero since currents and charges will be absent in free space. After some manipulation, this becomes the equations 2.3a-b.

$$\frac{\partial^2 E}{\partial t^2} - c^2 \nabla^2 E = 0 \tag{2.3a}$$

$$\frac{\partial^2 B}{\partial t^2} - c^2 \nabla^2 B = 0 \tag{2.3b}$$

These equations have a sinusoidal solution and can be useful to understand a host of phenomena including reflection, refraction, diffraction, and polarization. If it is assumed that there is only one frequency in the composition of the light wave, then the simplification leads to the Helmholtz equations for E or B. It is then possible to solve these equations in terms of multipole moments of order (l,m), and character E or M 2.4a-b, where l and m are angular momenta and projections respectively. The electric or magnetic character of a light wave comes from having two equations that need to be solved.

$$E = e^{i\omega t} \sum_{l,m} \sqrt{l(l+1)} [a_E(l,m) E^{(E)}_{l,m} + a_M(l,m) E^{(M)}_{l,m}] \tag{2.4a}$$

$$B = e^{i\omega t} \sum_{l,m} \sqrt{l(l+1)} [a_E(l,m) B^{(E)}_{l,m} + a_M(l,m) B^{(M)}_{l,m}] \tag{2.4b}$$

So, $E^{(E)}_{l,m}$ and $B^{(E)}_{l,m}$ are the electric multipole fields of order (l,m), $E^{(M)}_{l,m}$ and $B^{(M)}_{l,m}$ are the magnetic multipole fields of order (l,m) and a is the ampitude of the field. They are proportional to spherical Hankel functions, and vector spherical harmonics $\propto (r \times \nabla) Y_{l,m}$.

The electromagnetic theory of light describes light in terms of electric or magnetic character.

But for nuclear physics a quantum mechanical formulation is needed to understand the origination of the radiation. It can be shown that accelerating charges produce radiation. Typically the acceleration is a rotation or vibration that can be based upon all, some, or even a single particle in the nucleus. The acceleration is based on the charge density or the charged current density. The operators for a transition from the state (ψ) a $\rightarrow$ b (equations 2.5a-b) are as follows:

$$Q_{l,m}(a,b) = e\int r^l \rho Y^*_{l,m}(\theta,\phi)\psi^*_b(\vec{r})\psi_a(\vec{r})d\tau \tag{2.5a}$$

$$M_{l,m}(a,b) = -\frac{\mu_N}{l+1}\int r^l Y^*_{l,m}(\theta,\phi)\nabla \bullet [\vec{r}\times\vec{j}(a,b;\vec{r})]d\tau \tag{2.5b}$$

It can then be seen that the parity operation, which changes $\vec{r}$ to -$\vec{r}$, will be proportional to $(-1)^l$ for the $Q_{l,m}$ and proportional to $(-1)^{l+1}$ for the $M_{l,m}$. For simplicity, these characterizations of light emitted are called E1,E2,... EL for electric multipoles of Lth order and M1,M2,... ML for the Lth order magnetic multipoles. For a transition from a to b, E1,M2,E3 ... transitions will have a change in parity and M1,E2,M3 ... will not. More will be discussed of the nature and significance of these light rays in the paragraphs on gamma decay.

The spherical harmonics, $Y_{l,m}(\theta,\phi)$, introduced above are an extremely useful complete set of orthogonal functions that map out the angular part of the spherical coordinate system. The orthogonality and recurrence relations of this set have made them especially useful for simplifying complex summations and for describing geometrical distributions. They are used in quantum mechanics, astrophysics, computer science, and optics. For this study they are used to parameterize the shape of the nucleus (Fig. 2.3) and quantum mechanical operators as was discussed previously. For quadrupole deformation, it is convenient to define two parameters: β_2 and γ. Where the radius, R is:

$$R(\theta,\phi) = R_0[1+\beta_2\, Cos(\gamma)Y_{2,0}(\theta,\phi) + \frac{1}{\sqrt{2}}\beta_2\, Sin(\gamma)\{Y_{2,2}(\theta,\phi)+Y_{2,-2}(\theta,\phi)\}] \tag{2.6}$$

In this equation, β_2 describes the overall magnitude of the deformation and γ is a parameter that transforms the deformation from a prolate spheroid (γ=0°) to an oblate spheroid (γ=60°). The function repeats anti-symmetrically for every 60° and between 0° and 60° describes a triaxial shape.

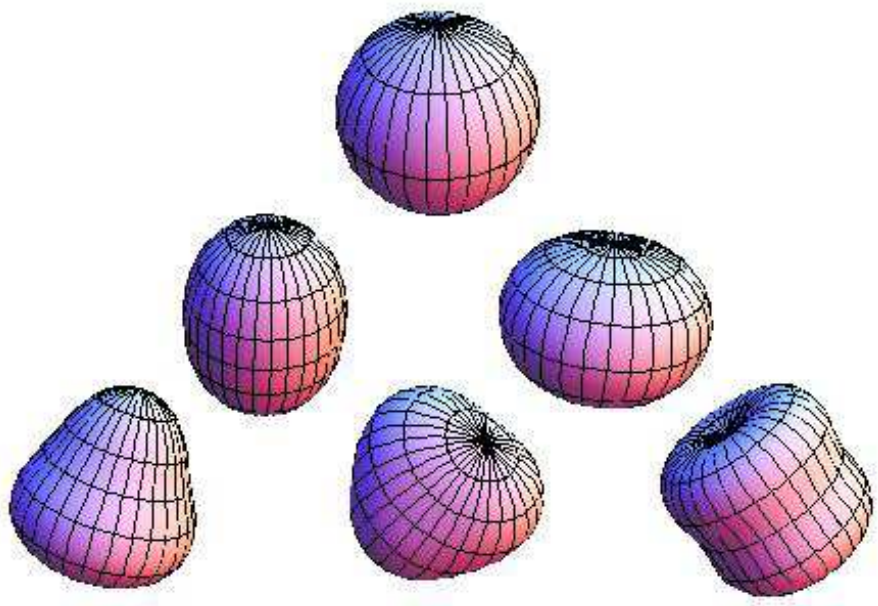

Figure 2.3: Nuclear shape in terms of spherical harmonics. In order from top to bottom, left to right, sphere, prolate spheroid (quadrupole deformed), oblate spheroid (quadrupole deformed), octupole (axial deformation), tetrahedral (octupole deformed, m=±2), and hexadecupole deformation.

The argument is that this variety of nuclear shapes occurs naturally. It is energetically driven, and this can be seen in a simple system. Consider the derivation in [23] as an example. The author begins with free particles bound in a sheet and solves Schroedinger's wave equation 2.7. Inside of a planar region one side of length a and the other of length b where the potential V is 0, and beyond V is ∞ so that no part of the wavefunction goes outside the box.

$$\frac{-\hbar^2}{2m}\nabla^2\psi + V\psi = E\psi \tag{2.7}$$

To put it in words: the Hamiltonian ($\hat{H}$) acting on the wave function ψ, is an operator that

returns the wavefunction and the energy ($\hat{H}\psi = E\psi$). Inside of the sheet, the potential part of the Hamiltonian is zero and the kinetic energy term remains, $\hat{H} = \hat{K} = \hat{p}^2/2m = (i\hbar\vec{\nabla})^2/2m$. Now, γ=a/b can be used to parameterize deformation and it can be chosen such that γ>1. The solutions are separable and go as Sin($\frac{n_{(x,y)}\pi(x,y)}{(a,b)}$), and n=1,2,3,... in either x or y independently. The total energy is then:

$$E = \frac{\hbar^2\pi^2}{2m}(\frac{n_x^2}{a^2} + \frac{n_y^2}{b^2}) \tag{2.8a}$$

$$E = \frac{\hbar^2\pi^2}{2mA}(\frac{n_x^2 b}{a} + \frac{n_y^2 a}{b}) = \frac{\hbar^2\pi^2}{2mA}(\frac{n_x^2}{\gamma} + n_y^2\gamma) \tag{2.8b}$$

where the area is A = a*b.

The minimum is found when the change in the function with respect to γ is 0. That is, $\frac{dE}{d\gamma} = 0 = n_y^2 - \frac{n_x^2}{\gamma}$ It is possible to see that if $n_x = n_y$ then the minimum of this function is γ=1, i.e. a square. But, if there is an energy degeneracy in one direction as opposed to the other, say $n_y^2 = 4, n_x^2 = 1$, then a deformation of 4 in one side over the other minimizes the energy.

This symmetry breaking is called the Jahn-Teller effect, and was first seen in molecular physics/ chemistry. It occurs when energetic degeneracies in a system can be removed by deformation. Typically, some states are pushed higher in energy and others are pushed lower in energy yet, the summation of energies is lowered. The same thing can happen in the nucleus and can be seen in section 3.3. The difference is the nature and strength of the forces/potentials and how these can drive various kinds of deformation. In order to see when this may be true and if so examine it in more detail, the science and methods of decay spectroscopy will be discussed.

2.1.2 Nuclear Decay Processes

To reiterate, the goal is to study neutron rich nuclei because this is the testing ground for nuclear models and is an important region where new physics is reasonably expected. They are tested as they decay and these decays are mediated by forces that can be studied, in the same way

as the strength of gravity from observation of falling objects might be studied.

Fission

The production mechanism for these neutron-rich nuclei, in this study was nuclear fission. There are two types of nuclear fission: spontaneous fission(SF) and induced fission. With spontaneous fission, a heavy nucleus like ^{252}Cf will release energy by splitting. The distribution of a light mass and a heavy mass fragment is shown in Fig. 2.4. Typically, there is a heavy fragment and a light fragment and several evaporated neutrons and it releases hundreds of MeV of kinetic energy. This can be shown by evaluating the masses of nuclei involved in this process. For example, ^{252}Cf will very likely fission into one barium(Ba) and one molybdenum(Mo) isotope with the emission of 4 neutrons. We then set up an equation (2.9a-c) representing the conservation of energy in units of MeV (i.e. the rest mass, $E_0 = mc^2$). The decay following SF: $^{252}Cf \rightarrow ^{102}Mo + ^{146}Ba + 4n$ will have the following energy balance, where m is the mass of the nucleus in parenthesis and KE is the residual kinetic energy.

$$m(^{252}_{98}Cf)c^2 = [m(^{102}_{42}Mo) + m(^{146}_{56}Ba) + 4 * m(n)]c^2 + KE \tag{2.9a}$$

$$KE = m(^{252}_{98}Cf)c^2 - [m(^{102}_{42}Mo) + m(^{146}_{56}Ba) + 4 * m(n)]c^2 \tag{2.9b}$$

$$KE = 234812.5 - (94928.8 + 135933.1 + 4 * 939.565)MeV = \boxed{192 \text{ MeV}} \tag{2.9c}$$

Notice that this accounts for all protons and neutrons, 98=42+56 (protons) and 252=102+146+4 (the sum of protons and neutrons). In some rare cases, an α particle or a ^{10}Be nucleus may be released as a ternary particle. Cold spontaneous fission, where no neutrons are released is also possible, but rare [24–26].

Fission, in some cases, may be induced by the energetic reaction between a small particle and a heavy nucleus. In the case of producing nuclides for beta decay studies, ^{238}U was bombarded with accelerated protons and the excited nucleus fissions. That distribution is shown in Fig. 2.5.

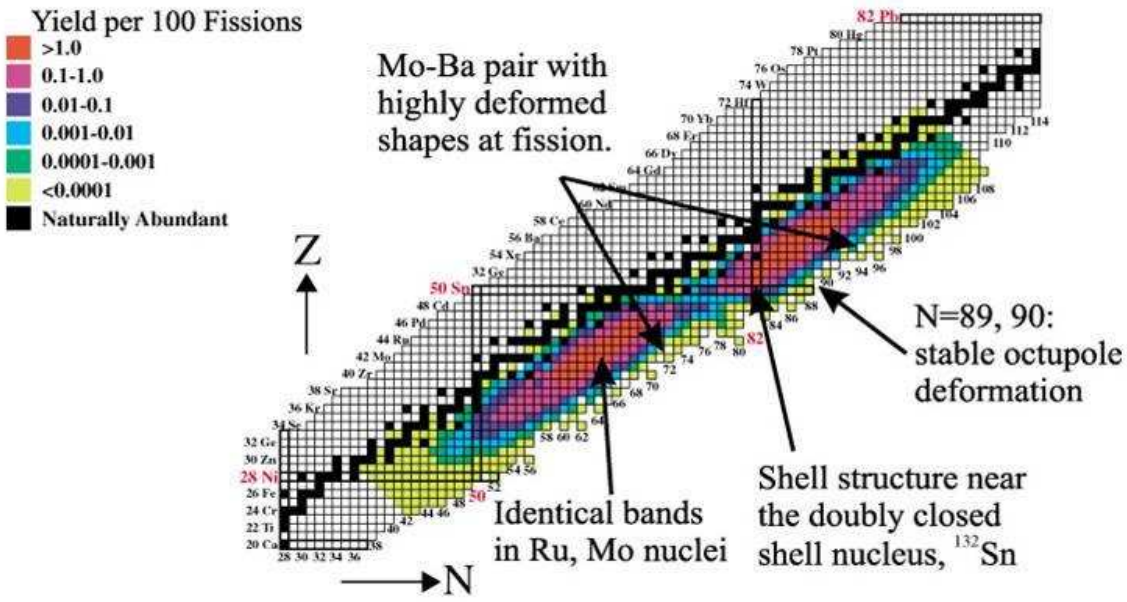

Figure 2.4: Figure of mass distribution from SF

This demonstrates that the distribution from these processes is different and each process can access different products. The uranium (A=92) fission distribution is centered around $_{52}$Te and $_{41}$Nb and spans from near $_{28}$Ni to $_{64}$Gd. However, the ^{252}Cf distribution is centered around $_{56}$Ba +$_{42}$Mo and goes from near $_{26}$Zn to $_{68}$Er. In practice, our study of ^{252}Cf fission has not found anything with more protons than $_{64}$Gd.

The nuclides produced from these processes are measured in different ways as well. In the first case, a fissioning source is placed in a detecting array and as soon as the fragments are produced, since they are created in an excited state, they will emit gamma radiation in order to de-excite. The radiation is measured in the detecting array, recorded and analyzed. This is prompt radiation and spectroscopy. This gives access to high spin states in nuclei because of the dynamical aspects of nuclear fission. It requires sophisticated data analysis techniques and database management, as all the data come in a single set.

Alternatively, fragments may be accelerated from the point of production (either induced fission or SF) to the measurement station. This is delayed spectroscopy, it requires an exotic beam facility such as the HRIBF at Oak Ridge National Laboratory. The fragments will beta decay after being accelerated to the measurement station and then will decay via gamma rays. Because there

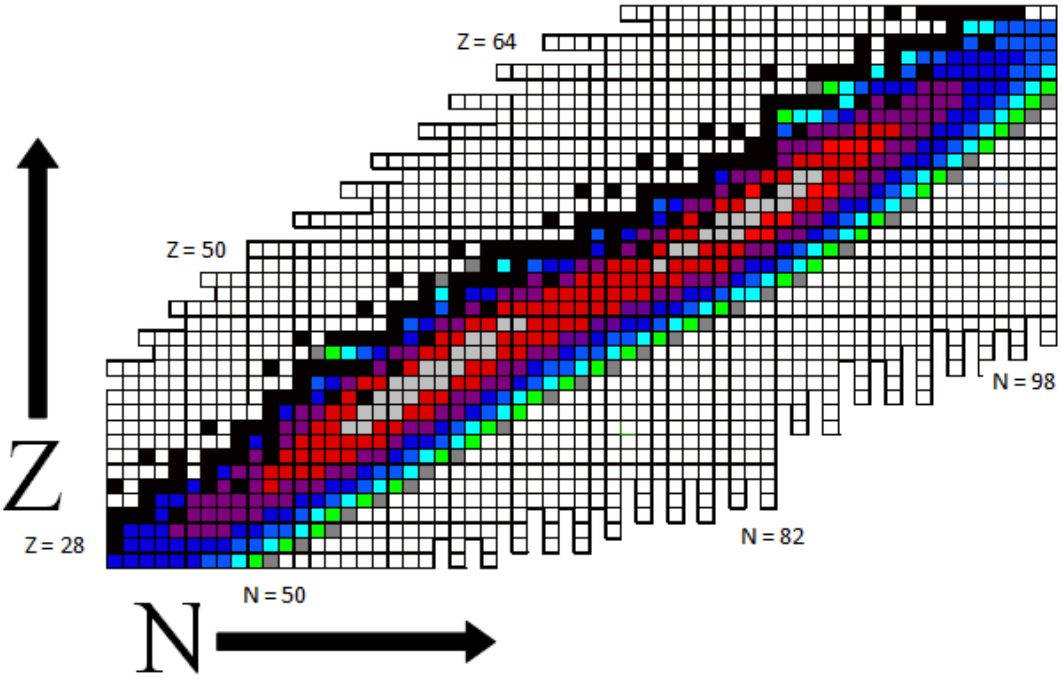

Figure 2.5: Figure of mass distribution from the proton induced fission of ^{238}U[Batchelder, J.C. (private comm.)]

is a hindrance against beta decays with large changes in spin between the states, the levels able to be accessed via delayed spectroscopy are limited by the spin of the parent nucleus. But, because the fragments travel along a beam line, they may be separated in a superconducting magnet by the charge to mass ratio. This gives better purity within the data set and may not require the statistics or data analysis techniques to be certain of the discovery. This was particularly useful in the case of gadolinium because many of the band structures in this region are very similar in energy and difficult to distinguish from each other.

Gamma Decay

In the case of prompt decay, when the nuclei are produced they de-excite via gamma radiation. In the quantum mechanics, order l of the multipole emitted is related to the angular momentum carried away from the initial state. Angular momentum is a vector that can only be coupled via an interaction in a certain way. This gives rise to a very important rule called the “triangle rule”. Given an initial nuclear state of spin I_i and a final state of spin I_f, the transition may carry angular

momentum anywhere between $\left|I_f - I_i\right| \leq l \leq I_f + I_i$.

The probability(λ) that a given type of transition will occur(2.10) is as follows, where X represents either electric or magnetic character carrying away angular momentum L, B(XL) is the reduced transition probability, E_γ is the transition energy in Mev and $\hbar c$ is 197.3 MeV fm.

$$\lambda_\gamma(XL) = \frac{8\pi(L+1)}{L[(2L+1)!!]^2\hbar}\left(\frac{E_\gamma}{\hbar c}\right)^{2L+1} B(XL) \tag{2.10}$$

Then, there are estimates as to what a transition probability would be if only a single particle were involved in the nuclear transition 2.11a-b. These are called Weisskopf Units (W.U.) [27], where e is the base unit of electrical charge and μ_N is the Bohr magneton. Also listed in table 2.1 are the first four estimates of each type of multipole transition.

$$B(EL)_{W.U.} = \frac{1.2^{2L}}{4\pi}\left(\frac{3}{L+3}\right)^2 A^{2L/3} e^2 fm^{2L} \tag{2.11a}$$

$$B(ML)_{W.U.} = \frac{1.2^{2(L-1)}10}{\pi}\left(\frac{3}{L+3}\right)^2 A^{2(L-1)/3} \mu_N^2 fm^{2(L-1)} \tag{2.11b}$$

Table 2.1: The single particle transition probabilities in the Weisskopf estimate for electric and magnetic transitions of multipole order 1 through 4. E_γ is in MeV

L	λ_γ(EL) (s^{-1})	λ_γ(ML) (s^{-1})
1	$1.02 * 10^{14}\, A^{2/3}\, E_\gamma^3$	$3.15 * 10^{13}\, E_\gamma^3$
2	$7.28 * 10^{7}\, A^{4/3}\, E_\gamma^5$	$2.24 * 10^{7}\, A^{2/3}\, E_\gamma^5$
3	$3.39 * 10\, A^{2}\, E_\gamma^7$	$1.04 * 10\, A^{4/3}\, E_\gamma^7$
4	$1.07 * 10^{-5}\, A^{8/3}\, E_\gamma^9$	$3.27 * 10^{-6}\, A^{2}\, E_\gamma^9$

Because of how drastically the probabilities change with regard to character and angular momentum, the typical gamma-ray transitions observed are of E1, M1, or E2 type and M1 and E2 transitions are often mixed. That is, there is a probability that the state will decay as an E2 and a similar probability that it will decay as an M1. This is also called dipole/quadrupole mixing. These estimates can also be used to give evidence that a given transition involves many particles

or is a collective transition as opposed to a single particle transition. The intensity I_γ is the actual measured quantity as the number of counts divided by the calibrated efficiency. Measuring lifetimes or a process called Coulomb excitation can be used to measure the absolute B(XL) and the relative intensities (probabilities) can then be inferred. The next paragraphs give specifics of other radiative processes and their transition probabilities and the experimental methods for determining them.

Depending on the energy, other processes may compete with gamma decay. At energy scales less than 200 keV, there is a competition between gamma decay and the process of internal conversion. The electrons orbiting the nucleus have a probability of existing inside the nucleus. When it interacts with the nucleus, the electron can be given energy and ejected, another electron from a higher orbital can occupy the vacancy created by the ejected electron via an atomic transition by emitting an X-ray. The ratio of the probabilities for electron conversion to gamma emmision is called the total internal conversion coefficient and usually labeled α. These X-ray energies are different for every element and are useful for identification purposes. They differ by about 1 keV for ΔZ=1 nuclei. The X-rays come in sets with diminishing probability for each higher electronic orbital, from $K_{\alpha,\beta,\ldots}, L_{\alpha,\beta,\ldots}, \ldots$ (K,L correspond to the vacancies created in the corresponding electronic shells and α, β are the subshells.) and all of the K_α and K_β X-rays are measured. Also, at energies greater than twice the rest mass of the electron (1.02 MeV), a photon can spontaneously create an electron-positron pair. The positrons interact within the electron in the detector and a peak at 511 keV will be in the experimental spectra.

Beta Decay

When delayed spectroscopy is performed, beta decay populates states in its daughter nucleus which, in our case (beta minus), has one less neutron and one more proton. It can be shown in the following decay from nucleus X to nucleus Y:

$$ {}^{A}_{Z}X_N \rightarrow {}^{A}_{Z+1}Y^{*}_{N-1} + \beta^- + \overline{\nu}_e + KE_{(recoils)} \tag{2.12} $$

where the * indicates that the nucleus Y is created in an excited state. These excited states then gamma decay. It is possible to measure the beta ray emitted from the nucleus, but often a more versatile array optimized for gamma ray detection is used and beta decay properties are inferred. Some details on the theory of beta decay are useful for understanding the relevant mechanisms. Unfortunately, the use of logft's are limited in their usefulness for determining spins and parities.

First it is necessary to understand the coupling of angular momenta in this process. From a wealth of observations in many different contexts, momentum is conserved. The β particle and neutrino both have spin 1/2$\hbar$, therefore there are two ways to orient them relative to each other, anti-parallel (to spin 0, called a Fermi decay) or parallel (to spin 1, called a Gamow-Teller decay). Succinctly, we can express the following:

$$\vec{I}_P = \vec{I}_D + \vec{L}_\beta + \vec{C}_{\beta,\nu} \tag{2.13a}$$

$$\pi_P = \pi_D \, (-1)^{L_\beta} \tag{2.13b}$$

Here is given, $I_{P,D}$, which is the spin of the parent and daughter state, respectively; L, which is the angular momentum associated with the electron; C, which is the coupling factor (1 or 0) for the electron and the neutrino; and π is the parity (+ or -) for the states considered. Because larger angular momenta require emmision farther from the center of the nucleus and therefore additional energy, the most favored process are decays from a nucleon at the center of the nucleus. These are decays from an initial state with spin 0 to a final state of spin 0 and no parity change (i.e. L_β=C=0) are most favored. This type of decay is called a superallowed transistion. If L_β=0, allowed transitions occur and $I_P \neq 0$ then spin changes of zero or one are available depending on whether it is Fermi or Gamow-Teller decay. Beyond this, if L_β>0, then the L value is the degree of forbiddenness for the transition (First Forbidden, Second Forbidden, ...). First forbidden transitions can have a ΔI= 0,1,2 and will have a change in parity. These degrees of hindrance to beta decay have an effect on the lifetime of the nuclear states with respect to beta decay. These effects are quantified in the following way.

Beginning with Fermi's Golden Rule 2.14, the probability of a decay occurring is given by some constants multiplied by a squared matrix element ($|H_{fi}|^2$) containing the interaction strength, the perturbative potential coupling initial and final wavefunctions and the available phase space factor ($\rho_F(E)$), which counts (statistically) the density of states available to the final state.

$$\lambda = \frac{2\pi}{\hbar}|H'_{fi}|^2\rho_F(E) \tag{2.14}$$

Using methods from statistical mechanics, the phase space factor can be expanded to show that it is the change in the number of available states verses the change in the Q-value or energy gap (E_0) for the reaction ($\frac{dN}{dE_0}$), which is equal to:

$$\rho(E) = \frac{1}{dE_0}\frac{4\pi p_e^2 dp_e}{(2\pi\hbar)^3}\frac{4\pi p_\nu^2 dp_\nu}{(2\pi\hbar)^3} \tag{2.15}$$

This can be shown via conservation of energy to have the following form:

$$\rho(E) = \frac{16\pi^2}{(2\pi\hbar)^6}\frac{pE}{c^4}[(E_0-E)^2 - m_\nu^2 c^4]^{1/2}(E_0-E)dE \tag{2.16}$$

This creates a bell shaped curve with zeros at p=0 and $E_0 = E$, that is when the electron is not emitted at all and when the electron carries away all of energy. However, this may be simplified further. The neutrino mass term (m_ν) and recoil energy term (implicit in E) are negligible and in that case the decay probability can be written 2.17a-b. The interaction term ($|H_{fi}|$) has been simplified as well in terms of g = 0.88 * 10^{-4} MeV fm, an interaction strength. It is also argued that to first order, the out going plane wave wavefunctions of the neutrino and electron are equal to unity. Therefore, $|H_{fi}| = g|M_{fi}|$, which contains only the interaction with the nuclear final and initial states.

$$\lambda = C\int_0^{pmax} p^2(E_0-E)^2F(Z',p)dp \tag{2.17a}$$

$$C = \frac{g^2|M_{fi}|^2}{2\pi\hbar^7 c^3} \tag{2.17b}$$

A correction factor, F(Z′,p), has been added and is a Coulomb term to acoount for differences in the spectra of β^+ and β^- decays. This term is well known, and can be found in tables, graphs or programmed [17]. The variable C is written separately to reinforce the idea that these are constants. Now, since $\lambda = \frac{ln(2)}{T_{1/2}}$ and this integral part, with some extra terms to make it unitless, is called f(Z′,E_0). Then, the following can be written:

$$f(Z', E_0)T_{1/2} = ft = \frac{ln(2) * 2\pi^3\hbar^7}{g^2 m_e^5 c^4 |M_{fi}|^2} = \frac{6190s}{|M_{fi}|^2} \tag{2.18}$$

Because the beta-decay half-lives of nuclei can range from 10^{-3} to 10^{20} s, it is useful to take the $\log_{10}$ of ft and call it a logft. The following Fig. 2.6 shows some systematics of logft values [28]. It should also be mentioned that in 2012 [29] the lowest known superallowed logft was measured to be $2.62^{+0.13}_{-0.11}$. Mainly, what this figure shows is the large role that nuclear structure plays in the determination of this parameter. It also shows the unfortunate overlap of many types of transitions. It is therefore very difficult to assign spins and parities firmly from the measurement of logft. This figure also shows, that by far, the most likely thing to occur is a ΔJ=0 or 1 transition.

There are other nuclear decay processes (such as alpha particle emission) that are important, but will not be discussed as they are not relevant to this present course of study.

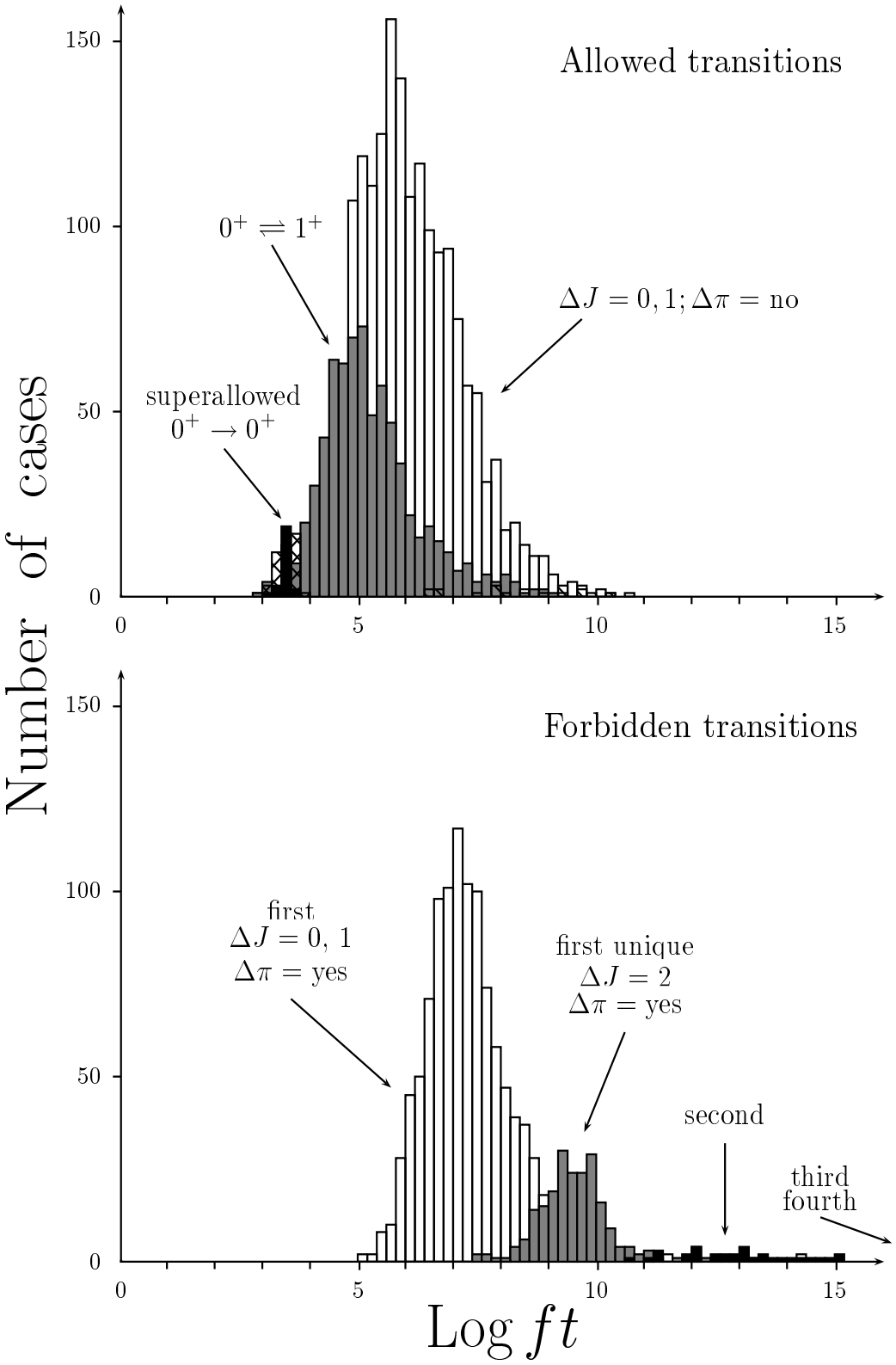

Figure 2.6: Histograms of the number of cases of a given type of transition versus log ft[28]

CHAPTER 3

NUCLEAR THEORY

This section describes the models that first predicted various phenomena that have or may be seen in nuclei. Many of the patterns, most notably shell structure and collective rotations and vibrations, have analogs in atomic and molecular physics. This section intends to explain a simple and qualitative picture of the origin of phenomena in nuclei and what is the expection as a result. These models are the most generally relatable theories to compare with experiment. However, also presented is a sketch of the modern approach that could be used in a specific case to give quantitative results. Nuclear theory can give band structures (patterns of levels, spins and parities), excitation modes, transition probabilities (half-lives), binding energies, and nucleon densities and currents. These observables can be compared either directly or indirectly to experiment. Just as much is learned, if not more, from examining in what ways these models fail as how they correctly explain phenomena.

3.1 Nuclear Shells

One of the most notable advances in nuclear physics was the description of various phenomena that indicated shell structure in the nucleus. Among those of importance were stability, neutron capture cross sections, and the energy of the first excited state when compared to those even one nucleon away. In 1955, Maria Meyer and Hans Jensen [30] summarized their findings, which showed that when a spin-orbit coupling term is added to the Hamiltonian in the mean field of a harmonic oscillator potential, it accurately recreates the regions where these phenomena of stability had been observed. These regions of increased stability lead to what are “magic numbers” of protons and neutrons and are shown in Fig. 3.1. When these shell groupings are filled, there is

a large energy gap between the full states and the next empty state available. Because the shape of the nucleus is spherical at this point, vibrational degrees of freedom are suppressed, all rotations are energetically degenerate, and all excitations are pushed very high in energy.

The potential used in this case was a spherically symmetric well, $V(r) = -V_0[1 - (\frac{r}{R})^2]$. The states in this model can be characterized by n, l, and j and are often written in spectroscopic notation in the form nl_j, where n is the principal quantum number related to the well solution of energies of the quantum harmonic oscillator, l is the orbital angular momentum and equal to 0,1,2,3.. (which can be written as s,p,d,f..., respectively) and j=l$\pm$1/2. This one half comes from the fact that the nucleons are fermions (spin s = 1/2). For example the $2p_{1/2}$ state has associated quantum numbers n=2,l=1,j=1/2. The direction and magnitude of the splitting was worked out and the schematic of spherical shell gaps can be seen. The quantum mechanical formalism can be used to show that these states have 2j+1 energetically degenerate substates.

This figure shows that there are regions of stability for neutron or proton number equal to 2, 8, 20, 28, 50, 82, ... and so on. A "doubly magic" nucleus is then a nucleus that has a magic number of protons and neutrons. Examples of such nuclei would be oxygen-16, calcium 40 and 48, nickel 56 and 78, etc.. As an example of the predictive power of this model, we can see that ^{16}O, with Z=N=8 has spin 0^+ in its ground state because all nucleons have paired off. Adding a nucleon to ^{16}O gives either, ^{17}F or ^{17}O both which have a ground state with spin $\frac{5}{2}^+$, can be seen to originate from the $1d_{5/2}$ orbital. If a nucleon is removed to create ^{15}O or ^{15}N, then it would be expected to have a valance particle in the $1p_{1/2}$ shell and they would be expected to have ground states of $\frac{1}{2}^-$ and so they do. This is only true, however, if it is only the last unpaired valence particle that contributes to the ground state. It is especially difficult to predict the ground state spins and parities of odd-N, odd-Z nuclei.

3.2 Collective Model

The collective model was developed by Aage Bohr and Ben Mottleson [31]. It was developed to explain the occurrence of larger quadrupole moments in certain regions that could not be

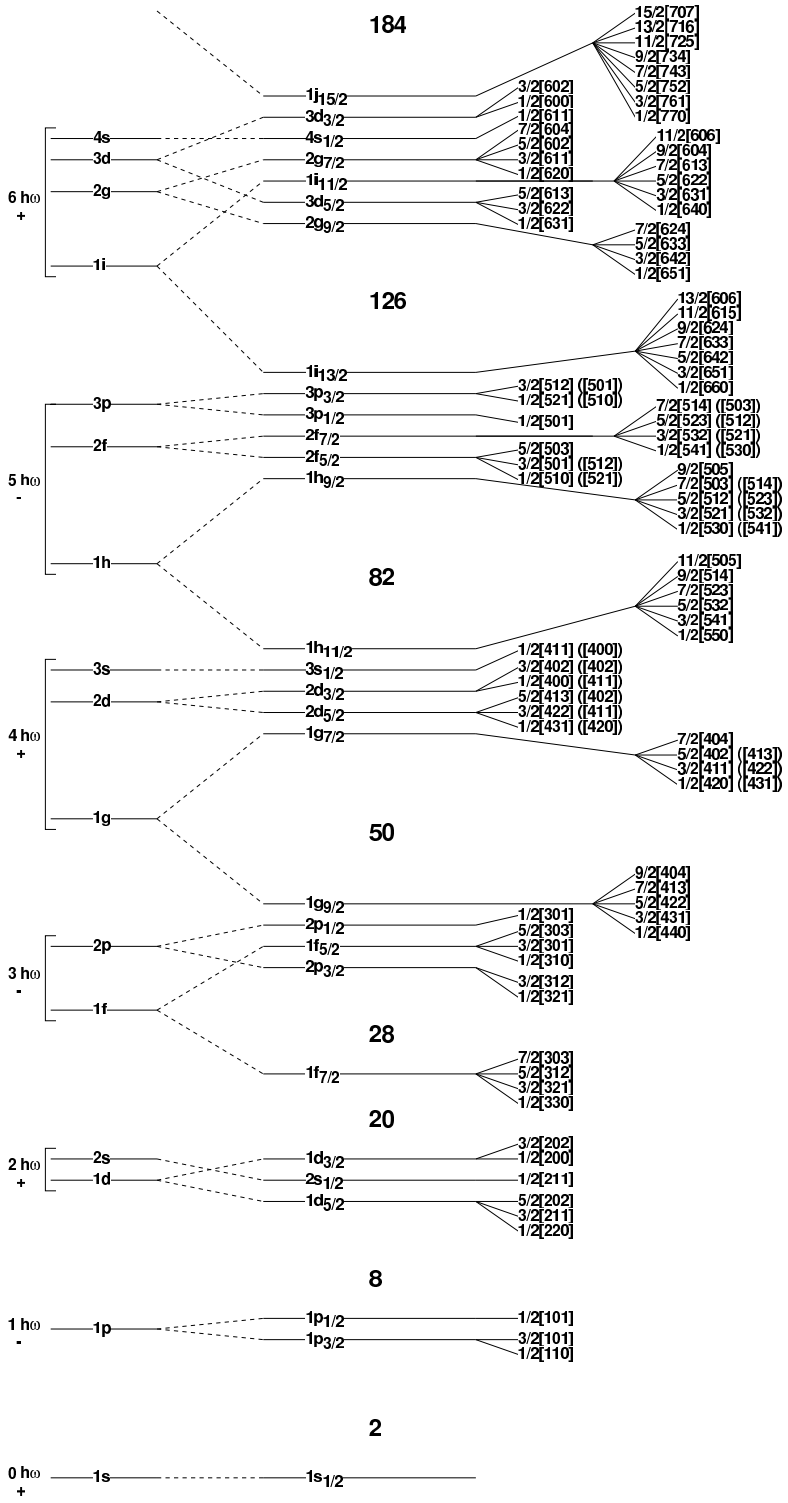

Figure 3.1: From left to right: The harmonic oscillator shells and spacings, the closed shells produced in the shell model that explained the phenomenon of particularly stable nuclei among other indicators of shell structure, the deformed shell model(Nilsson Model) with asymptotic quantum numbers for neutrons (and protons) $\Omega[N\ n_z\Lambda]$ Fig. 3.2.

predicted by the shell model. It predicted the observables that would be expected if all nucleons were involved in collective motion. This would have the physical chemistry analog to a dumbbell molecule (rigid rotor) such as the collective rotations and vibrations of H_2 or some other diatom. Rotations, vibrations, the K quantum number, and then band structures and decay strengths in and between these modes will be presented. For the collective model and the deformed shell model, it is helpful to see the following diagram of important quantum numbers for angular momenta (Fig. 3.2).

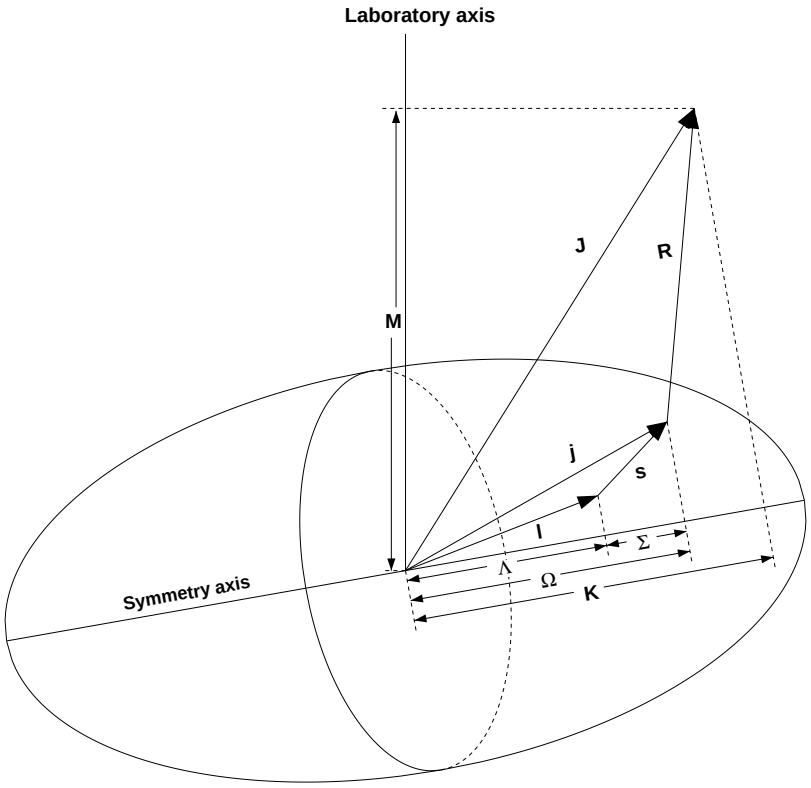

Figure 3.2: A schematic view of angular momenta and their projections onto the symmetry axis as used in collective and Nilsson models [32].

For collective rotations of a quadrupole deformed nucleus, the rotational energy is one-half the square of the angular momentum operator divided by the moment of inertia. The operator R^2 would act on the $Y_{I,M}$ characterizing the state and this solution is well known. It yields $E_I = \frac{\hbar^2}{2\Im_1} I(I+1)$. It is important to say as well that odd I are ruled out in this case, because the $Y_{I,M}$

change sign for odd I upon reflection in the x-y plane. However, the nuclear shape is symmetric under this operation. Therefore, odd I are disallowed on physical grounds for even-even nuclei. The ground state band or yrast band (meaning the lowest rotational state of a given spin), follows this spacing with the spin sequence 0,2,4,6 ... with positive parity. This spacing holds true if the rotation is aligned (K=0) and is pure rotational. For other interactions with the rotation, correction terms of the form $B(I(I+1))^2$, $C(I(I+1))^3$, and so on may be applied. If K$\neq$0, then $E_I = \frac{\hbar^2}{2}(\frac{I(I+1)-K^2}{\Im_1} + \frac{K^2}{\Im_3})$. Here, $\Im_1$ is the moment of inertia perpendicular to the symmetry axis and $\Im_3$ is the moment parallel to it. An example of a good rotor would be ^{160}Gd which has a 75.3 keV first excited 2^+ state with a half life of 2.72 ns. In the Weisskopf estimate, the half-life one would expect (for a single particle transition) is $\ln(2)/7.28 * 10^7 * 160^{(4/3)} * (.0753)^5$= 4.5 μs which is different by a factor of 1664. This indicates the collectivity of this transition. According to I(I+1) spacing, the 4^+ state built off of the 75.3 keV 2^+ state should have an energy of $\frac{75.3*20}{6}$ keV = 251 keV and the state is found experimentally to be at 248.5 keV.

Collective vibrations come in a variety of forms, surface oscillations about a spherical shape (discussed in section 3.4) and vibrations of deformed shapes such as beta, gamma, and octupole modes, which have associated rotational bands. The approximation of the nuclear medium as being incompressible, turns out to be very good even though it has a diffuse edge. Without going into to much detail, this limits the vibrational modes. In one quadrupole vibrational mode, the cross-section across the long axis remains circular, while the vibration across the other axes alternate. This mode changes the parameter β_2 as described in equation 2.6, and is called beta vibration. It should produce an excited spin sequence of K=0, and I=0,2,4,... with positive parity. The other mode describes an alternate compression in the direction of the short axes while the endpoints of the nucleus on the long axis remains fixed. This is a change in γ, and is therefore called gamma vibration. This produces a spin sequence with K=2 and I=2,3,4,... with positive parity. Axial octupole vibration has K=0, and describes a reflection asymmetric vibration, between a spheroid shape and that of a pear. It should produce a sequence of 1,3,5,... with negative parity, indicating its asymmetric shape.

In some cases, an excited state in a nucleus may be based on a high K quantum number. This is most likely do to single particle or quasiparticle pairs being excited in the nucleus. In which case there is an angular momentum barrier against making a transition of this type. A transition with a high $\Delta K = \mid K_i - K_f \mid$ can be hindered by a factor called $\nu = \Delta K - L$. Then the hindrance factor,

$$f = \tau_\gamma / \tau_{W.U.} \tag{3.1}$$

and reduced hindrance factor,

$$f_\nu = f^{1/\nu} \tag{3.2}$$

can be used to quantify the reduction in probability. This retardation factor may be applied to gamma or beta decay processes and is evidenced by an increased lifetime of the state over that which would typically be expected for the transition of the same order. This is is one reason that an isomer or a meta-stable state may occur in a nucleus. These isomers are called K-isomers.

The collective model also predicts estimates for different types of transitions. For a transition from a one phonon state to a non-phonon state the collective model([31] ch. 6) gives

$$B(E\lambda)_{ph} = \frac{3\lambda}{8\pi} Z^2 e^2 R_0^\lambda \frac{\hbar^2}{AME_\gamma} \tag{3.3}$$

for the reduced transition probability. For a transition from a beta vibrational state to a non-beta vibrational state

$$B(E2;\ I_i \to I_f) = B(E2)_{ph} \langle I_i\ 2\ K\ 0 \mid I_i\ 2\ I_f\ K \rangle^2 \tag{3.4}$$

and for a transition from a gamma vibrational state to a non-gamma vibrational state

$$B(E2;\ I_i \to I_f) = B(E2)_{ph} \begin{bmatrix} \langle I_i\ 2\ K \pm 2\ \mp 2 \mid I_i\ 2\ I_f\ K \rangle^2 & K \neq 0 \\ 2\langle I_i\ 2\ 2\ -2 \mid I_i\ 2\ I_f\ 0 \rangle^2 & K = 0 \end{bmatrix} \tag{3.5}$$

is what can be used. Where the formulae in bra-kets are Clebsch-Gordan coefficients derived from

vector geometry. Within a rotational band the E2 and M1 transitions are

$$B(E2;\ I_i \to I_f) = \frac{5}{16\pi} e^2 Q_0^2 \langle I_i\ 2\ K\ 0 \mid I_i\ 2\ I_f\ 0\rangle^2 \tag{3.6a}$$

$$B(M1;\ I_i \to I_f) = \frac{3}{4\pi}\left(\frac{e\hbar}{2Mc}\right)^2 (g_\Omega - g_R)^2 \Omega^2 \langle I_i\ 1\ K\ 0 \mid I_i\ 1\ I_f\ 0\rangle^2 \tag{3.6b}$$

where the M1 transitions require an additional factor for K=1/2. If there is more than one option for decay out of a state, the branching ratio is given by

$$\frac{B(L\ I_i \to I_f)}{B(L\ I_i \to I_{f'})} = \left(\frac{\langle I_i\ L\ K_i\ K_f - K_i \mid I_i\ L\ I_f\ K_f\rangle}{\langle I_i\ L\ K_i\ K_f - K_i \mid I_i\ L\ I_{f'}\ K_f\rangle}\right)^2 \tag{3.7}$$

These formulae along with those given in equation 2.10 can be helpful in analyzing what should be expected for decays from various states.

3.3 The Deformed Shell Model

Not long after the development of the collective model S.G. Nilsson [33] created the deformed shell model. It added deformation parameters and an l^2 term to the Hamiltonian. From the plots of the migration of single particle shells, shown in Fig. 3.3, one can see new magic numbers arise for deformed nuclei where there are gaps that arise in the shells at $\beta_2 \neq 0$.

In this case, because the 2j+1 degeneracy of the spherical shell states are broken, new quantum numbers are needed. They are called asymptotic quantum numbers, and are listed in the diagrams as $\Omega^\pi[Nn_z\Lambda]$. Where Ω is the total angular momentum j=l+s projected onto the symmetry axis, N is the number for the oscillator shell, n_z is the number of quanta in the z direction, and Λ is the projection of l onto the symmetry axis. These numbers are sufficient to label these states.

3.4 Interacting Boson Model

The collective model provides a description of harmonic vibrational states that are vibrations on the surface of nuclei. Phonons, that is vibrational quanta, can be excited and will create at the

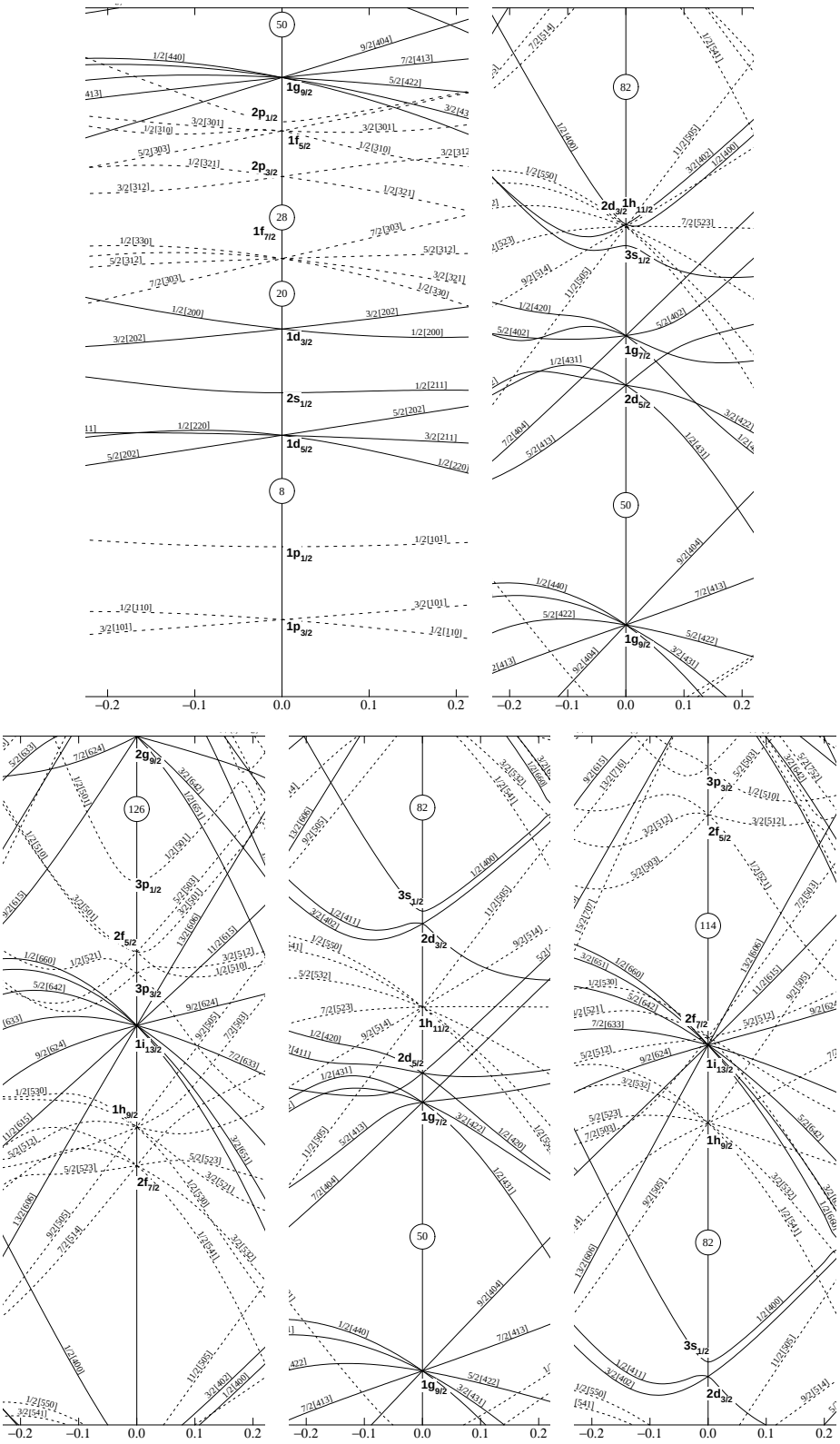

Figure 3.3: Plots of the migration of deformed shells from spherical in the collective model[32].

one phonon level a 2^+ singlet, at the two phonon level a triplet of states with spins and parities of 0^+, 2^+ and 4^+, and at the three phonon level a quintuplet of states of 0^+, 2^+, 3^+, 4^+ and 6^+.

In energetic terms, rotational bands have ≈100keV and I(I+1) spacing. Vibrational levels, however, should be evenly spaced that is "R" the ratio of the 4_1^+ level to the 2_1^+ level should be 2, because each phonon should have the same energy. R for the rotational levels by contrast should be, via $I(I+1)$, 4*5/(2*3) = 10/3 = 3.33. In terms of selection rules, the phonons can only be created one at a time. Therefore, the decays are limited to $\Delta N_{ph} = \pm 1$. So that the 2_2^+ level ($N_{ph} = 2$) should not decay to the ground state 0^+ (N_{ph}=0).

From very early on in the collective model(≈1960) Cd isotopes near stability, specifically A=110 and 112, have been thought to be very ideal candidates to describe a surface vibrational mode. In order to explain these nuclei, the Interacting Boson Model (IBM) has been employed [34]. It has be used either with or without distinguishing protons and neutrons, IBM-2 and IBM-1 respectively and accounts for 2p-4h (two particle - four hole) excitations across the Z=50 shell gap called intruder states. The IBM has two core assumptions. First, that the valence nucleons (those in the highest shells) are the only ones that contribute to the excitations of the nucleus. Second, that they act pairwise and the pairs of fermions couple to form s and d bosons, that are 0^+ and 2^+ respectively. The bosons can have magnetic substates of multiplicity (2I+1). That is, 1 state for the s boson and 5 for the d boson. Therefore, the operators that can be formed out of this group are subsets of the U(6) algebra or unitary operations in six dimensions. This group has 3 limiting subsets, U(5), SU(3), and O(6). The important algebra for harmonic vibrations is U(5). The predictions of the levels and their expected spins and parities are shown in Fig. 3.4 from [35] along with the expected B(E2)'s. These B(E2)'s are first predicted by the Bohr model and then modified to IBM in the following way.

$$B(E2; n_d \rightarrow n_d - 1)_{IBM} = \frac{N - n_d + 1}{N} B(E2; N_{ph} \rightarrow N_{ph} - 1)_{ph} \tag{3.8}$$

The following is a list of the fit parameters in IBM-2 that are also used to fit the level energy and transition strength: ε_d, κ, χ_ν, χ_π, $C_{0\nu}$, $C_{2\nu}$, $C_{4\nu}$, ξ_1, ξ_2, ξ_3, $e^{(0)}_{\nu_n}$, $e^{(0)}_{\pi_n}$, $e^{(2)}_{\nu_n}$, $e^{(2)}_{\pi_n}$, g_{ν_n}, g_{π_n}, α, β,

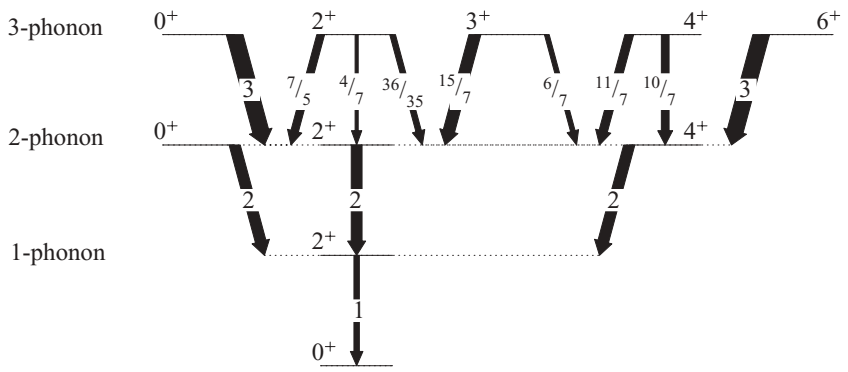

Figure 3.4: The schematic pattern of spins, parities and B(E2)'s expected for a vibrational nucleus for a spherical quadrupole vibrator.

Δ, $e_I^{(2)}/e_n^{(2)}$, g_I/g_n, $e_I^{(0)}/e_n^{(0)}$.

The goal is then to connect these terms to real physical observables. But, as with all of these models it does not specifically address anything but the pure case. It does not give any hint as to what to expect in the physical (non-ideal) world where mixing of these pure modes with other modes is likely to occur. For example, an experimental result somewhere between a U(5) nucleus towards something that looks like an SU(3) nucleus would not be able to be explained in this limiting framework. Primarily however, there is a concern that this view of the nucleus is quite narrow and perhaps misleading. If the experimental data does not fit this picture rather exactly, then it is limited in its ability to explain those things which may be physically realized yet outside of its rather narrow model space. Namely, this framework has provided a description of the intruder states that may interfere and mix with the vibrational states, but it does not address the possibility of non-bosonic or higher order couplings nor more collective degrees of freedom. As in the collective model, the IBM is limited in its description of mixing and correlations outside of its model space.

3.5 Geometric Model for Octupole Deformation

Reflection asymmetry in the intrinsic frame was first predicted for nuclei near ^{145}Ba, in the form of octupole deformation[36]. This was based on the single particle energy levels from the

deformed shell model, which showed shell gaps for Z=56 and N=88 for $\beta_3 \approx 0.1$ (see Fig. 3.5). Reflection asymmetry should be evidenced [37] by two ΔI=1$\hbar$, alternating parity rotational bands with opposite parities distinguishing the two. In addition, in octupole deformed nuclei, a displacement between the charge center of mass and the total center of mass should cause strong E1 transitions to populate and depopulate the negative parity levels in contrast to a band built on octupole vibrations.

This geometrical model defines the simplex operator as a combination of parity and rotation (by 180°) operators, S = Π R^{-1}. R is called the signature operator and is used to explain phenomena in quadrupole deformed nuclei, which are symmetric under this operation. The eigenvalue of this operator is s and $s^2=(-1)^A$, that is, s= $\pm$1 for even-A nuclei or s= $\pm i$ for odd-A nuclei. This gives parity eigenvalues as a combination of simplex and signature quantum numbers as p= s $e^{-i\pi I}$ [37]. Therefore, parity alternates with spin changes of one $\hbar$. Explicitly this is:

$$s = 1 \rightarrow 0^+, 1^-, 2^+, 3^-, \ldots \tag{3.9a}$$

$$s = -1 \rightarrow 0^-, 1^+, 2^-, 3^+, \ldots \tag{3.9b}$$

$$s = i \rightarrow \frac{1}{2}^+, \frac{3}{2}^-, \frac{5}{2}^+, \ldots \tag{3.9c}$$

$$s = -i \rightarrow \frac{1}{2}^-, \frac{3}{2}^+, \frac{5}{2}^-, \ldots \tag{3.9d}$$

There is an important note that should be made about the signature quantum number. The algebraic solution of this model is that r may equal $\pm$1, but physics discards algebraic solutions on physical grounds all the time. It is suggested [20] that in even-even nuclei the preferred signature is the lowest energy configuration of a pairing of r=$\pm$i to $I^\pi = 0^+$. It is not requisite that the r=-1 band should exist. In fact, it seems to be rare. In the cases where it could be assigned, different signature rotational bands came, not from intrinsic symmetries, but from quasiparticle couplings to the core in nuclei near N=Z=40 [38]. In terms of octupole deformation and simplex, there is the case proposed in $^{224}_{89}$Ac where the odd valence particles have formed a 0^- ground state and a s= -1

and a s= +1 band have been seen and these bands are very nearly degenerate in energy.

A detailed review of octupole deformed nuclei and some of their properties and importance is given in reference [11]. More recent calculations have been done that continue to support the assignment of octupole deformation for these nuclei [39, 40]. These studies also give motivation to pursue experiments in ^{148,150}Ba. More detail on them will be shown in the following section.

The geometric model [37] provides helpful analysis of new states and trends in these nuclei. We show the analyses in Fig. 7.18. They are found in three formulae. That these nuclei have mixed rotational/vibrational character closer to the ground state is well established. We give the extension of these formulae to analyze new higher spin states. Rotation should stabilize the vibrational mode and these formulae reveal the qualitative balance between these degrees of freedom.

$$\delta E(I) = E(I)^{-} - \frac{(E(I+1)^{+} - E(I-1)^{+})}{2} \tag{3.10}$$

The energy displacement formula is a way to quantify deviations from an asymmetric rigid rotor, where negative parity levels would lie halfway between the positive parity levels. Therefore, $\delta E \approx 0$ is an indication of the stabilization of octupole deformation.

The rotational frequency ratio is a collective model measure, which assumes pure rotational levels and each gamma-ray depopulating a level has an energy of $\hbar\omega$. The ratio of the positive parity states to the negative parity states is then expressed in terms of the level energies.

$$\frac{\omega(I)^{-}}{\omega(I)^{+}} = \frac{2[E(I+1)^{-} - E(I-1)^{-}]}{[E(I+2)^{+} - E(I-2)^{+}]} \tag{3.11}$$

The limits we expect to see are, $\frac{\omega(I)^{-}}{\omega(I)^{+}} = 1$ for angular momentum stabilized octupole deformation and the limit we expect to see for a rotational level built off an octupole phonon is, $\frac{\omega(I)^{-}}{\omega(I)^{+}} = \frac{2I-5}{2I+1}$, called the vibrational limit.

Furthermore, the intrinsic dipole moment [41] is expressed as:

$$D_0 = \sqrt{\frac{5B(E1)}{16B(E2)}}\ Q_0 \tag{3.12}$$

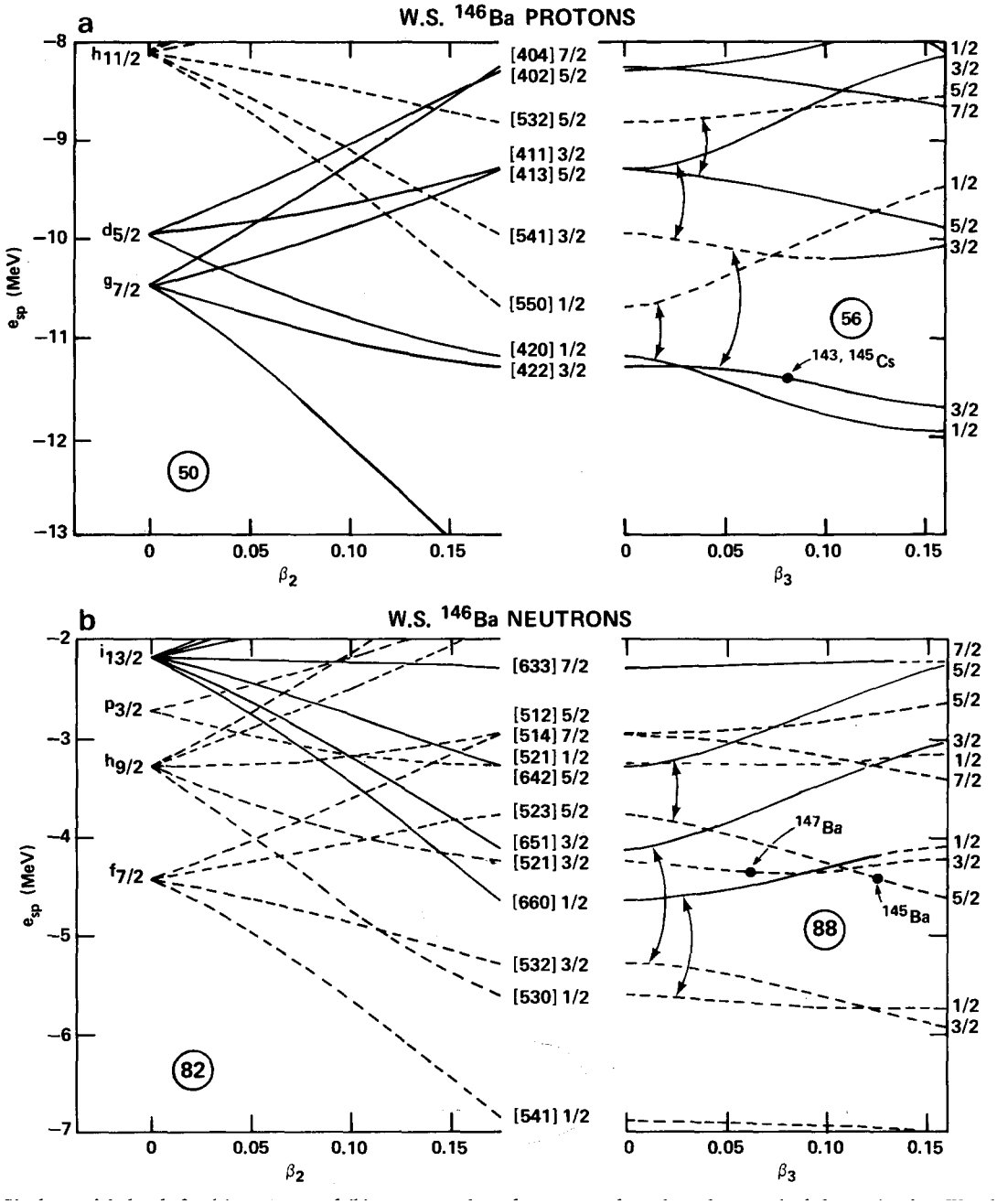

Figure 3.5: The theoretical migration of single particle energies with respect to changes in deformation, first in β_2 to a physical result then in β_3 until shell gaps are seen [36].

It is a way to analyze deformation as well as other effects that may be present in the nucleus [37, 41]. $\frac{B(E1)}{B(E2)}$ ratios are found from relative transition intensity measurements. However, the aforementioned E1 transitions and their strengths give strong evidence that a band is rotational rather than mixed rotational/vibrational in nature. However, this is stated cautiously because octupole deformation is not the only thing that can cause a non-zero dipole moment [11, 37, 41]. The interpretation of the drop in D_0 in ^{146}Ba is that there are several cancellation effects in the shell correction contribution as well as the macroscopic contribution to D_0. This theoretical approach, from reflection asymmetric mean field theory, as well as others are reviewed in [11].

Very recently, S. Frauendorf has presented an alternative model to the axial coupling of an octupole phonon to the intrinsic quadrupole shape. He suggests that Coriolis forces should anti-align the rotation of an octupole phonon ($Q_{3,3}$). At higher spin values, this phonon condenses or synchronizes with the rotation of the quadrupole and shows the alignment with spin properties described above as a rotating stable reflection asymmetric shape, which he calls a "rotating heart" shape. The intent is to eventually use the new results found in this present work to further analyze this new model.

3.6 Modern Theory

Now that the basic phenomenology is understood, the modern approach is more understandable. Because the basic phenomena should be able to be reproduced as well as a more quantitative picture of moments, levels and transition strengths. The most important connection between the phenomenological approach and the modern approach is the successful assumption that underpins the spherical and deformed shell models: that the nucleons can be treated as independent particles moving in a mean field.

It is always necessary to make simplifying assumptions in any nuclear theory. The more modern approach, as can be seen from the UNEDF [42] and similar efforts, is to provide a microscopic description that would connect the entire nuclear landscape. For nuclei with few particles, each nucleon can be treated as individually with its own set of initial conditions: the *ab initio* ap-

proach. This works well for only the lightest nuclei($< {}^{40}$Ca) and becomes intractable very quickly. For the heaviest and most neutron rich nuclides found from fission, it is necessary to use a mean field description. Hartree-Fock(HF) theory and its extensions which could be thesis topics in their own right, will be outlined only.

3.6.1 Hartree-Fock (HF)

Following the procedure in [20, 43], the derivation of the HF equations begins with an understanding of the variational principle. It can be shown that the time-independent Schroedinger's equation,
$(H-E) \mid \Psi\rangle = 0$, is equivalent to the variation of the energy functional, $\delta E[\,\Psi\,] = 0$. Where,

$$E[\,\Psi\,] = \frac{\langle\Psi \mid H \mid \Psi\rangle}{\langle\Psi \mid \Psi\rangle}. \tag{3.13}$$

Carrying out the variation with respect to Ψ, one finds $\langle\delta\Psi \mid (H-E) \mid \Psi\rangle + \langle\Psi \mid (H-E) \mid \delta\Psi\rangle = 0$. This variation is arbitrary and can therefore in principle be complex. It can then be shown that this is equivalent to $\langle\delta\Psi \mid (H-E) \mid \Psi\rangle = \ (H-E) \mid \Psi\rangle = 0$, the static Schroedinger's equation. More importantly, it can be shown that an approximate state($\mid \Phi\rangle$) can be written in terms of the exact state($\mid \Psi\rangle$). That is, $\mid \Phi\rangle = \sum_{n=0}^{\infty} a_n \mid \Psi_n\rangle$. It is found that the exact energy, $E_0 \leq E[\,\Phi\,]$ which is the functional of the approximate state $\mid \Phi\rangle$.

After making the assumption that the Hartree-Fock state assumed is a single Slater determinant,
$\mid HF\rangle = \prod_{i=1}^{A} a_i^+ \mid -\rangle$, where the a_i, a_i^+ are single particle operators that correspond to the single-particle wave functions. The HF ground state energy can then be written as,

$$E_0^{HF} = \sum_{k=1}^{N} \langle k \mid t \mid k\rangle + \frac{1}{2}\sum_{k,l=1}^{N} \langle kl \mid \bar{v} \mid kl\rangle \tag{3.14a}$$

$$\text{where, } \langle kl \mid \bar{v} \mid kl\rangle \equiv \langle kl \mid v \mid kl - lk\rangle \tag{3.14b}$$

where t is the kinetic energy term and $\bar{v}$ is the potential energy term which has a part "kl-lk" which represents the character of the mean field. Namely, that it should be anti-symmetric under the particle exchange operation. The HF expression for the ground state energy can be written as a density functional which depends on nucleon densities, kinetic energy densities, as well as spin and current densities. This is the outline for finding the ground state density or energy. Constrained HF can be used to find the ground state deformation and the energy difference between one deformation and another.

More can be done after calculating the ground state. Excited states can be found by adding constraints, like ωJ to find rotational excitations. Vibrational excitations (surface and giant resonances) can be built on the HF ground state using the Random Phase Approximation (RPA). Other physics can be added on to this basic formalism: using the quasiparticle transformation (QRPA), or even pnQRPA considering distinct proton-neutron correlations can be done, and pairing forces can be added through the HF+BCS (Bardeen-Cooper-Schrieffer) approach. A more general formalism is the self-consistent mean field + pairing theory called Hartree-Fock-Bogoliubov(HFB). Yet another approach is shown in the next subsection, which begins with the Langrangian instead of the Hamiltonian, which leads to a relativistic approach.

3.6.2 Reflection Asymmetric-Relativistic Mean Field (RAS-RMF) Theory

One example of the application of this methodology from [40] will be detailed. The approach used here is Reflection Asymmetric-Relativistic Mean Field (RAS-RMF) theory. Relativistic, in this sense, refers to the generally relativistic approach to quantum mechanics. An equation is chosen with the correct relativistic properties (effective Langrangian) and the variational principle is applied as outlined above. Instead of Schroedinger's equation, one instead gets the Dirac equation (for fermions i.e. nucleons) and Klein-Gordon equation (for mesons used as exchange particles defining the interaction). Then trial wave functions are chosen (the carefully chosen $\mid \Phi \rangle$ mentioned before) to be the eigenfunctions of the Two Center Harmonic Oscillator shown in equation 3.15.

$$V(r_\perp, z) = \frac{1}{2}M\omega_\perp^2 r_\perp^2 + \begin{cases} \frac{1}{2}M\omega_1^2(z+z_1)^2 \ , \ z < 0 \ , \\ \frac{1}{2}M\omega_2^2(z-z_2)^2 \ , \ z \geq 0, \end{cases} \tag{3.15}$$

This equation describes harmonic oscillations in an intersecting double spheroid(1,2) system. Constraints are applied simultaneously for quadrupole ($\langle\hat{Q}_2\rangle$) and octupole ($\langle\hat{Q}_3\rangle$) moments in the form of

$$\langle H'\rangle = \langle H\rangle + \frac{1}{2}C(\langle\hat{Q}_2\rangle - \mu_2)^2, \tag{3.16}$$

and a total energy surface(TES) can be created. The interaction has fit terms, but they are not individualized. Instead what is used is a global, physically accurate parameterization based on measured inputs (binding energies, lifetimes, etc.). The parameterization of terms in the effective Lagrangian is PK1 [44] and pairing is treated via the BCS approximation. The authors reproduce the binding energies of known neutron-rich barium to within 0.5% and the measured β_2 to within 10%. This is near the experimental errors.

They also produce two interesting figures (from private communication with the authors [40]). They predict quadrupole and octupole deformations for these nuclei by finding the energetic minimum in the β_2, β_3 plane. These regions are shown in Fig. 3.6. This figure shows a comparison of plots from $^{144-154}$Ba. The flatness of the minimum in the TES for $^{144,\ 154}$Ba means that there is equal likelihood (in the ground state) to have β_3 = 0 and $\neq$0. Therefore, one could expect to see vibrational excitations in these nuclei. However, in ^{148}Ba there is a well defined barrier against β_3 oscillations. One might then be convinced to attempt a measurement of octupole deformation properties for the ground state of this nucleus. Spectroscopic information could only be inferred with additional constraints, because these moments may change with spin [45, 46] and therefore, the spectroscopic observables like simplex band structures may change.

As was shown before, the strength of the octupole deformation is very sensitive to the location of the Fermi level to the gaps in single particle energies of the nucleons. It is asserted that this is because the interaction between these orbitals is the driving force behind octupole deformation.

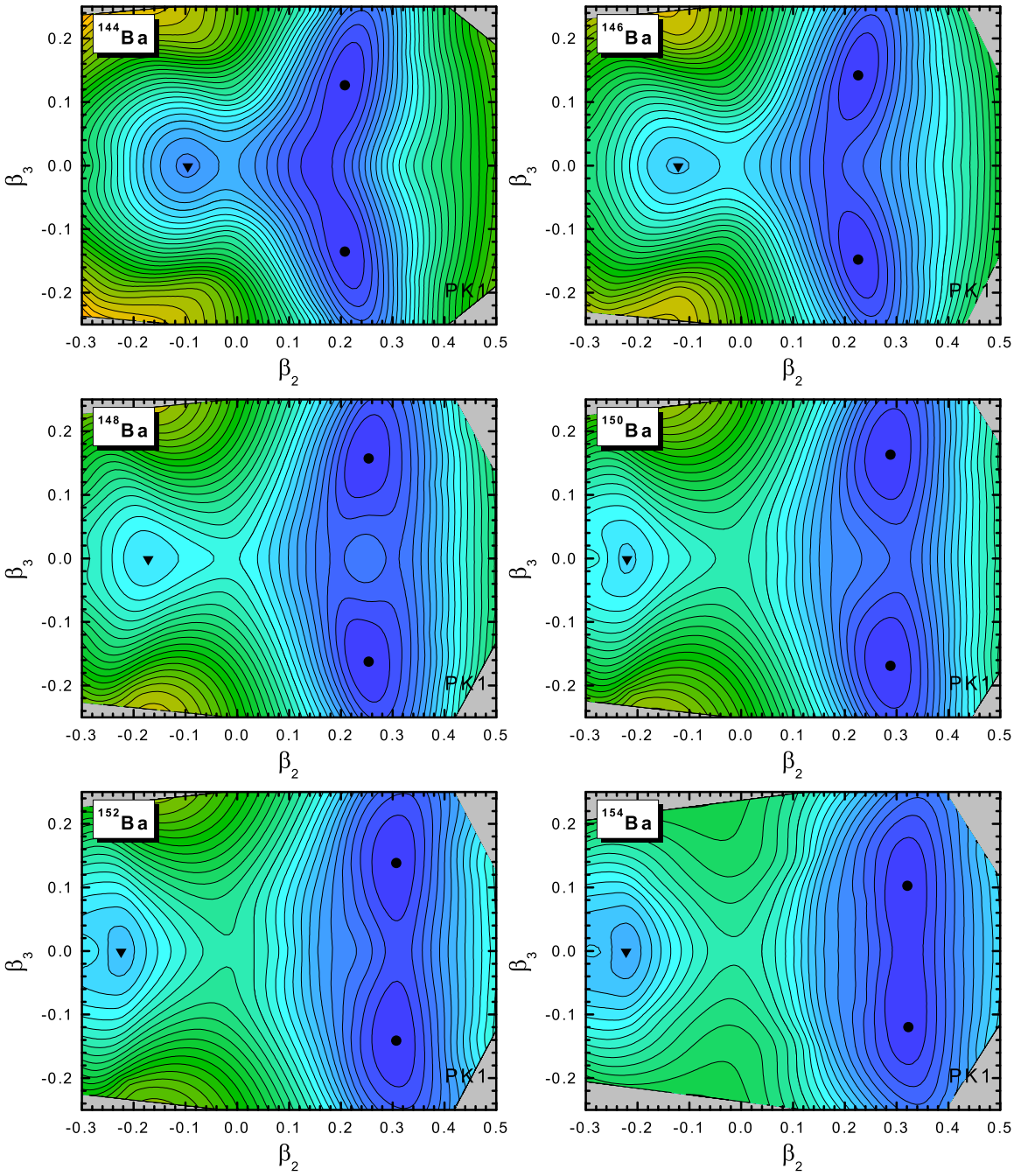

Figure 3.6: The ground state TES's for neutron rich Ba isotopes (from private communication with the authors of [40]).

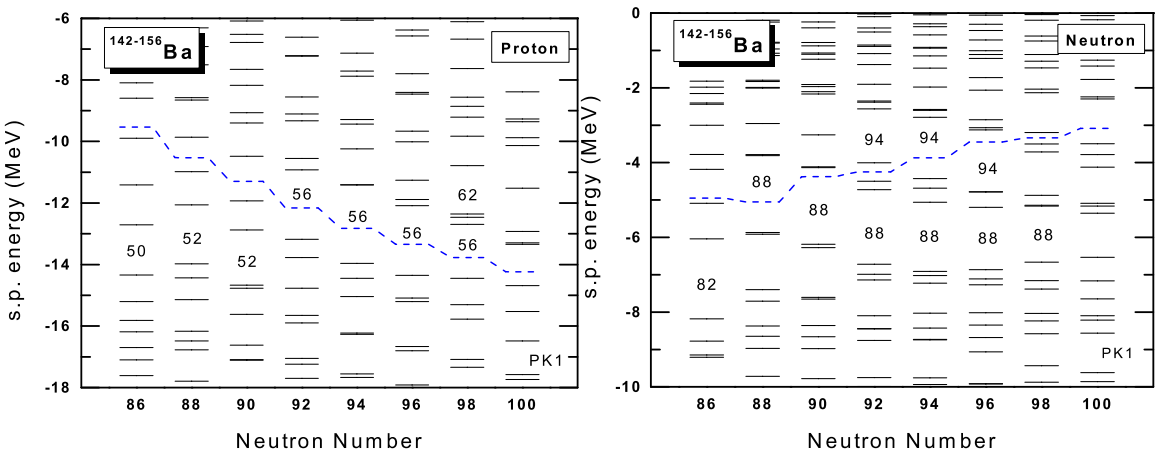

Figure 3.7: Migration of the s.p. shells and Fermi level of the nucleons with respect to neutron number [40].

Fig. 3.7 shows that Z=56 for a N=90-100 is a very good octupole magic number. However, there is a difference in the migration of the Fermi level for the neutron orbitals. It shows that N=88 and N=94 show a more pronounced gap in between the Fermi level and the nearest s.p. level. So an octupole region of particular interest is Z=56 and N=94 or ^{150}Ba, where both neutron and protons shells have large energy gaps. In fact, in the ground state the TES plot for ^{150}Ba has the minimum which is largest in $\beta_3 \approx 0.18$.

The explanation of these theories gives tools to explain the phenomena observed in each of the cases that have been explored experimentally. Near the Z=50 shell gap, the rigidity of shell structure has been thought to limit the vibrational modes of cadmium nuclei to pure harmonic oscillations. In the rare earth region, near the Z=66 midpoint between spherical shells at Z=50 and 82, strong quadrupole deformation is expected and indeed has been seen. Gadolinium at (Z=64) is probed for the structures that would be expected for a quadrupole deformed nucleus. Quadrupole deformation is fairly common in the nuclear landscape and yet there is still room to probe the systematics, expectations and characterization of various kinds of bands one would expect from the collective model. More exotic is a higher order deformation, octupole deformation, which occurs near Z=56, in the barium and cerium region and also in the Z=88, radium and thorium region. The study of Ba and Ce nuclei will focus on axial octupole deformation (pear shaped nuclei).

CHAPTER 4

EXPERIMENTAL TECHNIQUES

This section discusses the methodologies in general and the specific setups that were used to obtain the results in this thesis. The results came from two different studies: Cd and Gd studied from beta-decay at the Low-energy Radioactive Ion Beam Spectroscopy Station(LeRIBSS) at Oak Ridge National Lab(ORNL) and Gd, Ba and Ce studied from ^{252}Cf SF and Gammasphere. LeRIBBS at the HRIBF at ORNL utilized the induced fission of uranium and accelerated the nuclei so that the beta-delayed radiation was measured. The Gammasphere experiment took place large detecting array that utilized a fixed source of spontaneously fissioning Cf and measured the prompt radiation of these fragments.

4.1 Interaction of Radiation with Matter

In general, when radiation (ionizing or non-ionizing) enters a detector a it must interact with the atoms in the material in such a way to release charge carriers from a bound state to a continuum state and create current. A bias is placed on the detector and the freed charges are collected and the number of charges i.e. the current is directly related to the energy of the incoming radiation. The trouble comes because there are multiple ways to interact with a given material. Radiation may enter a detector and scatter off an atom and perhaps back out of the detector only depositing a portion of its energy. If this scattering occurs it is called a Compton event. Gamma radiation, if it has greater than the $2m_ec^2$=1.022 MeV required, can spontaneously produce an electron-positron pair. This can then produce false counts in the detector at 511 keV and at the energy of the gamma minus 511 or 1022 keV, depending on whether or not one or both particles escape the detector. Because light can interact with electrons in this way, photo-electric events occur when the incident

light is totally absorbed by one or more electrons and ejected from the atom(s) with some kinetic energy. The cross-section(probability) for each of these events is dependent on energy and can vary. There is a balance in detection methods between position sensitivity, energy resolution, detection efficiency, and electron drift velocity (how fast a signal can be read out of a detector).

Therefore, detecting systems are tailor made to fit a specific application. The detection of gamma rays is most commonly done with High-Purity Germanium (HPGe) crystals maintained at liquid nitrogen temperature. Because of the small band gap, 0.74 eV, a gamma ray (50 keV to several MeV) will produce one electron-hole pair per $\approx$3 eV of incident energy. Therefore, statistical fluxuations that would lead to poor resolution are reduced, and a high signal to noise ratio is achieved. Unfortunately, it performs very poorly for detecting below 30 keV. Efficiency at low energy, is proportional to cross-sectional area and at higher energy to detector volume, so a different detector is needed for low energy measurements. In germanium, Compton scattering is the dominant process in the region where most radiation is emitted. One way to handle this in a large array of HPGe detectors would be to place a high Z absorber like copper coated lead shielding in between detectors. In that case the partial energy is still detected, but the remainder is not redetected. It is also possible to place an additional detector in between the HPGe to detect and reject those Compton events that had just happened. This detector would need to be very fast. Gammasphere uses bismuth germinate (BGO) to do just that. The peak to background can be further improved by obtaining segmented HPGe so that it could be known where in the large volume a signal originated. Then, if it left that detector and went into another one it could be determined where it hit and where it came from. In this way, using gamma ray tracking, a very large effective volume is utilized and takes full advantage of the dominant Compton process making it work positively instead of negatively. This is the idea behind the GRETA and GRETINA detection projects.

A similar semi-conductor material used for detection of low energy X-rays and also conversion electrons is lithium doped silicon(Si(Li)). It is used with a different geometry to achieve better detecting efficiency at low energy. It is a lower Z material, so its photoelectric effect cross

section is significantly lower. Silicon in a grid formation called a Double-sided Silicon Strip Detector(DSSD), has a vertical row of strips on one side and a horizontal row on the other and can be used to detect heavy ions or alpha particles. This is another way of getting position sensitivity in a detecting system.

Electrons emitted as β radiation or neutron emmission may be detected with scintillation type detectors. In this case, radiation enters the detector and its energy is absorbed and re-emitted as light. At one end of the detector is a photo-multiplier tube which gathers the light and boosts the signal through a series of multiplication stages and sends out the information. Plastic scintillators are most common, but if fast timing is desired La(Br) detectors are the tool of choice. One main advantage of scintillating materials is their ability to be used at room temperature. In addition, especially plastic, their physical characteristics allow them to be manufactured into novel geometries.

After detection of one radiation, and recording its energy there is much left to be done. Some of the nuclei that have been studied by our research group have hundreds of gamma ray transitions. Many nuclei share similar radiation characteristics, so how can a particular radiation energy be associated with a specific nucleus? The key is to make a radioactive ion beam (RIB) and have a magnetic field steer that beam to a detecting station. The magnetic field's bending radius is proportional to the mass to charge ratio, B r$\propto$m/q. Therefore, in a magnet of fixed r, a beam of mass component A can be steered through the curvature by adjusting the magnetic field. These isobaric beams can then be further purified through other beam optics to give a singular nucleus. There are other ways to do particle identification and radiation simultaneously like the time-of-flight technique or through reactions where the reactants and residuals are known. In other cases, the knowledge from previous studies is used as a basis for the identification and the study progresses from that point.

In general, the coincidence technique is also required to make any study of the structure of nuclei. The desire is to be able to make a statement like the following: the energy of the first radiation measured was rad_1 *then* rad_2 *then* rad_3 were measured. This implies that timing

and multiple detectors are necessary. There are several ways to do this, but a few things are common. First realize that the detector signal is analog to the point we have described thus far. It is a voltage spike that occurs at a given time and needs to go through a preamplifier and an amplifier and then to a analog to digital converter (ADC). At the same time, it is necessary to know *when* that energy was recorded. This can be done via a TDC(time to digital converter) or an MCA(multi-channel analyzer). In principle all processing after the ADC could be done in the computer, though sometimes it is necessary to employ hardware filters. The important thing is that for accurate coincidences and to not lose efficiency through dead time a fast clock and fast digital readout system is best. With that recorded, a time window can be chosen for coincidences. Then, anything that happened within a time window as rad_1 is recorded as well as the time from the beginning of the first signal. It is also important to state that there are physical restrictions on the time window. Each detector takes a finite amount of time to send an electron from one place in the detector to another. It also takes a finite amount of time to read out a coincident event and store it to a file for analyses later. This analysis would consist of picking out a radiation's energy and setting a "gate" on that energy, then the analysis program would then show a histogram of energies of the coincident radiation.

These histograms are subject to the laws of statistical measurement so if 25 counts in rad_2 are detected then the standard deviation(σ) in that number is σ=$1/\sqrt{N} = 20\%$ error$\rightarrow$ 5. Then the true measure of 25 counts in a peak in a histogram is 25 ± 5 or 25(5). There may also be systematic errors or error estimates that also should be considered.

4.2 LeRIBSS at ORNL

Experiments at LeRIBSS [47] at ORNL have recently made very important contributions [2–7, 48, 49] to our understanding of nuclear structure in several key areas. Further advancements have been made in neutron-rich nuclei with a series of experiments, including nuclei approaching ^{132}Sn and the evolution of shell structure and levels in Cd as well as decay spectroscopy of well deformed rare-earth nuclei. There has also been a successful effort by our collaboration to measure single

particle states and lifetimes of nuclei around the r-process path near ^{78}Ni [2–7, 50].

A schematic of the experimental setup at Oak Ridge National Laboratory is shown in Fig. 4.1. A 10 to 18 μA current of ≈50 MeV protons is used to bombard an UCx target on a High-Voltage(HV) platform. As was mentioned in 2.1.2 this process creates many fragments in a distribution from 26≥Z≥68, the HV platform ensures that fragments begin to move through the beamline. From there, the different masses are separated to one part in 1000 by passing them through a magnetic field. The beam is again isobarically separated in a second magnet to ≈one part in 10000. At this stage there is a fast beam deflector (kicker) in place which prevents the desired beam from reaching the detecting station. This kicker is put into and pulled out of the beamline in a correlated way with the tape cycle, so that grow in and decay of activities can be measured. There is also a charge exchange cell for the elimination of some contaminants for some masses or to prepare to send negative ions to the tandem (not done at LeRIBSS). The setup is capable of accelerating negative and positive ions (this has been done up to the ++ charge state), which allows for isobaric separation far exceeding that of previous studies. The detecting station is placed after the isobar separator which eliminates the need for post-acceleration in the tandem (which has a factor of ten loss of intensity). This has the effect of lowering the kinetic energy of the nuclei, but for these decay studies this is not an issue. The result of this new setup has dramatically improved our rates and opened up our capabilities to be able to study nuclides that typically have low fission yield, long hold-up times in the target or poor separation. A previous setup at the facility [2, 6, 7, 51], detailed here for comparison, utilized much of the same technique, except in this setup the charge exchange cell is used to create negative ions. These ions are then sent to the 25 MeV tandem accelerator and at the point of terminal voltage are stripped to return them to a positive charge state. The singly charged positive state is selected to be sent to the experimental station. Then, a CF_4 filled gas cell ionization chamber is used to identify the isobars and to enhance low Z ions versus high Z components which are typically larger in the beam. This ranging out (RO) technique has the ability to give great selectivity of ions, but suffers losses from stripping efficiency and in target hold up times.

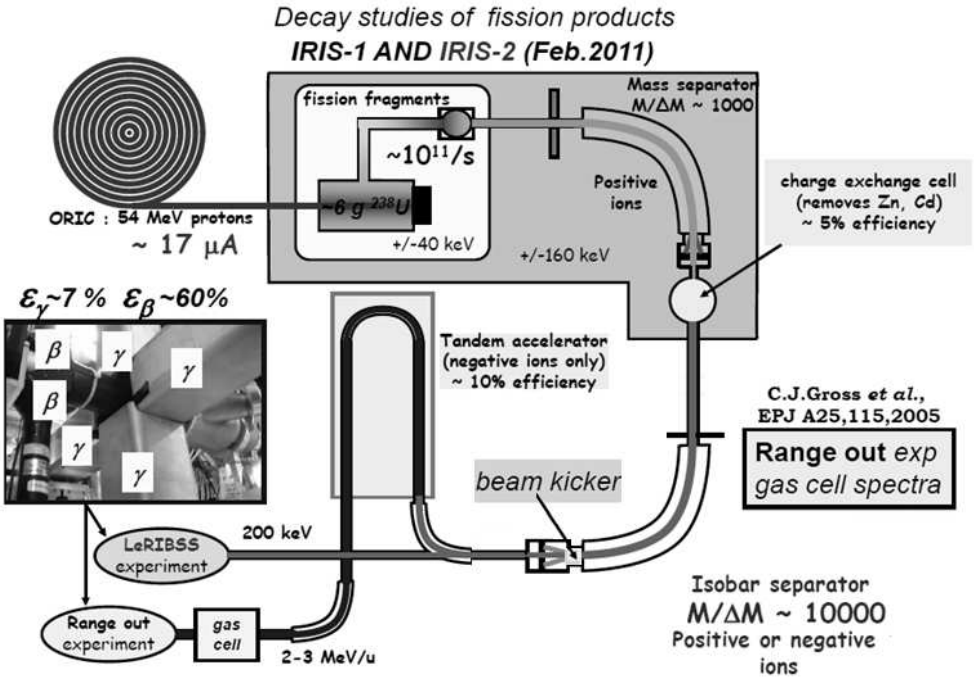

Figure 4.1: A schematic of ORNL facilities: LeRIBSS and the previous ranging out experiment.

The detector array used with LeRIBSS consists of 4 HPGe detectors in a close configuration around 2 plastic scintillators for beta ray detection. The beam is deposited on a tape, which is then moved behind shielding to avoid contamination of longer lived daughters and other contaminants. The scintillators are placed in a co-axial arrangement around the tape position to give excellent solid angle coverage. Using digital electronics [52], the signals were read out and analyzed. The detectors have a 30% peak efficiency at 100 keV and 4% efficiency at 1.33 MeV. This detector array is versatile and can accommodate Compton shields and a conversion electron detector, though these were not used in the experiments presented here.

The main coincident histograms used are then $\gamma-\gamma$, $\beta-\gamma-\gamma,\gamma$- tape cycle time, $\beta-\gamma$- tape cycle time and related projections(the ungated sums of all detected energies). It is important to emphasize that a β coincidence in the plastic gives only a starting signal. The detecting volume of these detectors is too small to give the beta energy spectrum. For online use, the spectra are compressed by a factor of 10 for online use and a 10ns pulse is used for the clock.

Shown in Fig. 4.2 is the difference in ion rates for studying a beam of neutron rich Ga at LeRIBSS compared to the RO method. The top spectrum shows results for the RO method [6] and

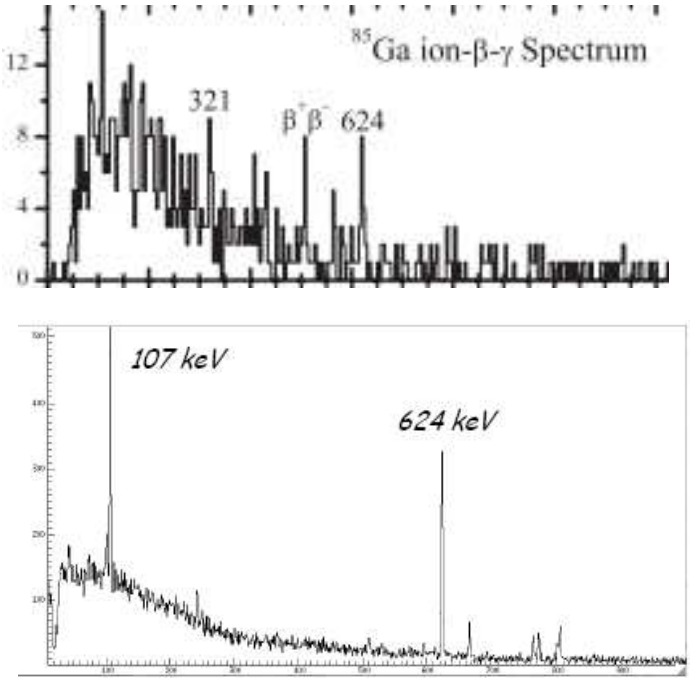

Figure 4.2: Online spectra of ^{85}Ga+ from LeRIBSS (bottom), show better rates over the previous study (top). Note: the 107 keV is present in top spectrum but is unmarked. [3, 6]

the bottom spectrum shows new results [3] from LeRIBSS. It should be noted, although it is not marked, the 107 keV line can be seen in the RO study but is now clearly observed. By accelerating positive ions, beam intensity is not reduced in the charge exchange cell, nor is beam lost in the stripping process and transmission through the tandem. The previous RO rate [6] of ^{85}Ga was $\approx$1 ion/ 10 s, now at LeRIBSS we have observed a rate increase to 50 ions/s, which represents two orders of magnitude of enhancement.

Results from the UNISOR isotope separator[48, 53] at ORNL are shown in Fig. 4.3, comparing the experiment where there was no isobaric separation of ions, and only separation of mass to about 1/2000. The spectrum on the bottom is from UNISOR and LeRIBSS is on the top. This is an excellent example of improvements made in beam purity via isobaric separation and the use of the charge exchange cell. For example, the study of Ag decays is dramatically improved and indicated the plausibility to study the decays of 128 or even 130 (N=82) Ag. Significant suppression of cadmium and indium beam components has been accomplished. The strongest decay from ^{124}Ag ($2_1^+ \rightarrow 0_g s^+$ in ^{124}Cd at 612.8 keV) decay was seen at UNISOR only as a doublet with a

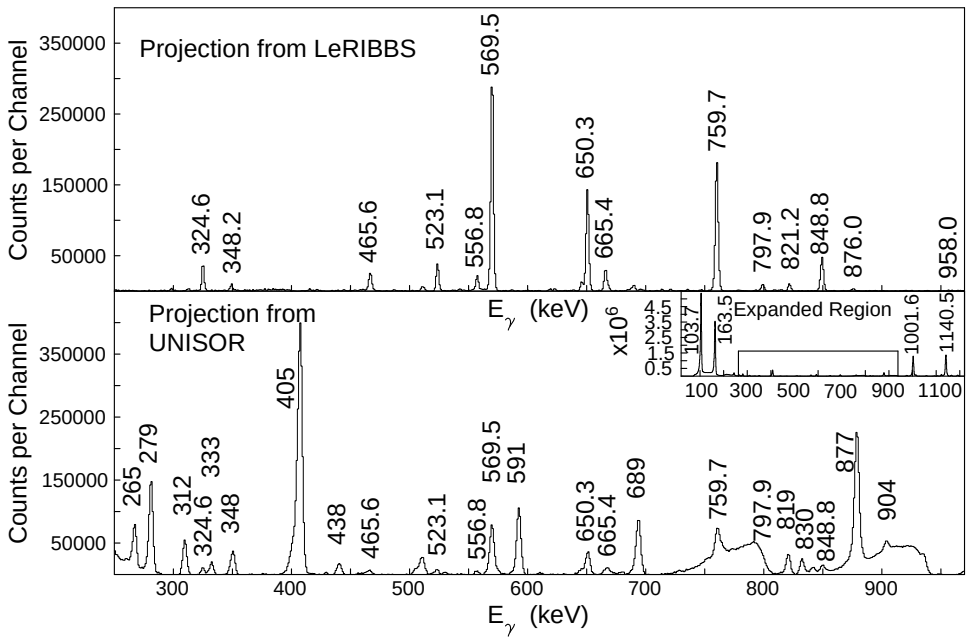

Figure 4.3: Spectra comparing UNISOR (bottom) and LeRIBSS (top) experimental results from ^{122}Ag decay

^{124}In decay peak ($3_1^+ \rightarrow 4_2^+$ at 614.7 keV). Shown in Fig. 4.3, in the ^{122}Ag decay study, the most intense line seen was from indium decay into tin (2_1^+ -> $0_g s^+$ at 1140.5 keV) and dominates the projection spectrum from the run at UNISOR. This line is suppressed to 3% of the 2_1^+ -> 0gs$^+$ transition at 569.4 keV in ^{122}Cd. The peaks associated with ^{122}Cd are essentially pure in the top spectrum. Experiments were performed on ^{122}Cd from both setups and both were used for these studies to ensure that transitions and levels reported are surely in the isotope of interest and not from contamination. That is, a contaminant peak is assumed to be a larger beam component in the UNISOR data and is more easily identified to be contamination from that experiment. The UNISOR run also had BESCA (a conversion electron detector) in place, in an attempt to identify conversion electrons from the high spin isomers present in Ag. No successful measurement could be obtained from the ^{122}Ag decay.

In summary, LeRIBSS witnessed beam rates and purities far exceeding expectations and have allowed for much progress along the leading edge of knowledge of neutron-rich nuclei.

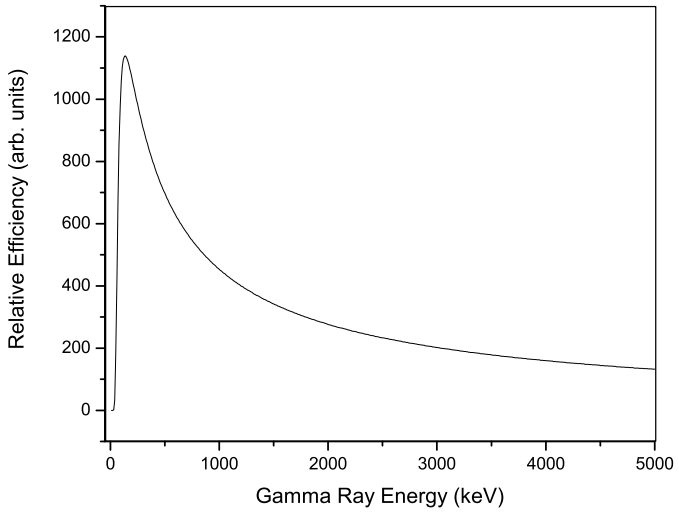

Figure 4.4: Curve of the Relative Efficiency of Gammasphere

4.3 Measuring Gamma-rays from ^{252}Cf Fission Fragments

In order to study a variety of nuclei, we have also measured the prompt gamma rays from the spontaneous fission fragments of ^{252}Cf. For details of the experiment consider reference [54]. This experiment was performed using Gammasphere with 101 Compton suppressed gamma ray detectors and a 62 μCi source. This gives us access to high statistics and access to high spin states. In addition, Gammasphere also has excellent angular coverage ($\approx$47%) and is well suited to angular correlation measurements [55]. Shown in Fig. 4.4 is the fit of the relative efficiency of this detecting array.

The efficiency of this array is 9.9% with a peak to total ratio of 0.6% for 1.33 MeV. The relative efficiency for the experiment done in 2000 is fitted to an exponential of the form in equation 4.1.

$$Eff = exp[(A+Bx+Cx^2)^{-H} + (D+Fy+Gy^2)^{-H}]^{-1/H} \tag{4.1}$$

Here E is energy in keV, x = Ln(E/100) and represents the low energy part and y = Ln(E/1000) represents the high energy part, and the parameter H is the coupling factor between them and is

Efficiency Parameters	Value	Energy Calibration Parameters	Value
A	14.1597	a	-6.2734*10^{-1}
B	9.18559	b	3.337*10^{-1}
C	-2.7907	c	-9.0093*10^{-8}
D	6.36297	d	4.7999*10^{-12}
F	-0.65056		
G	0.0		
H	2.09765		

Table 4.1: Parameters of the efficiency and energy calibration of Gammasphere

typically near two. The values (which are very sensitive to the choice of H) are shown in table 4.1. The energy calibration is fitted to a third order polynomial as:

$$E = a + b\,N + c\,N^2 + d\,N^3 \tag{4.2}$$

where N is the ADC channel number on the recorded tape. The values for this fit in table 4.1 are essentially a 0 keV offset and one third of a keV per channel.

The ^{252}Cf was placed as a source inside the detecting array housed in a polyethylene ball to partially moderate fission neutrons and to act as a beta ray absorber. Anti-Compton veto detectors made of BGO were placed coaxially around the germanium crystals and at the front to prevent the re-absorption of backscatter gamma rays and to veto events coming from inside the detector and scattering back out the front. BGO was also used as a back stop to ensure that most of the events detected would be those of the full energy peak.

Because it was placed as a fixed source and no additional detectors were used (like a time-of-flight detector), mass number cannot not be directly determined. Our identification of various nuclei relies mostly on previous research for the identification of isotopes and transistions that are also in the data set. From that point relative yields may be determined and compared to nuclei neighboring in Z. The basic argument is that protons are not lost in the fission process and trends for the average number of neutrons emitted in the fission process do not vary greatly systematically. Therefore, comparing the relative yields of known fission partners to the yields seen in gates in known and an unknown nuclei reveals the element (Z) and the mass (A) of the isotope of interest.

Beneficially, the most well known nuclei are nearer to stability, and since relatively few neutrons are emitted in fission, a gate on a known isotope reveals very neutron rich isotopes.

4.3.1 Methodology

In order to analyze these data, containing more than 150 nuclei and nearly 3000 gamma rays it is necessary to use the coincidence method for identifying individual isotopes. In our case we now have coincident events in cubes of up to four dimensions. A cube is a matrix of values that is symmetrically built in all axes. For example, a cascade of four gamma rays is included in the cube such that a gate on any three gamma rays shows the fourth and higher fold coincidences. But, a double gate on the 4d cube will double count the third gamma ray in the cascade.

By building a higher fold coincident cube, significant statistics may be lost. In general, the gamma rays from prompt fission are rather low multiplicity. That is, in most cases less than 5 or 6 events happen simultaneously. The 3 dimensional cube has an estimated $5.7*10^{11}$ triple and higher events, while the 4 dimensional cube has about a factor of 3 fewer events. This means that any given triple gate in the 4d cube may have a factor of ten fewer events than a double gate in the 3d cube. The raw data have a size on disk of 664GB, the 4d cube takes up 15GB of space and the 3d cube uses only 1.3 GB.

However, in many cases, even with lower counts, many weak peaks that would otherwise be disguised in the background counts can be made visible with the use of additional coincidences. Because of the high line density (about 3 lines/keV between 100 and 300 keV) many gates are very complicated and show a great deal of contaminant peaks. Random background from each of these contaminant peaks also adds to the already present random background from the peaks belonging to the isotope of interest. Adding an additional gate removes contaminant and associated background in out spectra. Examples of these spectra will be shown in chapter 7.

All of this was done using the intrinsic programs in the current version of Radware [56–58]. Much of the work on the 4d hypercube was done by E.H. Wang by properly defining the events in the scanning program and making some decisions to ensure that the files did not get to large.

As was mentioned previously, electron conversion may compete with gamma emission. With the coincidences in Gammasphere, it is possible to measure these internal conversion coefficients. In the tables presented in chapters 6 and 7 for the intensities of transitions found from ^{252}Cf SF the intensities decrease dramatically with increasing spin. In the yrast band, the efficiency corrected intensity may be less by a factor of $\approx$2 for each higher gamma ray. This is mostly affected by the probability of producing a nucleus at high spin. However, if a gate is set from one gamma ray that decays through two others and a gate is set on a fourth at the end of this cascade, and this is the only decay path, then the relative intensity between these two transitions should be 100%. Alternatively, one may state that the branching ratios for the intermediate gamma rays is 100%. My measurements of these decays where electron conversion should not compete (E> 4-500 keV) limit the deviations from 100% to less than 5% which is consistent with the statistical errors in these measurements. Therfore, missing intensities and conversion electron coefficients can be measured. These coefficients can then be related to the electro-magnetic multipole of the transition of interest. We assume in this gating scheme that the ratio of two gamma rays in a cascade with a gate on the top and on the bottom is 100% and choose the gate such that one of the transitions is not appreciably converted. Then the conversion coefficient α is:

$$\alpha = \frac{I_\gamma(unconverted)}{I_{gamma}(converted)} - 1 \tag{4.3}$$

Where I_γ is the measured counts divided by the efficiency. The measured coefficients are then compared to the theoretical coefficients from the BRICC online computer program [59] to determine the multipolarity of the gamma ray.

4.3.2 Angular Correlation

Angular correlations between successive quanta are a small ($\approx$ 10%) effect in nuclei, but given sufficient statistics it is effective for determining the spins and parities of nuclear states. More details of this technique can be found in [55]. The software developed by Andrey Daniel, Chris Goodin and Ke Li is based in root [60], the graphical analysis tool developed by CERN. This

is a way to build on knowledge of previously done experiments and assign the quantum mechanical values of spin and parity to states in nuclei via the characterization of transitions in nuclei. It takes advantage of the fact that we can arrange the data from 110 detectors into 64 separate angular bins and draw conclusions based on the intensity of the gamma ray measured as a function of the angle between detector pairs.

The angular correlation function was first developed by D.R. Hamilton in 1940. It describes the angular correlation between "two successive quanta". We use a form of the function that has been tabled [61, 62] and implemented in computers as, $W(\theta) = 1 + A_2\ P_2(Cos(\theta)) + A_4\ P_4(Cos(\theta))$. This comes from the explicit evaluation of the probabilities of decays from an initial state to a final state via a definite intermediate state. It physically originates in the small coupling between radiation and matter. The initial evaluation included simplifying assumptions, including an oscillator basis giving rise to outgoing plane waves, a small nuclear velocity compared to that of the propagating radiation, and a choice of initial quantization axis as the direction of the initial emission (with the consequence that m, the magnetic projection quantum number, only changes by ± 1 unit of $\hbar$). This is then expanded in terms of multipoles to evaluate dipole (D) and quadrupole (Q) content. It gives a way to measure the spin of a state if the two others are known. That is, it would not discriminate between a 8(Q)$\rightarrow$6(Q)$\rightarrow$4 and a 4(Q)$\rightarrow$2(Q)$\rightarrow$0 transition. Later formulations of the angular correlation function included considerations of longer lived states that might precess around a nuclear magnetic moment, along with (2,3) (Quadrupole, Octupole) mixing, considerations of high spin states, as well as first-third and higher correlations. To reiterate, if the mixing ratio (δ) is large this indicates that the higher multipole dominates in the transition. Because only the changes in angular momentum between states are taken into consideration, this would not reveal direct measurement of electric or magnetic character. Though, as discussed previously, inference based on the transitions likely to occur (gamma ray selection rules) in an experiment can give guidance.

Since only E1, M1, and E2 type transitions are typically observed, and mixing between E2/M1 are the only likely ones possible out of this set, if an angular correlation gives a mea-

surement without mixing and is consistent with spin state that is greater by one unit of angular momentum, it is most consistent with an E1 transition. Then an angular correlation measurement allows for the assignment of the spin and the mixing ratio may indicate the parity of the state. We always need as a given a pure transition between two states of known spin; this is typically chosen as an E2 transition (and likely yrast), because M3 mixing is very unlikely and E2's are assumed (and can be experimentally confirmed) to be pure E2's. The A_2/A_4 for a I+2$\rightarrow$I$\rightarrow$I-2 pure E2 cascade is 0.102/0.009 and I$\pm$1$\rightarrow$I$\rightarrow$I-2 is -0.071/0.000.

Some examples from a variety of different curves are shown in Chap. 7. In some cases, many additional gates on these transitions are summed and in that case, each additional gate is checked to ensure that contamination from other similar transitions is minimized.

CHAPTER 5

NEW LEVELS IN ^{122}CD AND THE STRUCTURE OF CD NUCLEI

In the recent LeRIBSS campaign the beta-decays of even-A Ag have been examined, and in the case of the decay of ^{122}Ag, for at least the third time. to understand the extent to which the U(5) symmetry (vibrator) IBM explanation of Cd isotopes is valid. Nature is kind to us, giving various medium spin beta-decaying isomers in these parents so that different spin levels in their daughters can be studied. When these nuclei were first studied, the prevailing paradigm was that cadmium isotopes were ideal vibrators, i.e. a multi-phonon, IBM (Interacting Boson Model) seemed to describe the levels and their decay properties. However, it has been shown [35, 48, 49] that a close analysis of what one would expect for such nuclei reveals many inconsistencies with this simple picture. In addition to quadrupole vibrations, there are levels that have been described as 2p-4h intruder states and mixed octupole-quadrupole levels that give rise to anharmonicities in the vibration. These anharmonicities may affect the transition strengths and phonon selection rules in the decay. In our present study, these intruder states are higher in energy and become a simpler testing ground for the systematic description of these levels.

Fortunately, in mass 122 there have been many studies done on both the Ag[63, 64] parent and Cd[65–68] daughter nuclei in this region. Unfortunately, the data are not completely consistent with the new observations made in ^{122}Cd. There is clear evidence of isomerism in ^{122}Ag from the mass excess measurements reported in Ref.[69] that are consistent with predictions from the atomic mass evaluation for an isomer to have an excitation of 80(50)keV. According to Ref.[64] there is a low spin isomer ($T_{1/2}$=550(50)ms) and a high spin isomer ($T_{1/2}$=200(50)ms). The high spin isomer “can be associated with” a 9^- spin and parity and the low spin isomer “could arise from” a configuration resulting in 1^-. The softness of this language suggests that there is not a

certainty to these spin and parity assignments. The authors also state that the intent of this study was to demonstrate the selectivity of the laser ionization of short-lived nuclei. The half-life had been measured in [63] to be 520(14) ms, but it is unclear in this two page report if this is the ground state or a combined half life. The half-life reported in Ref.[67] is 480(80)ms, which is consistent in their report with a 3^+ assignment via logft assignment. An earlier work[70] suggests an even higher half-life of 1.5(5) s which was thought by Ref.[66] to be an isomer in this isotope. The combined half life reported in Ref.[71] of 357(24) ms is also seen. The summary of what is known from these studies is the existence of three isomers: a 3^+ ground state (0.529(13) s), a 1^- excited state (0.55(5)), and a 9^- 80(50) keV state (0.20(5) s).

One difficulty with these kinds of studies is called the "pandemonium effect". The pandemonium effect is what occurs because there is not sufficient efficiency at high energy. For example, a peak in the current calibration (which is extrapolated and very uncertain as well) with 1 or 2 counts near 4 MeV may have 5-10% of the intensity in the $2^+ \rightarrow 0^+$ transition. The Q-value has been estimated to be 9.5(2) MeV from the systematics of atomic masses[72]. With such a high Q-value and a level scheme that only goes as high as 3.7 MeV there is certainly still a great deal of missing intensity. Since values of logft and spin and parity arguments are dependent on highly accurate intensity and beta feeding measurements, the pandemonium effect ensures that a woefully incomplete picture is presented in the present work. That said, even in the present work, there are some inconsistencies.

5.1 Level Scheme of ^{122}Cd

Shown in Fig. 5.1 are the levels and transitions found in this work with all save one spin and parity listed coming from the studies mentioned previously. The line width is proportional to intensity up to 2% and written in italics above the energy. The parent states listed are the most consistent view that is possible considering the experimental data and the previous research but should not be considered certain. This effort is helped considerably by the work of Ref.[65] from the ^{252}Cf SF data which shows the levels in the ground state band up to (14^+). There is an

indication in this study as well as in Ref.[68] that there is no feeding to the 4^+ state at 1329.2 keV which was the main evidence in Ref.[67] for the assertion of a 3^+ isomer in the parent. However, *if* there is a 3^+ state, since the 1909.3 keV level is a very likely spin 3 state with only a 792.0 keV transition decaying into it, the isomer is reported here to have a half-life measured from the feeding into that state of 0.32(5)s. The proposed 9^- isomer would decay into the level assigned as an (8^+) and the associated half-life measured in the activity 645.6 keV gamma ray is 0.39(5) s. However, a 9^- isomer should feed the known (10^+) state at 3057.3 equally as well as the (8^+) level at 2823.6 keV because the energy of these states is not very different. No 233.6 keV transition is seen. The previous studies and the current measurement are consistent when considering a 1^- isomer with a longer half-life. The measurement of 0.69(13) s comes from the activity curve of the 1135.5 keV transition depopulating the level at 1705.2 keV. A gate on this transition shown in Fig. 5.2 shows no measureable feeding from higher energy states. The level of the background in this gate limits gamma rays feeding to <1% of the 569.5 keV transition for gamma rays <1 MeV.

There are a number of gamma rays that are degenerate in energy. Shown in Fig. 5.3 are three spectra, in the middle spectra are the coincidences with a 650.3 keV gamma ray and the bottom shows a gate on 523.1 keV. In the 650.3 gate several decay chains can be seen: 348.0 $\rightarrow$ 113.9 $\rightarrow$ 523.1, 348.2 $\rightarrow$ 465.6 which sums to 813.8 which is also seen in the spectrum. The 523.1 keV gate shows only the 348.0 keV transition which is evidenced here in the relative intensity between the 113.9 and 348.0 keV transitions. The reason the 113.9 keV(3.8%) gamma is placed lower than the 348.0 keV(0.7%) transition in the level scheme, in contrast to the placement of the 349.1 keV gamma ray in Ref.[65], is because of the difference in intensity. The gate on 848.8 keV in the top spectrum, shows the difference between the 466.8 keV shown here and the 465.6 keV transition seen in gate on the 650.3 gamma ray. These transitions had previously been placed and this study agrees with that placement. This gate also reveals a troublesome feature at 1084.3 keV, which is the detection of two separate events as one event with the sum of the energies of the two real transitions. The probability of a “sum peak” occuring is quite low but such peaks could interfere with low intensity transitions, of the same energy. This feature can be revealed via coincidence

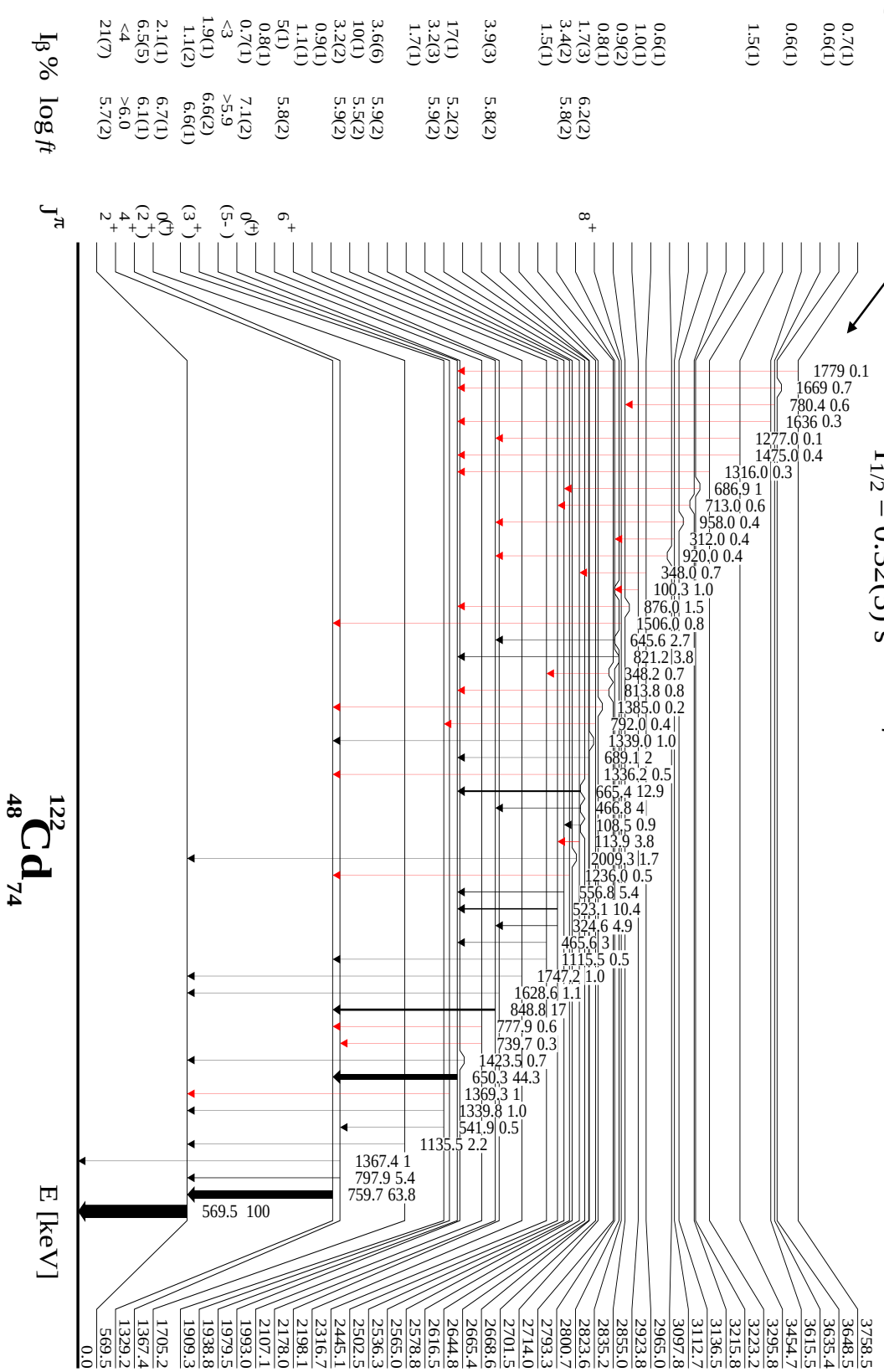

Figure 5.1: New level scheme of ^{122}Cd. New transitions compared to [66] are shown in red.

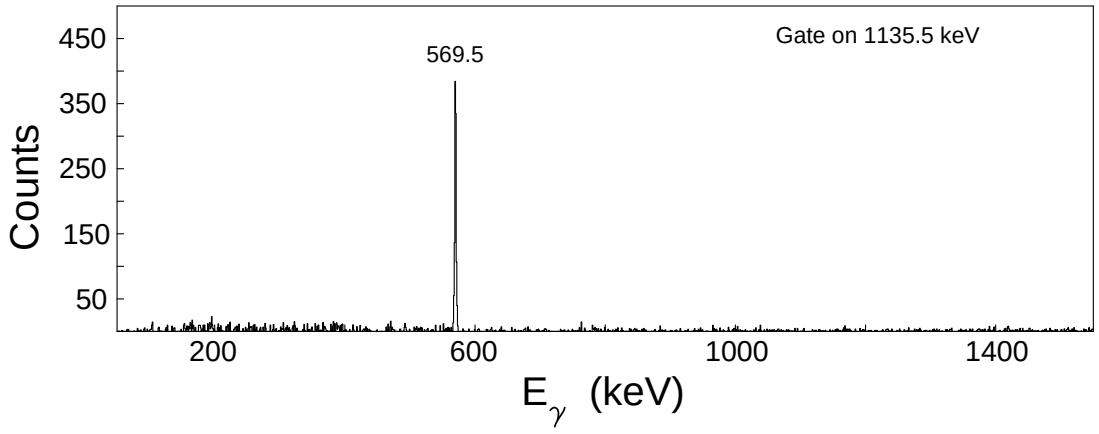

Figure 5.2: Spectrum showing the absent or week gamma feeding into the level at 1705.2 keV in the gate on 1135.5 keV.

relationships or by adjusting the coincidence timing in the analysis software. A gate on the 1085 keV peak shows 848.8 and 569.5 keV transitions but not the 759.7 keV line, which does not make sense if the 1085 keV peak were a real transition. Other examples are seen as sums of 466+760 = 1226 keV and 560+760 = 1320 keV and these can also be seen in the spectrum.

5.2 Analysis of Near Spherical Nuclei

Shown in Fig. 5.4 are the systematics of levels in $^{110-122}$Cd. The top four are all very nearly stable in the ground state and ^{114}Cd is the midshell nucleus with the first excited 0^+ state at 1134.5 keV. This state is associated with the intruder levels[73] and the lowering at midshell of these kinds of states are seen in other mass regions as well. As nuclei farther from stability and farther from midshell are examined, the expected behavior of these states is for them to move higher in energy, as they do. It was unexpected that the vibrational levels that one would expect to see are not seen. Even with the very strong statistics of a recent study[49], at the 3-phonon level, no 0^+ state is seen in ^{120}Cd and in this present work there is no clear candidate for the 0^+ or 2^+ members in ^{122}Cd. This is a negative argument and it cannot be said that these states are absent only unobserved. This is only the beginning of the inconsistency with this model.

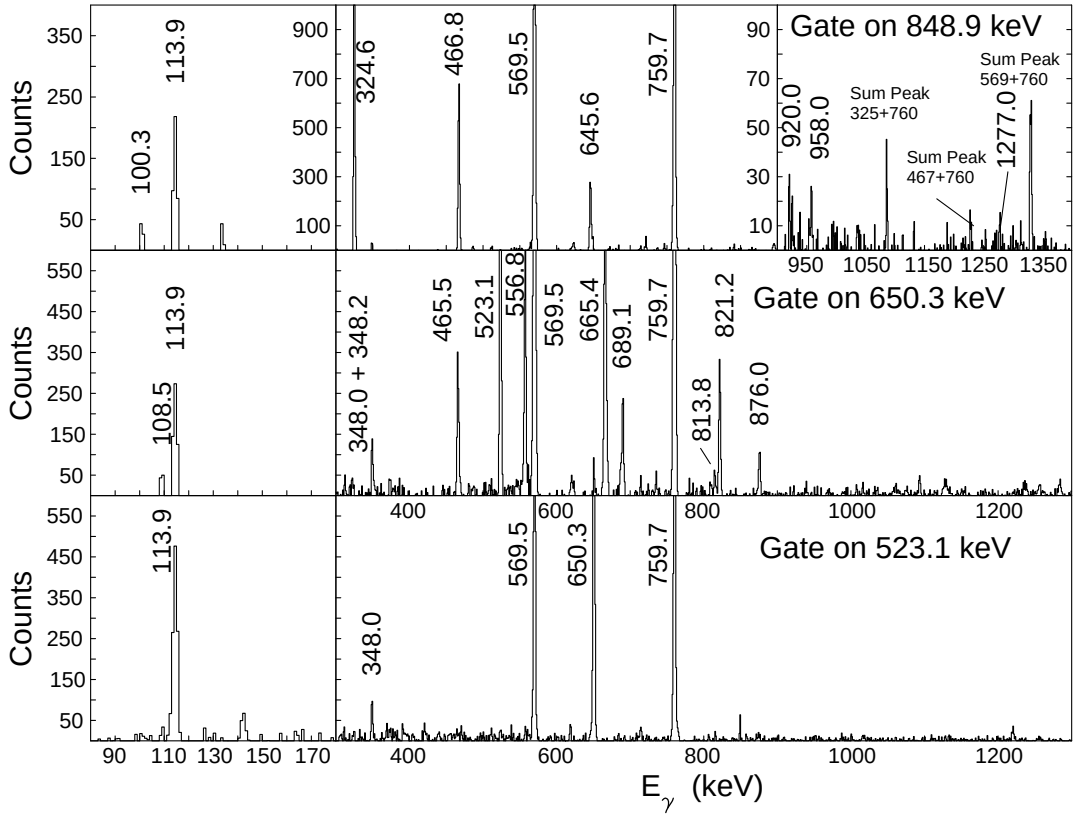

Figure 5.3: Spectra showing gates on 523.1(bottom), 650.3 keV(middle), and 848.8(top) keV. These gates reveal doublet structures. The doublet at 348 keV can be seen in the comparison to the 113.9 keV. The doublet at 466 keV is also revealed along with many of the new transitions compared to [66] marked with an *.

Shown in Fig. 5.5 are the low energy (2.5<MeV) levels that would be in the correct energy range to be candidates for three phonon levels or could have an interpretation as members of an independent band structure. As was shown in Fig. 3.4, the expectation for phonon levels is that they should decay to the N-1 levels and decays to the N-2 levels would be forbidden. On this basis the proposed 2-phonon $(2)^+$ state at 1367.4 keV would be questionable because 15% of the intensity from this level goes to the ground state. In addition, only the (6^+) level at 2178.0 keV and the 2107.1 keV (4^+) level decay to only the proposed N-1 states. In the harmonic model, the decays from the 3-phonon 4^+ level should favor decays slightly (11/7 vs. 10/7) to the 2^+ 2-phonon level. What is seen experimentally is a intensity ratio of 2 to 1 favoring decay into the 4^+ level at 1329.2 keV. Even though this is intensity and not B(E2) the energy is nearly the same and so this

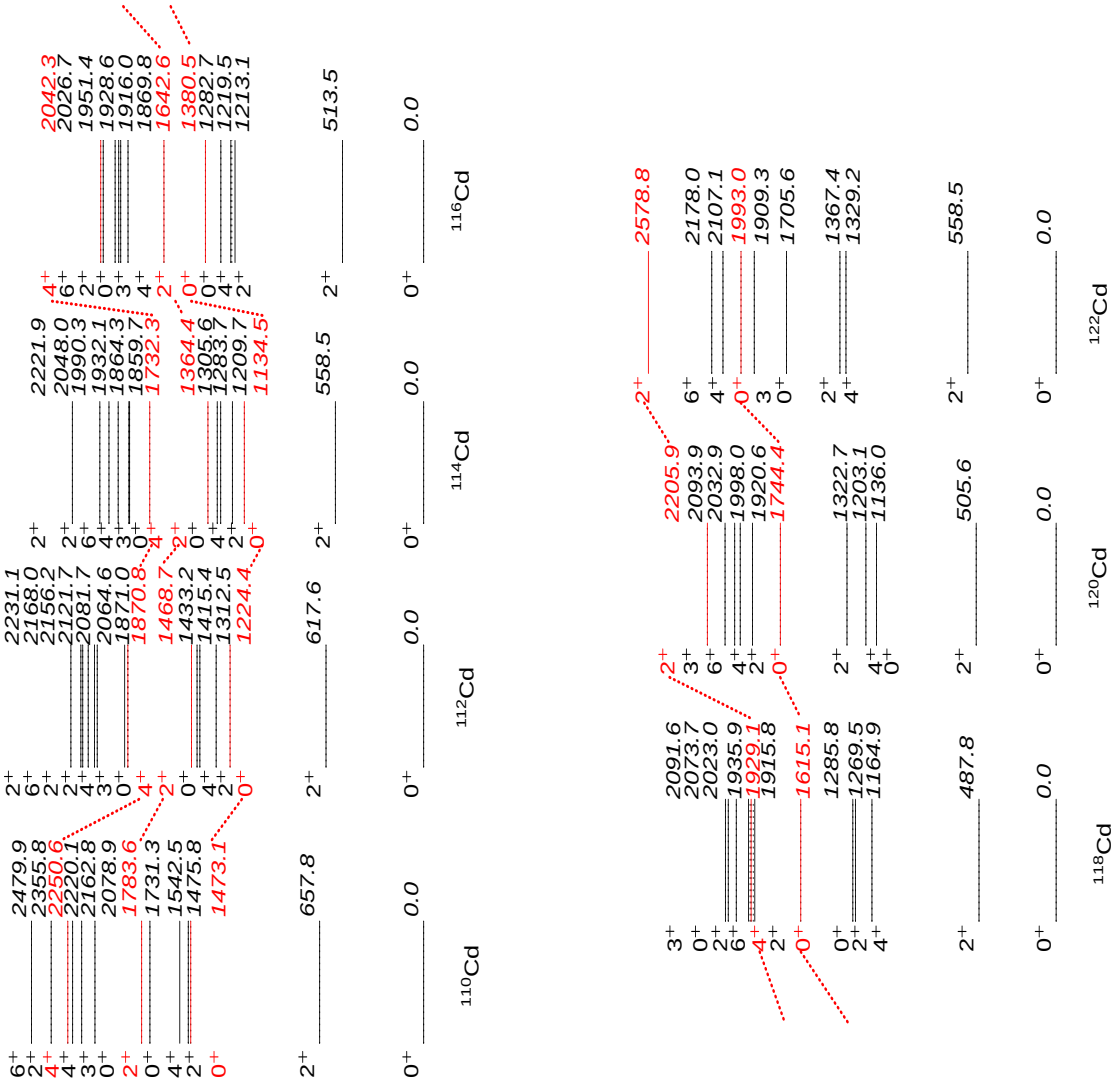

Figure 5.4: Systematics of even-even nuclei from near stability to approaching the N=82 Shell closure.

proportion should also favor decay into the 4^+ when considering the B(E2) values.

Therefore, because of qualitative and quantitative inconsistencies with the data, it seems more reasonable to group certain states in terms of an independent band structure. This is shown in Fig. 5.5 with two side band structures. The first is a negative parity band which has been seen in Refs.[65, 68] and nanosecond lifetimes measured for the (7^-) and (8^-). This band has been associated with either a quadrupole-octupole coupled(QOC) band or a high-j/low-j quasiparticles band in these isotopes[65]. It has also been proposed, based on systematics, the 1909.3 level has been thought to be a 3^- level also associated with the negative parity band or a 4^+ level. Based on how these levels decay it is sensible to group them into a band structure that begins to look very much like a gamma vibrational band.

Further calculations were done in the TRS (Total Routhian Surface) framework[65, 74] in the $\beta - \gamma$ plane to look for any evidence of triaxiality in these nuclei. The plots for even-A $^{118-122}$Cd are shown in 5.6 the surfaces are calculated with a constraint on rotational frequency (ω=0.0-0.2). The top plots are for ^{118}Cd and show a secondary minimum which may indicate shape co-existance in these nuclei. The defomartion characteristics of this secondary minimum decreases in β_2 from 118 to 122 cadmium and increases in the triaxiality parameter gamma from nearly 0 to nearly 30° (the triaxial maximum). It also appears to become the primary minimum in ^{122}Cd where there also is little change in the mean value of β_2 or γ parameters with increasing rotational frequency. The tentative positive parity band structure reported in this work may provide helpful evidence for a microscopic description of that sort.

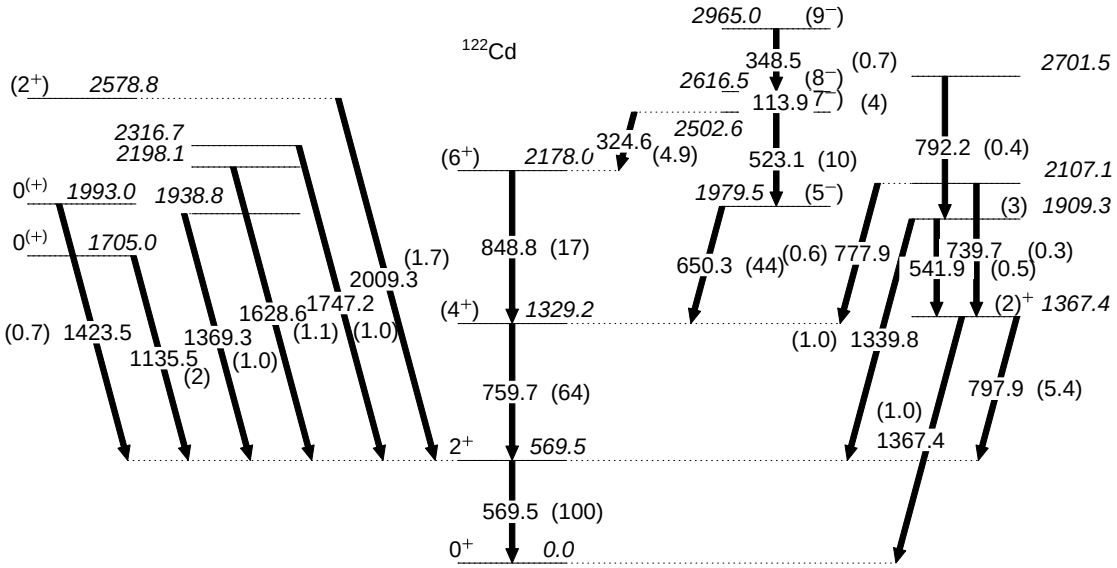

Figure 5.5: Proposed band structures in ^{122}Cd and states that are in the correct energy range to be potential three phonon candidates.

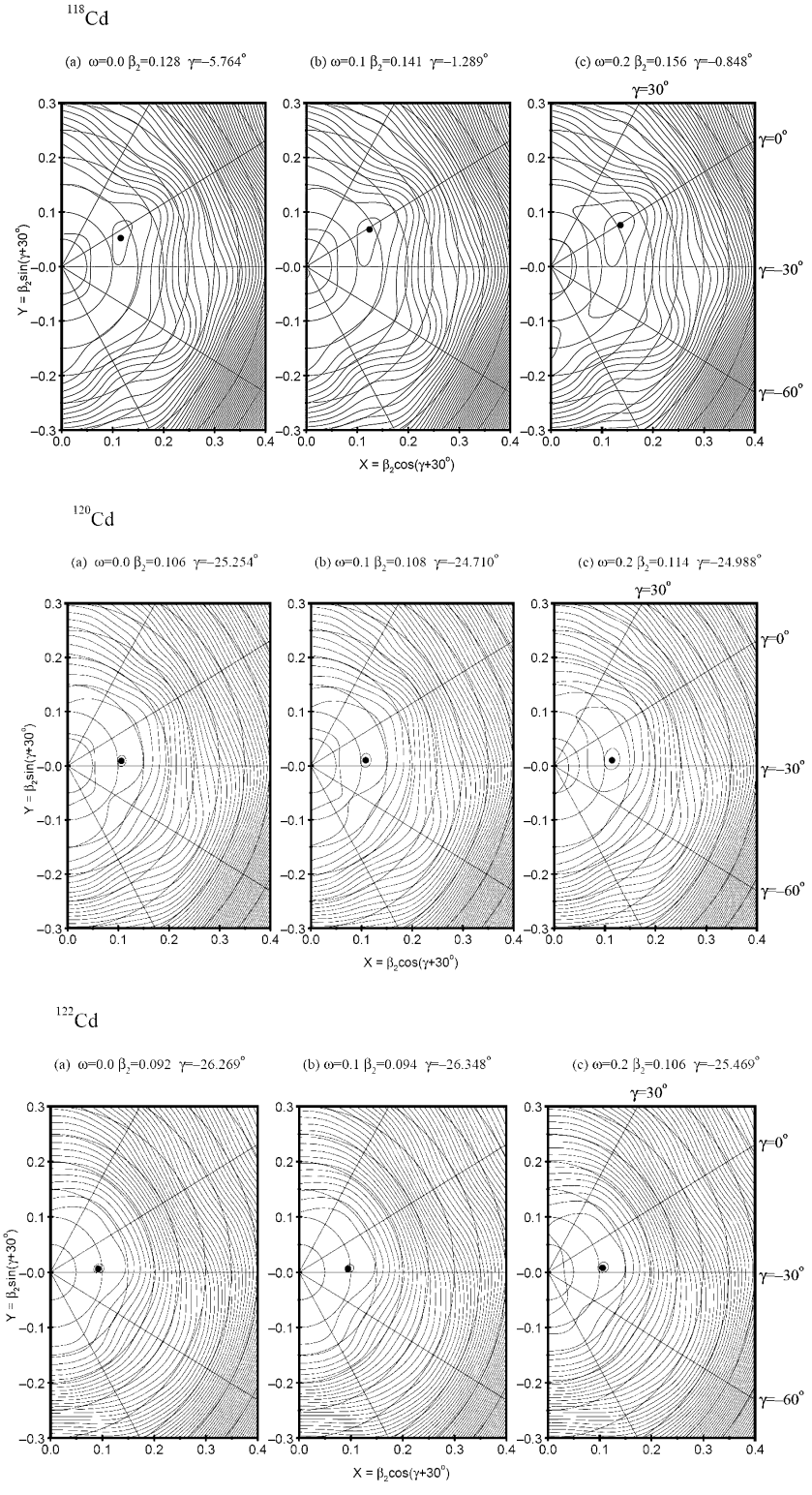

Figure 5.6: TRS calculations for even-even Cd nuclei A=118-122.

CHAPTER 6

STRUCTURE OF $^{162-165}$GD

This section describes the structure of nuclei near midpoints between spherical shells (the exact midpoint being $^{166}_{66}$Dy) in the rare-earth region, which are known to be well deformed and form good rotors. This means that for these isotopes the variation in first order I*(I+1) spacing is at the 5-10% level at high spin. New levels and vibrational excitations in ^{162}Gd and ^{164}Gd are reported. For ^{163}Gd, where only 5 gamma rays had been published before, a level scheme has been established for the first time. Also the first gamma rays from ^{165}Gd will be reported. This chapter is unique because it represents work done from both experimental setups. The work was performed in collaboration with a local high school student, B. Doll from Nashville Big Picture High School. It required, especially in the case of ^{163}Gd and ^{165}Gd a very careful analysis utilizing many different measurement techniques. These experiments were analyzed at the same time and were highly complementary to one another. The discussion will first detail structures in mass 162 and then 164 from both studies and show spectra and analysis from both. Then the odd mass, which are only seen from the beta decay study will be discussed.

First shown in Fig. 6.1 is a very impressive work [75] showing the large number of collective structures that are available to a strongly deformed nucleus and their extensions to high and medium spin values. This is then the motivation for studying these nuclei. It is important in the light of the phenomenon of shifted identical yrast bands [76–80] to see how the systematics of non-yrast states compare. The first non-yrast band is shown is the gamma vibrational band followed by two octupole bands one with K=2 and another with K=0. The octupole vibrational levels are followed by a beta-vibrational band which is followed by a rotational band built on a quasiparticle excitation and a K=4 vibrational band that has been hypothesized to be a hexadecupole vibrational

band. This is followed by five other band structures.

Knowledge of these isotopes has been limited especially at high spin for the rare earth region because it is at the edge of the production for fission. Studies had been done in Gd 160 and 162 from two neutron transfer on ^{158,160}Gd by bombarding them with tritons (^{3}H), this reaction process is called a (t,p) reaction [81]. This method only revealed levels and not gammas depopulating them. This method revealed angular correlations between the fragments and were able to assign spins and parities as well. However, because of the age of the study, the level energy errors were estimated by the authors to be about 7 keV. Some levels found previously in this study (only shown are the levels seen in both their study and ours) and from spontaneous fission [80] are shown in Fig. 6.2. This study had begun to reveal important properties of the gamma vibrational band and added to knowledge of the systematics of excited 0^{+} states [82].

Also known in Eu were the half lives of very neutron rich isotopes [83, 84] which guided our study and were able to be re-measured in some cases. Because the half-life had been previously measured, the LeRIBSS tape cycle could be set to match that half-life appropriately. The thought process used was to allow for the accumulation of data for as many half-lives as possible but to move the activity behind shielding before the daughter isotopes half-life began to interfere. Table 6.1 summarizes the half-lives known and tape cycles used.

Table 6.1: Table of known half lives and tape cycles used at LeRIBSS

Isotope Mass Number	Known Eu Half-life	Known Gd Half-Life	Tape Cycle On/Off
162	10.6(10) s[84]	8.4(2) min[85]	22 s/22 s
163	7.7(4) s[83]	68(3) s[85]	30 s/55 s
164	4.2(2) s[83]	45(3) s[86]	22 s/22 s
165	1.7(3) s[83]	10.3(16) s[87]	10 s/7.5 s

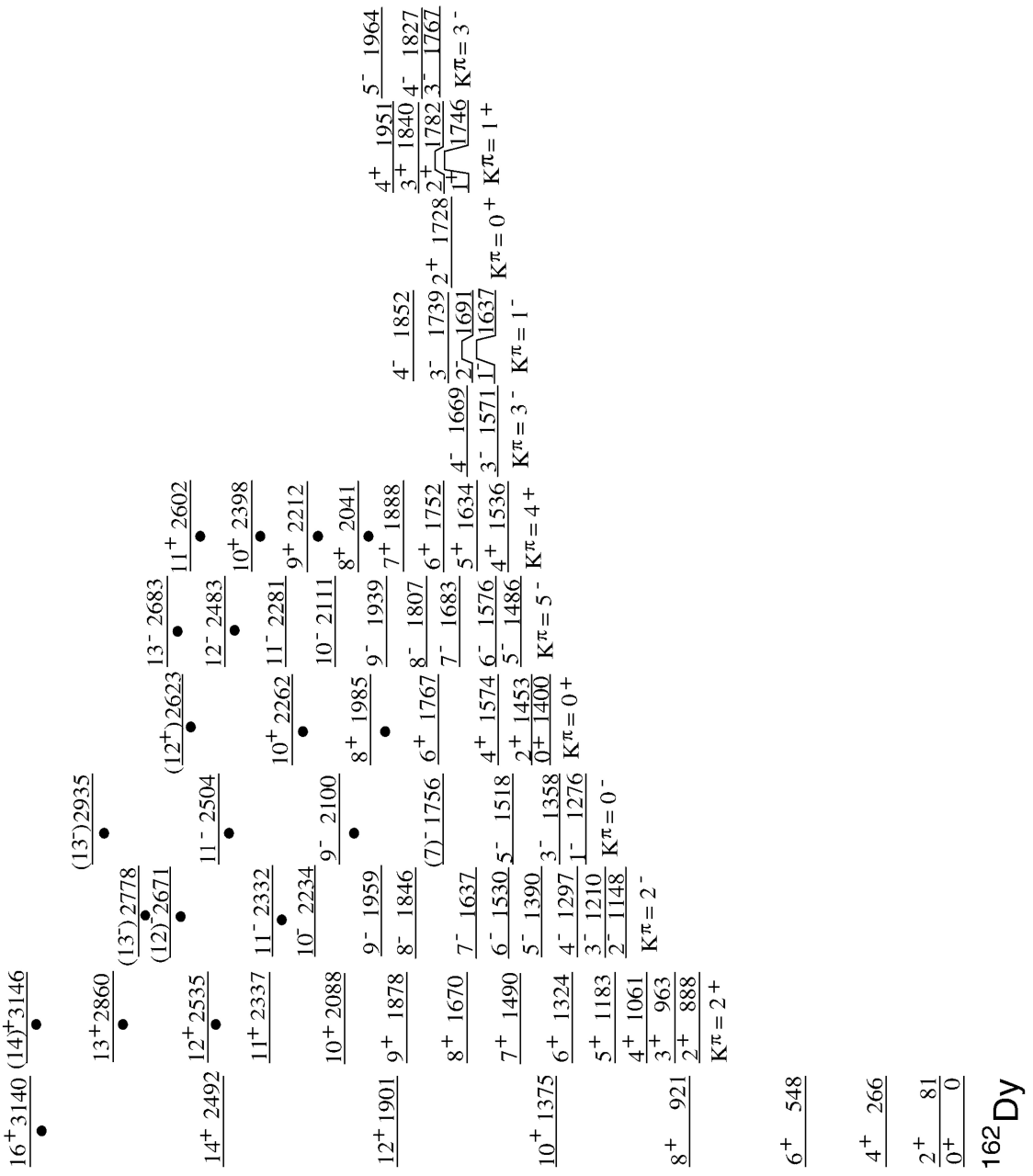

Figure 6.1: Figure of the complete spectroscopy of ^{162}Dy [75].

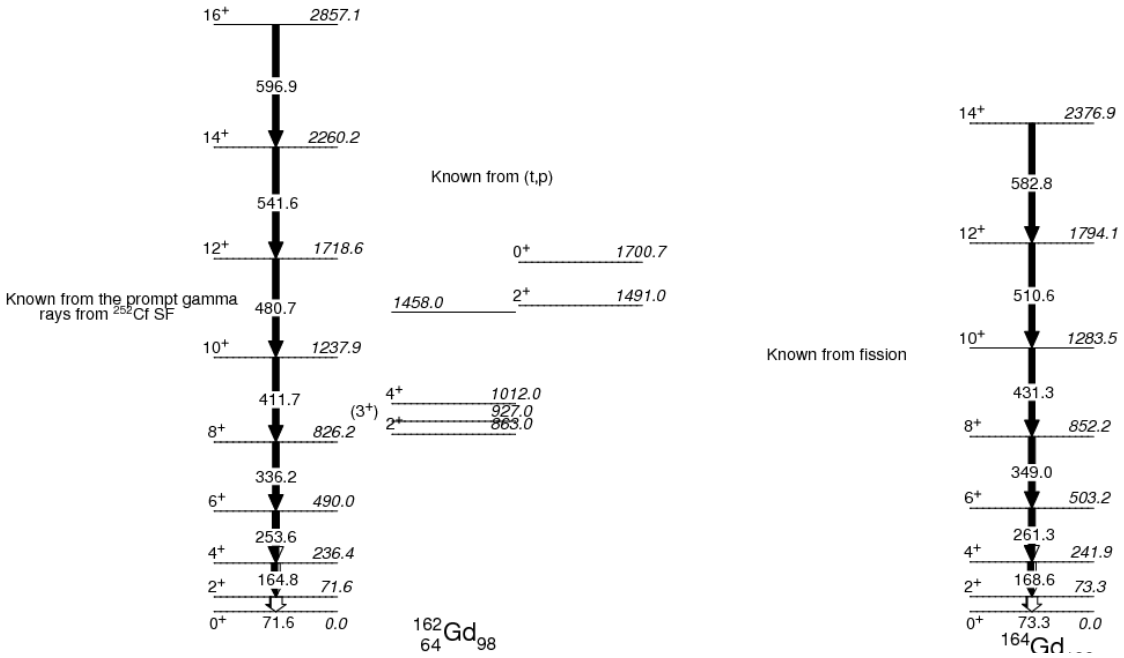

Figure 6.2: Previously known levels and gammas in ^{162}Gd and ^{164}Gd

6.1 Even-A Gd

6.1.1 ^{162}Gd

Shown in Fig. 6.3 are the levels and gamma rays found from the beta decay of ^{162}Eu. Found are several collective band structures. The first band structure is based on known levels previously assigned to be part of the gamma vibrational band. The extensions of this band that have been found continue to support this assignment as will be discussed. Also seen is a level at 1353.5 keV, which fits best systematically with the K=4 vibrational levels that have been seen in neighboring nuclei. Also seen are a number of levels that are of interest, which will be discussed.

Identification of this isotope is made by mass separation of the beam and then confirmed by the observation of known peaks as well as elementally unique X-ray radiation. An example of the spectra seen in this study is shown in Fig. 6.4. In this spectra 13 of the 34 new gamma rays found in this work are presented. This spectrum from ^{162}Gd is very pure though the data does contain some contamination from the mass 81 region (Zn, Ga, Ge, As). The highest intensity line at 351.3 keV from ^{81}Zn $\rightarrow$ Ga decay is 7.5% of the 71.9 keV transition. These isotopes were studied explicitly

as part of the campaign to measure isotopes near ^{78}Ni. Different magnet settings were used in that case and better rates of mass 81 isotopes were seen. The gamma rays seen in this study were compared to those focused on mass 81 to assure their proper placement.

Before the structure of Gd is discussed further, the analysis of what can be inferred about the parent isotope is presented. In Fig. 6.5 are some examples of the half life curves that have been linearized by plotting the logarithm of the counts against time in seconds. The slope shows the decay constant from which the half life of 10.7(7)s is inferred from the weighted average of several of the strongest transitions. Unfortunately, there were fewer counts able to be used for half life measurement than there were for coincidences, thus this figure shows significant statistical fluxuation. This is consistent with the previous measurement of 10.6(10)s. The strongest transitions were used in order to minimize the error in this value. There is an indication however in the half life curves of the 862.7 and 792 keV transitions of a longer half-life that may be able to be associated with an additional beta decaying state in the parent nucleus. Analysis of these curves is still ongoing.

There is no firm assignment of the spin and parity of ^{162}Eu. There is currently a mixed view of the decay properties. The best systematics unfortunately are not more recent than the work done in 1973 [88]. Yet, even in that work[88] there is a suggestion that the ground state is 0 or 1^- and there may be the presence of a high spin isomer in this isotope due to the "apparent population" in ^{160}Gd of the 6^+ state and due to the probability that the $5/2^+$ (proton) and $5/2^-$ (neutron) orbitals would favor a 5^- ground state.

Apparent population is the key phrase in the decay of ^{160}Eu and could perhaps be an issue in this present work. Table 6.2 shows gamma rays found in this work, the intensity coming into a state should equal the outgoing intensity and all missing intensity is assumed to come from direct population by beta decay. The pandemonium effect is not as likely to be an issue here as it was in ^{122}Cd because of the lower Q value. However, the highest excitation is still only 1/3 of the total β Q value, so there is a certainty of missing intensity. Nonetheless, it is necessary to say a few things about the population that is observed. The only levels where there is little or no feeding from beta decay is seen are the levels at 236.0, and 1012.1 keV which are both likely 4^+ states. Note that

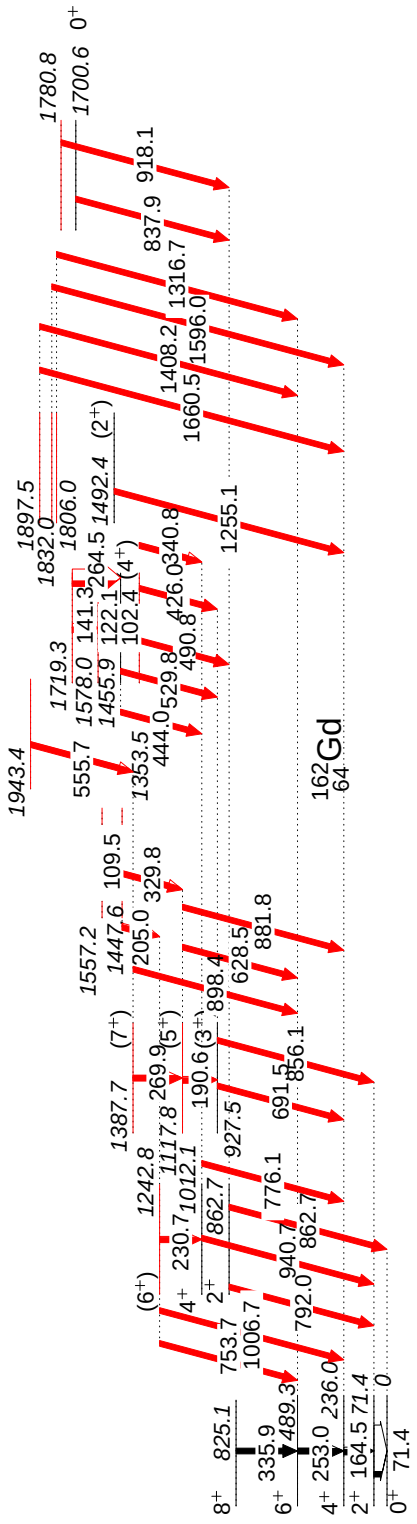

Figure 6.3: New levels in ^{162}Gd populated by beta decay of ^{162}Eu

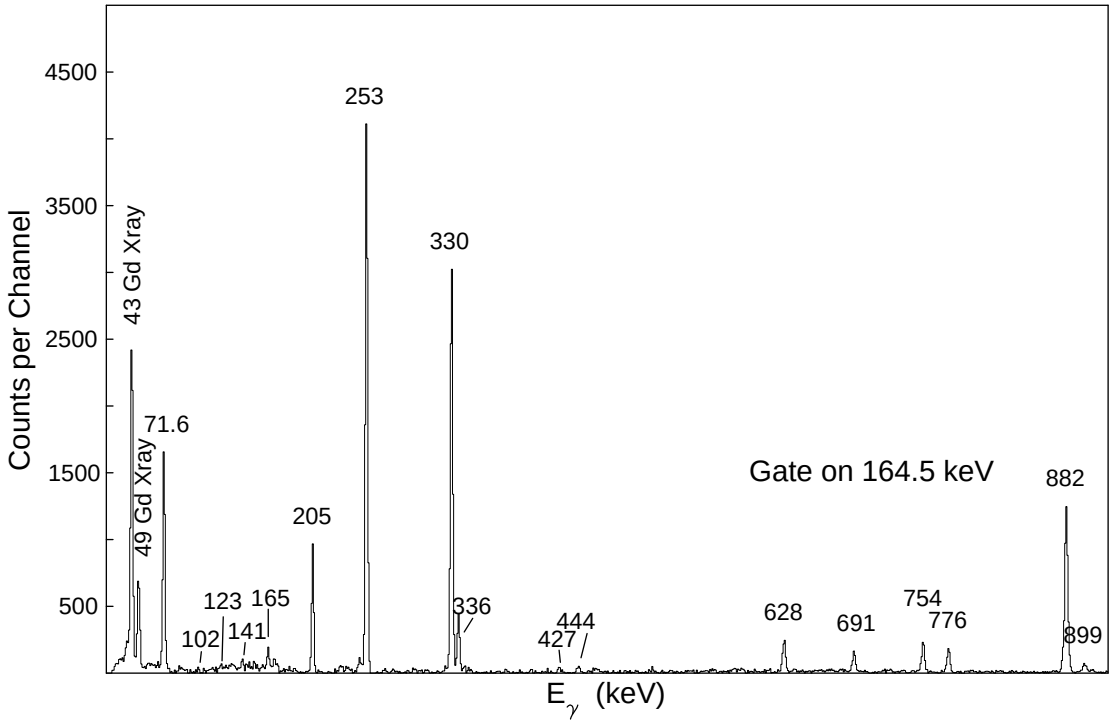

Figure 6.4: Spectra of ^{162}Gd from beta decay

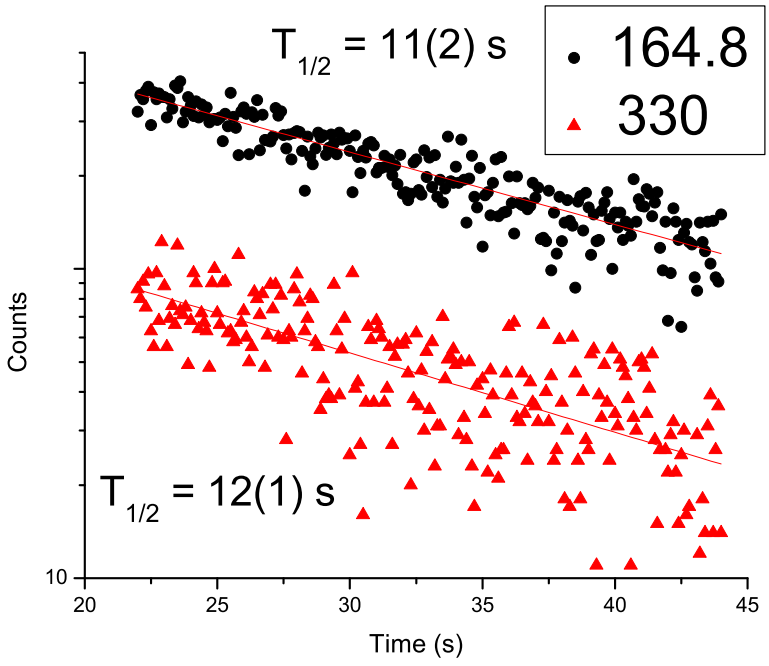

Figure 6.5: Half life curves of the ^{162}Eu parent from beta decay

the level and gamma ray energies are slighly different between the study from beta decay and the SF study. The largest feedings seen are to the levels at 71.4, and 862.7 keV which are both 2^+ and to the level at 1447.6 keV with unknown spin and parity. In addition there are two low spin states seen from (t,p) at 1492.4 and 1700.6 keV that do not seem to have any gamma ray feeding from above. However, the level at 1447.6 keV decays to both a (6^+) and a (5^+), and is therefore limited to spin between 4 and 7 and is most likely spin 5 as an estimation from systematics. This state and the gamma vibrational band states are close in energy but see very different feedings. Since those states are positive parity, the level at 1447.6 keV is presumed to be a negative parity state. This means that there is either significant missing intensity to this state or there is a high K isomer in ^{162}Eu, which is more likely.

It is problematic to assign the beta decaying state as 5^- because then there should be some first-forbidden decays to the 4^+ and 6^+ states which have very little β feeding. From the gamma intensities there is seen beta population of both the 6^+(489.3, and potentially 1242.8, and 1578.0 keV) and 8^+ states(825.1 keV). The 253.0 keV $6^+ \rightarrow 4^+$ transition is seen very strongly in 6.4 and the $8^+ \rightarrow 6^+$ transition is also seen at 335.9 keV. This could be explained by a beta decaying 7^- state in the parent, but this would change the likely interacting valence orbitals that form the ground state of ^{162}Eu.

This suggests that there is not a way to determine from this work the potential spins and parities of the ground state and isomeric levels in the parent isotope, but there are hints of isomerism as in ^{160}Eu and it would be beneficial to have direct studies of isomers in these isotopes. It will also be beneficial to have studies in the odd mass isotopes in this region, this would allow for the analysis of potential orbital couplings as well as give an opportunity to study half lives and energy levels of single particle states which inform r-process abundances in the rare earth peak.

Results from spontaneous fission in Gammasphere are shown in Fig. 6.6; many of the collective levels are seen and much of the same decays are seen. There were a number of challenges with this approach, most notably the fact that Gd nuclei (Z=64) are the highest Z that have been seen in the spontaneous fission data and have the weakest statistics. So, having the beta decay data allows

Table 6.2: Table of gamma ray intensities found from the beta decay of ^{162}Eu.

E_i	E_γ	I_γ	β Feeding	Log*ft*
71.4	71.4	94 (6)	30 (9)	6.1 (1)
236.0	164.5	41 (1)	2 (5)	7.3 (1)
489.3	253.0	15.5 (5)	4 (2)	7.0 (1)
825.1	335.9	12.4 (5)	1.7 (1)	7.2 (1)
862.7	792.0	12.1 (7)	11 (2)	6.4 (1)
	862.7	6.1 (4)		
927.5	691.5	2.3 (8)	7 (3)	6.5 (1)
	856.1	8.9 (5)		
1012.1	776.1	2.2 (5)	2 (2)	7.1 (1)
	940.7	1.5 (2)		
1117.8	628.5	2.3 (2)	3 (2)	6.8 (1)
	881.8	13.3 (6)		
1242.8	753.7	3.1 (5)	2 (1)	7.0 (1)
	1006.7	1.4 (2)		
1353.5	340.8	0.9 (2)	7 (2)	6.4 (1)
	426.0	1.2 (9)		
	490.8	5.6 (7)		
1387.7	269.9	0.5 (2)	1.5 (6)	
	898.4	1.4 (3)		
1447.6	205.0	3.3 (5)	16 (1)	6.0 (1)
	329.8	12.7 (5)		
1455.9	102.4	1.1 (5)	0.2 (1)	
	444.0	0.3 (7)		
	529.8	2.1 (2)		
1492.4	1255.1	1.8 (3)	1.8 (3)	6.9 (1)
1557.2	109.5	0.09 (3)	0.09 (3)	
1578.0	122.1	1.2 (1)	0.5 (2)	
1700.6	837.9	0.7 (2)	0.7 (2)	
1719.3	141.3	0.8 (1)	1.7 (3)	
	264.5	0.9 (2)		
1780.8	918.1	0.8 (2)	0.8 (2)	
1806.0	1316.7	0.15 (9)	0.15 (9)	
1832.0	1596.0	1.7 (1)	1.7 (1)	6.8 (1)
1897.5	1408.2	3.2 (2)	3.7 (3)	6.4 (1)
	1660.5	0.5 (1)		
1943.4	555.7	0.4 (2)	0.4 (2)	

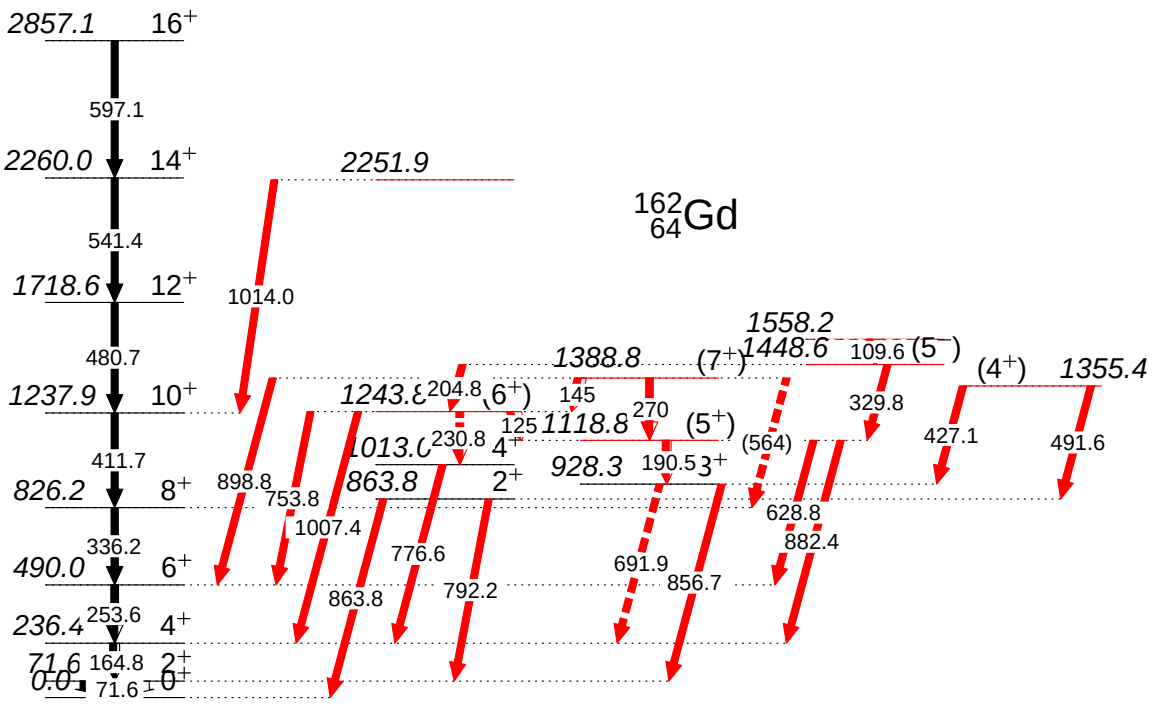

Figure 6.6: New levels in ^{162}Gd from SF. Note that level and gamma ray energies are slighly different than those found from beta decay.

us to pick out very weak peaks from the background in this region. It also allows us to develop better methods for gating and background subtraction in weak channels. In total 19 gamma rays were found, 3 of which were not seen in beta decay and 5 new levels, all of which are also seen in beta decay.

Most important is the observation of the gamma rays at 125.0 and 145.0 keV, because these gamma rays serve to link these levels to each other and support the assignment of a gamma vibrational band to these levels.

In Fig. 6.7 the difficulties in measurements of gamma rays in side bands are illustrated. It is easily seen how gamma rays at 329.8 and 753.8 keV could easily have been mistaken for background in this spectrum. Once these gamma rays are known, they can be used in gates and new transitions can be sought after.

In order to analyze the qualitative nature of these decays we can re-examine the decay selection rules seen in section 3.2. The gamma vibrational band is analyzed first. According to equation 3.7 there is no difference for the expected decays from a beta or a gamma vibrational band to the

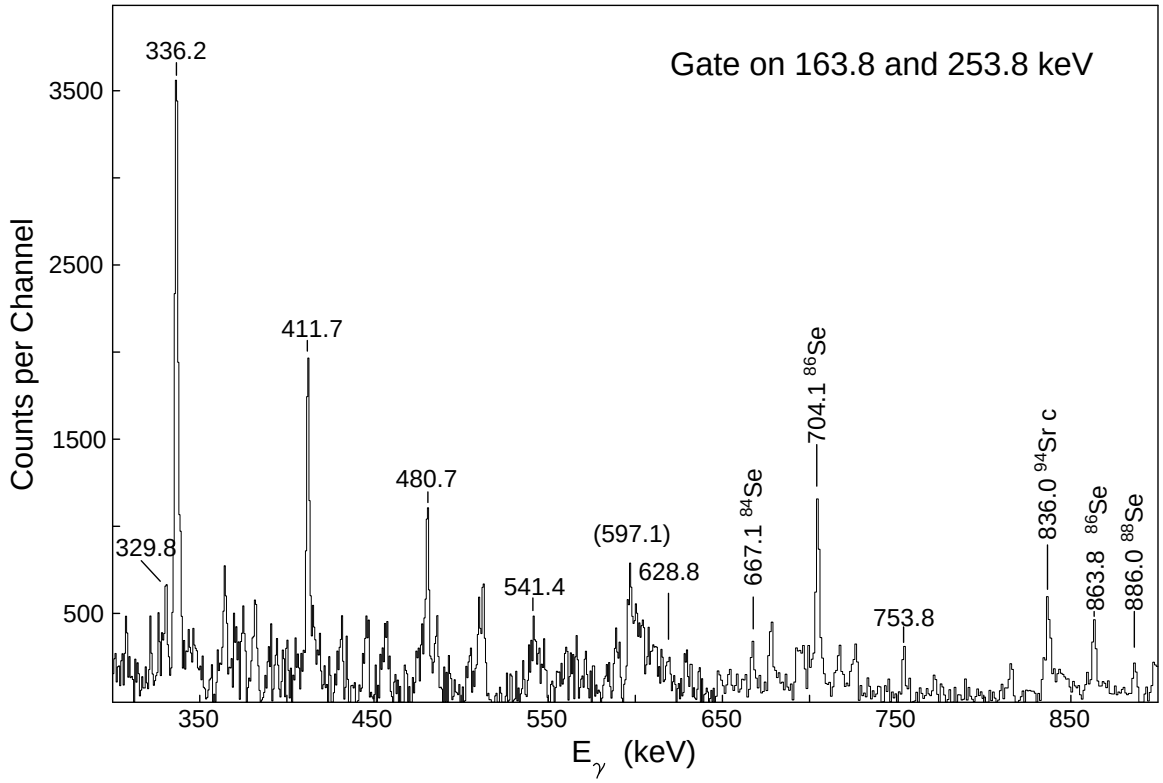

Figure 6.7: Spectra from the gate on 163.8 and 253.6 keV in ^{162}Gd from SF

yrast band. To put it another way, the Clebsch-Gordan coefficients explain the fact that K=0 and K=2 are equally likely quadrupole transitions. They also predict that the $2^+ \rightarrow 2^+$ is more likely than the $2^+ \rightarrow 0^+$ by a factor of 10/7 or about 1.4. But a pure beta vibrational band would not have the signature components giving rise to odd spin members and interband M1 transitions. Because we see both of these things, even though there is not a claim to have measured any more of the spins and parities of levels in this isotope, the gamma vibrational band is still reported to have been observed. If a different spin and parity were to be measured in future experiments, then this assignment would need to be re-evaluated.

Considering the level at 1448, there are two possibilities if it is a 5^- level. It is either the 5^- member of a K=0 or 2 octupole band or a K=5 isomeric level built on a two neutron quasiparticle configuration. Unfortunately, in ^{162}Dy and in other nearby isotopes these levels are very close in energy. In ^{162}Dy the K=0 and K=5 5^- levels are different by only 32 keV (Fig. 6.1 [75]), so no assignment based on systematics can be made. The only way an assignment could be made is if

a half-life could be measured for this state. There would be a measurable half-life for this state if it originated as an excited quasiparticle because of the degree of K-forbiddeness in this transition. But if it were an octupole member with K=0 or 2 there would not be an appreciable hindrance factor. Therefore equations 3.1 and 3.2 may be employed to ascertain what might be expected from this decay. From [89] decays from these levels in Nd and Sm have half-lives near ≈50-100 ns. According to the methodology presented in reference[90] the states in ^{158,160}Sm at 1279 and 1361 keV respectively are remeasured to be 54(9) ns (83(12) ns previously) and 72(6) ns (120(46) ns previously). The difference is that these states decay directly to the ground state (K=0) instead of the gamma vibrational band (K=2). So what would be the expected K-hindrance factor for a decay into the gamma vibrational band?

Hindrance factors called ν must be determined. This is ν=4 ($\Delta K - \lambda$) for the K=5 to 0 transition and ν=2 for the K=5 to 2 transition (to the gamma band). Taking the ^{160}Sm level at 1381 with a $T_{1/2}$=70 ns for comparison, the ratio of the observed half-life to the Weisskopf estimate for this transition is found. $T_{1/2}(E1)_{W.U.}$=ln(2) $160^{-2/3}$ $(0.878)^{-3}$ / (1.02*10^{14} = 0.15 ps, therefore f=$T_O/T_{W.U.}$= 4.6*10^8 and f_4=147. Then this reduced hindrance factor should be the same for the case of f_2=147. Continuing to work backwards the decay into the gamma band should have a half-life of somewhere between 0.2 to possibly 2 ns, which is consistent to the quasiparticle band in ^{162}Dy which decays into the gamma band and has a half life of 1.9(1)ns. This measurement would be beyond the capabilities of the Gammasphere setup because the clock used in this study was limited to a 8 ns minimum, though this measurement would not be beyond the capabilities of modern techniques which can have ps timing resolution. Despite this prediction, the measurement was still attempted and, as expected, no half-life is measurable (Fig. 6.8), therefore one is not able to establish the structure of this level.

In the same framework of K-hindrance, it not surprising that the states built on a level at 1353.5 keV, thought to be a K=4 band, show exclusive decay to the gamma band instead of the ground state band. This is what we expect from the CG coefficient for the transition to the K=0 band is $\langle 4\,2\,4\,-4 \mid 4\,2\,2\,0\rangle$=0. This assignment is further corroborated by the energy level spacing

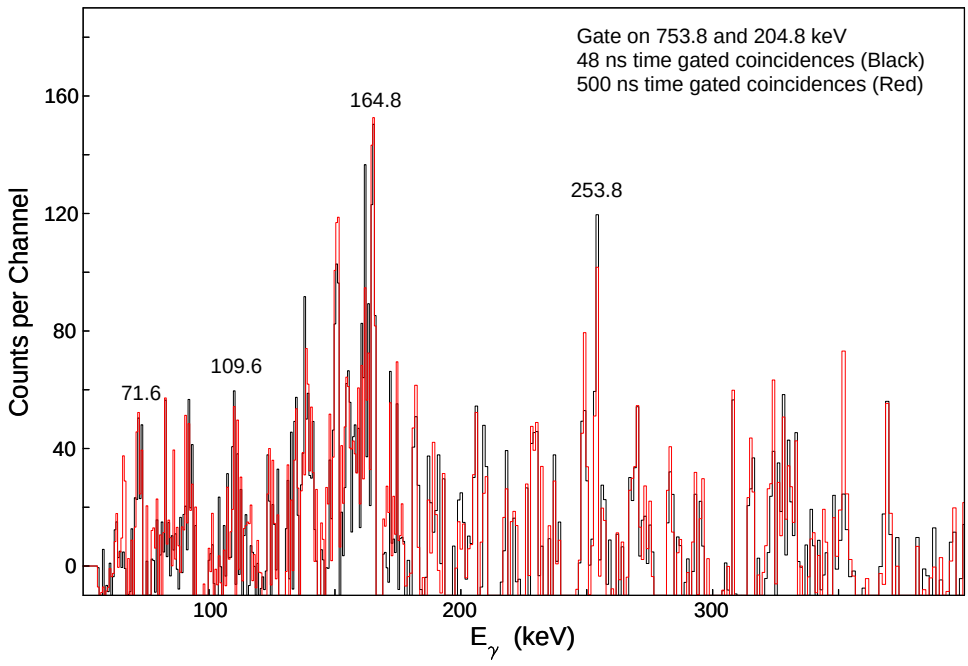

Figure 6.8: Spectra from a short and long time gated cube from ^{252}Cf examining the transition at 109.6 keV.

which is consistent with K=4 bands in nearby isotopes. More important is that for the level at 1354 keV which, via the selection rules and probability to decay by a certain multipole order, the spin is limited to 2, 3, or 4 $\hbar$. Then the relative strengths of these decays can be examined. Since the 426.0 transition has the highest relative error in its intensity measurement, the ratio of the decay to the 4^+(340.8 keV) and the 2^+(490.8) members of the gamma band is considered. If K=I for the state at 1354 then the intensity ratio of the 340.8 keV to the 490.8 keV is 0.75, 0.54, or 0.20 for spin 2, 3, or 4 respectively. The experimental value of 0.16(25) is most consistent with the assignment of (4^+) for this level. There are then two possibilities for this band: it is either a two-phonon gamma vibrational band or, as has been suggested by ref. [91], a hexadecupole vibrational band. The only qualitative difference that seems to exist is that every expectation would be that the two-phonon band would be nearer to twice the excitation of the 2^+ gamma bandhead, which would be nearer to 1700 keV instead of 1354 keV.

6.1.2 ^{164}Gd

Shown in Fig. 6.9 are the levels and gamma rays found from the beta decay of ^{164}Eu. Unfortunately, the counts were not high enough to measure the half-life. Known previously, were the levels in the yrast band[78] shown in Fig. 6.2 as well as a few gamma rays found in the work reported in ref.[83] which are marked in the figure with an asterisk. These decays are now placed in the level scheme in what appears to be the gamma vibrational band. In addition to what was known previously this study found 8 new transitions and 9 new levels.

In Fig. 6.10, two gates are shown as evidence for this level scheme. First, the identification of peaks associated with the X-ray (42.5 keV) is seen in the top spectrum. From there, subsequent gates on known and new peaks seen in this first gate, like the 491.0 keV shown on the bottom spectrum, can be used to construct the level scheme. Note that the 91.3, 192.5, and 301.0 keV lines are not seen in the gate on 491.0 keV and are placed decaying into the 1094.8 keV level because the are seen in coincidence with the 854.0 keV transition.

The new levels and gamma rays found for ^{164}Gd from SF are shown in Fig. 6.11, where 6 new gamma rays are seen that are not present most notable is a higher transition in the proposed gamma band at 142.0 keV, which is placed tentatively in the level scheme based on some evidence for an 826.7 keV decay to the 503.0 keV level. If this band is a gamma vibrational band, then the level at 1329.7 keV should be a (6^+) level. Since the 503.0 6^+ level is observed, the level at 1329.7 could also be populated.

It is proposed that the four levels at 1034, 1095, 1186, and 1329.7 keV are part of the gamma vibrational band. There is a difference however, the spin 3-5 levels in the gamma band in ^{162}Gd have an interband transition from $5^+ \rightarrow 3^+$ at 190.5 keV and no other interband transitions, while the proposed gamma band in ^{164}Gd has only $5^+ \rightarrow 4^+$ and $4^+ \rightarrow 3^+$ transitions. Therefore, even though this band energy and spacing would be most consistent with the systematics of the gamma vibrational band in this region, this assignment is made only tentatively. No conclusions can be made regarding the structure of the remaining levels without a comparison to a more precise theory.

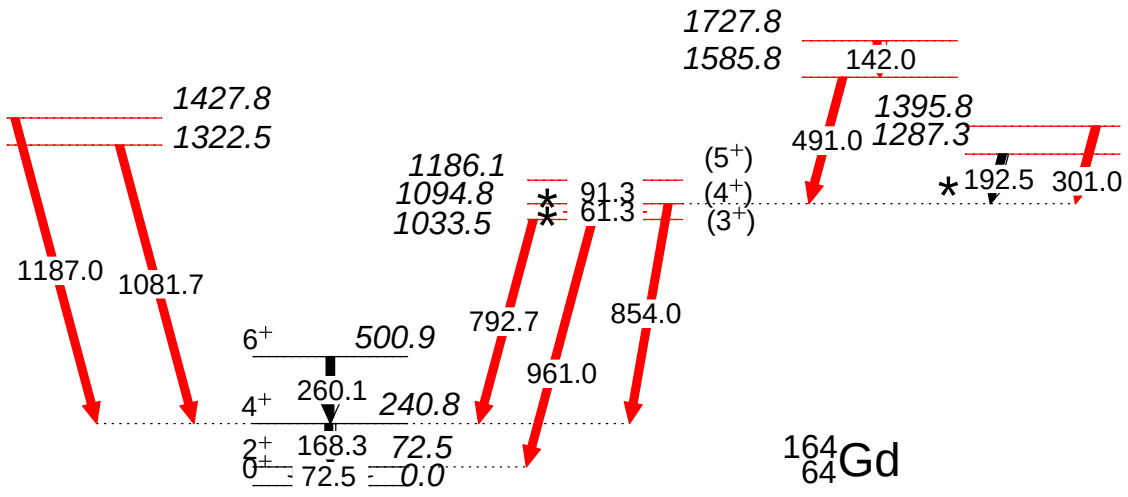

Figure 6.9: New levels in ^{164}Gd seen from the beta decay of ^{164}Eu. Gammas previously reported [83] shown with an *.

6.2 Level Systematics and Quadrupole Deformation of Even-A Gd

All of what has been said regarding systematics in this chapter in the even mass Gd species are shown in Fig. 6.12 as a summary. Note, that the first excited 2^+ state in N=100 isotones is nearly midway between the N=96 and N=98 isotones for a each isotope considered. This state is also systematically lower in Gd than in Dy. The gamma vibrational bandhead in the Dy isotopes also follow this same trend, with a maximum excitation at N=96, a minimum at N=98 and near a midpoint at N=100. Since, ^{160,162}Gd follow this same trend, it is most reasonable to guess that the spin and parity of the level at 1033 keV is 3^+, because it would be a deviation from systematics for the 2^+ level of the gamma vibrational band to be so high in energy. This is an argument for a motivation to measure the spin and parity of this state, not evidence for its assignment. If this state is the 3^+ member of the gamma band, it would fit with systematics, therefore this is the suggestion. Also the relative excitation energy of the gamma band is noted, which is about 100 keV higher in Gd than in Dy. This would also make the 1033 keV level a likely 3^+ gamma band member level. There is also a very consistent 3^+ - 2^+ spacing within these bands of ≈70 keV in Dy and ≈65 keV in Gd.

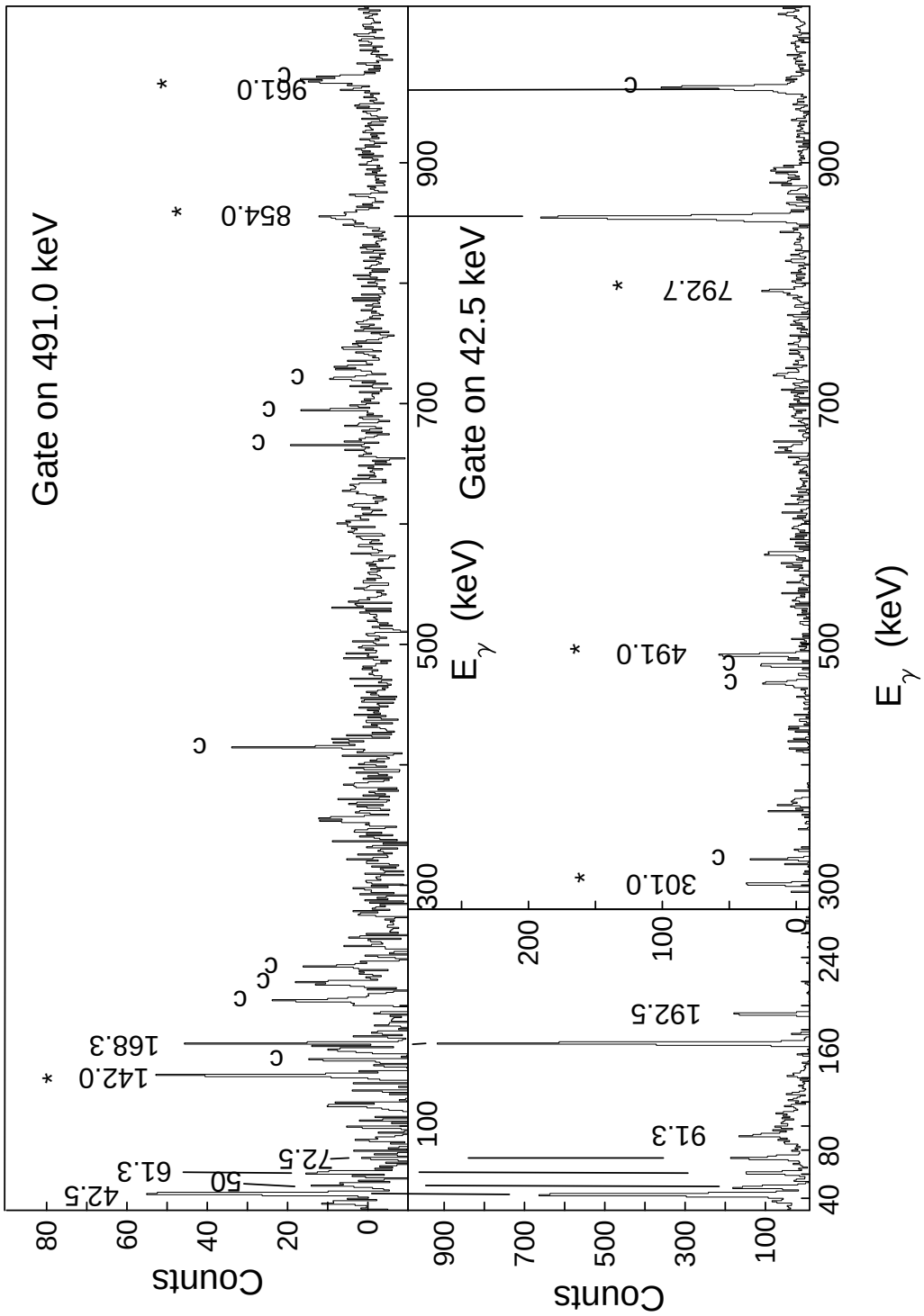

Figure 6.10: Spectra from gates on peaks determined to be associated with the beta decay of ^{164}Eu. The top spectrum shows a gate on the Gd x-ray peak and the bottom shows a gate on the new transition 491.0 keV. Contamination peaks (c) are known from lower mass (A= 81 and 82) region and known background. New peaks are labeled with an *.

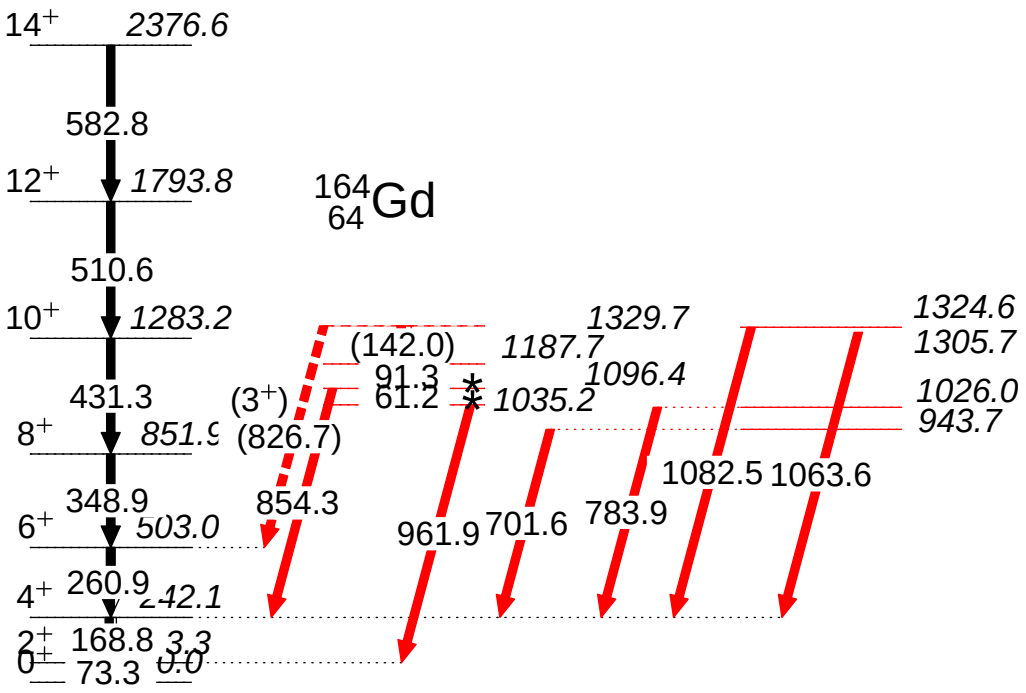

Figure 6.11: New levels in ^{164}Gd as seen in SF. Gammas previously reported [83] shown with an *. Note that the level and gamma ray energies are slightly different than those found from SF.

The K=4 π=+ band in N=96 lowers dramatically in ^{160}Gd almost to the same level as the gamma vibrational band. The most consistent thing across isotones for this band is the interband spacing of about 100 keV between the 5^+ - 4^+ band members. If it is determined that the nature of these levels are two phonon rather than hexadecupole vibrational in nature some detailed theoretical explanation is required for the behavior of this band in ^{160}Gd.

The octupole vibrational band is only very well known in the N=96 isotones, where this band does not change its energy very much at all. However in the case of ^{164}Dy, both the octupole and the quasiparticle band are moved to very high in energy, but it appears that this may not be the case for ^{162}Gd. The 3^- - 1^- spacing of 83 keV is similar in the Dy isotopes shown and if systematics hold a 65 keV spacing could be possible in ^{162}Gd. No levels were seen with this spacing. A suggestion could be made however, that the level at 1897.5 keV seen in beta decay would be a possible candidate for the 5^- member of the octupole band. It is important to suggest this because if the parent has a 5^- ground state, this level should be an allowed transition and strongly populated

from beta decay.

6.3 Odd-A Gd

6.3.1 ^{163}Gd

Now shown in Fig. 6.14 and Fig. 6.15 are the new levels and gamma rays populated from the beta decay of ^{163}Eu. In this study, 66 new levels have been placed where only 5 gamma rays had been previously assigned[92]. The Q_β value[93] and half life[83] were also known. Some transitions are placed tentatively because they are seen in the projection at the same energy for which there is a level in the level scheme but not in coincident gates. These are high energy transitions that may feed a state that does not gamma decay but corresponds to a level energy existant in the level scheme placed by other evidences. There are several gamma rays with considerable intensity, like the 2297.9 keV transition with 16.7(8)% intensity, shown in the level scheme in Fig. 6.14. Setting gates on these transitions reveals that they are not inconsistent with their placement feeding the ground state in this isotope but cannot be confirmed by setting gates on them. There are also low energy transitions depopulating levels above 1200 keV and these are problematic as to how they can compete with the very high energy transitions. In Fig. 6.15 there are two such dashed transitions. All transitions from levels in Fig. 6.15 are placed here because there is minimal coincidence information available for their placement in the level scheme.

There were significant difficulties in the analysis of these data. There was a nearly equal population of daughter (gamma ray intensity of 70.7(6)% of 191.8 keV) and granddaughter (intensity of 73(5)% of the 213.9 keV gamma ray in ^{163}Tb) decays. It has not been determined what proportion of Gd decays into Tb comes from the decay chain starting with Eu and how much comes from direct production from fission. There were also many large Compton events that appear as diagonal lines in the two dimensional histogram. There are more than 20 such constant sum peaks between 20 and 500 keV that are comparable in height to the real peaks. In addition, there are several peaks which have nearly the same energy and are placed in up to three different places in the level scheme. The peaks are revealed to be different because the spectra can be uncompressed to the

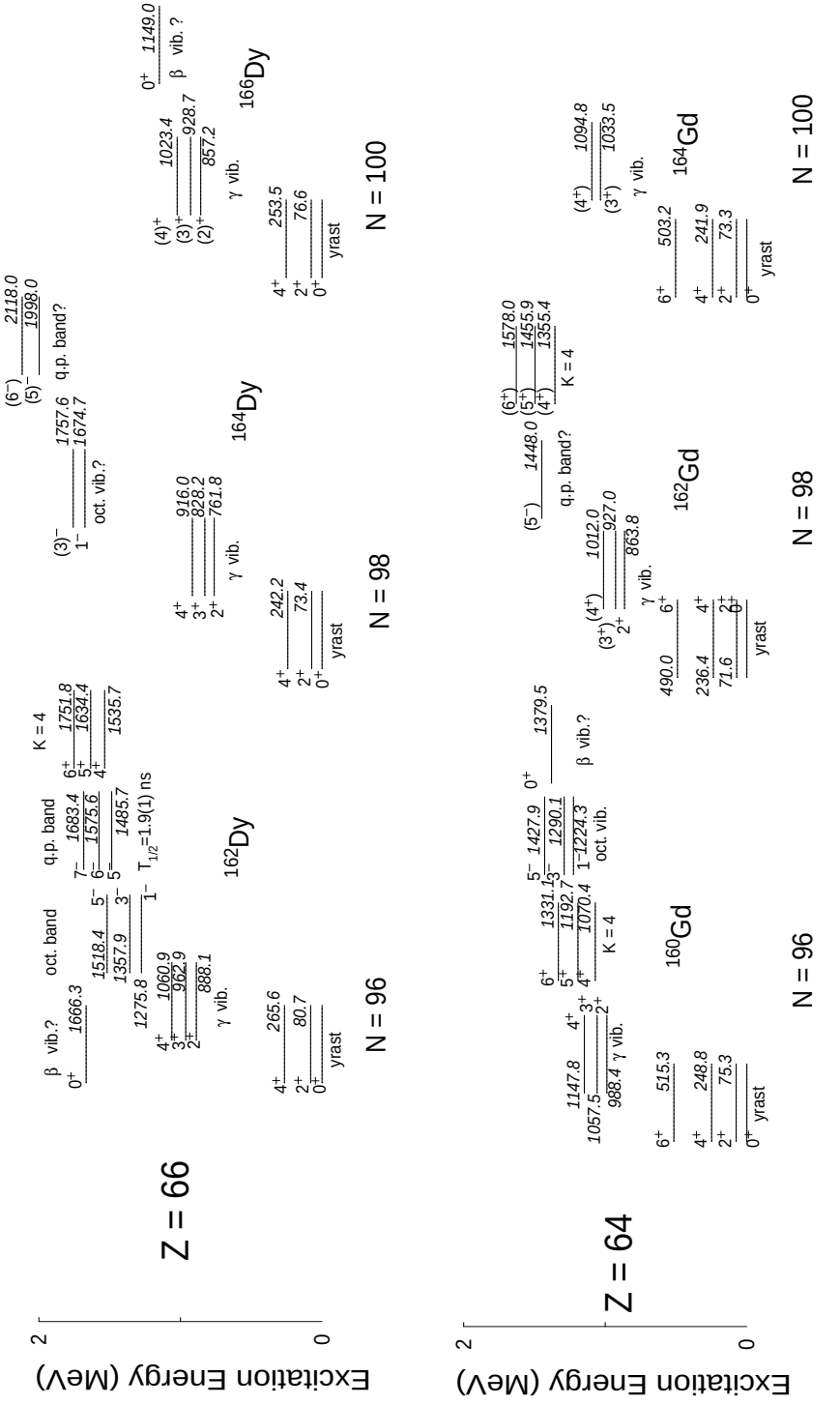

Figure 6.12: Systematic comparison of collective structures in even-even nuclei near ^{162} Gd

level of 0.1 keV per channel. The Compton events were found to be drastically reduced by taking only the coincidences from detectors that directly face one another. Since most of the Compton events are into neighboring detectors and because our statistics are sufficient enough this method proved very useful. Different scans of the data with different time windows for coincidences were also used.

There may only be a few cases where it is possible to measure the electromagnetic mixing ratio. This is because there are few cases where the decay chain has more than three gamma rays. Unfortunately, this means that the physics that can be discussed is limited until more can be known. This is to be expected in new territory. The best technique was to gate on the 42.8 keV Gd X-ray and compare this to the gate on the Tb 44.4 keV X-ray. This is shown in Fig. 6.16; here the top spectrum is a gate on Gd X-rays, the middle is a gate on Tb X-rays, and the bottom spectrum is a gate on Nd X-rays. Time gated spectra were also used in the analysis but are not as clear in some ways. The most important thing to emphasize is the fact that the X-ray peaks can be resolved, as well as other peaks which are degenerate in energy. Not shown in this spectrum are many high energy peaks that are also clearly seen. All peaks placed in the level scheme are seen in the top spectrum or in coincidence with these gamma rays and not in either of the other two spectra. For example, the peaks at 213.9 and 287.6 keV are seen most clearly in the gate on Tb X-rays, and peaks at 556, 578, and 642 are most obviously associated with the Nd X-ray spectrum; in fact all of these transitions and many others have been seen previously in these isotopes. Based on a weighted average of the 85.0 (minus 87 keV background) and 191.8 keV lines a new half life of 7.9(1) s is now reported. These half life curves are shown in Fig 6.13

One of the difficulties in this study is the attempt to build a level scheme for ^{163}Gd for the first time. All other level schemes in this thesis are based on some known transitions and a determination of the ground state. The evidence for the placement of the ground state is based on gates shown in Fig. 6.17. The first gate shown in this figure is on a 400.9 keV transition (this is seen in the Gd X-ray gate in Fig. 6.16 which shows 2 transitions, one at 1713.7 and another at 1758.0 keV. The remaining spectra that are shown are the coincidences with these two gamma

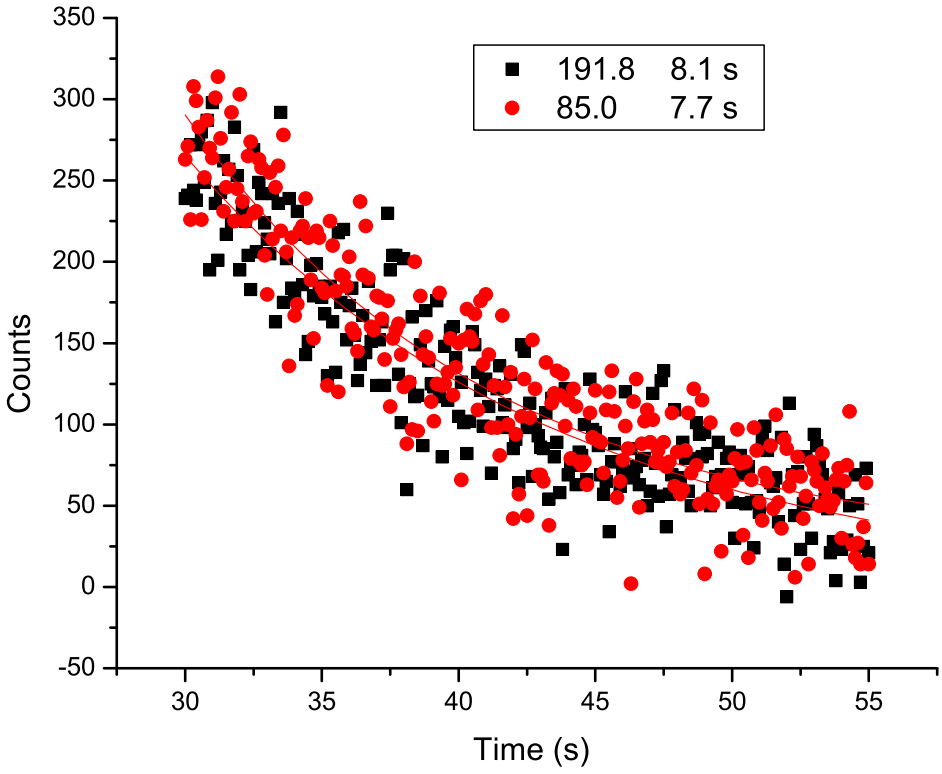

Figure 6.13: The half life curves from the 85.0 and 191.8 keV transitions.

rays. Importantly, the 1713.7 keV has coincidence with the 85.0 keV and not the 191.8 keV transitions, while the 1758.0 keV gate shows a peak at 191.8 keV and not 85.0 keV. These gates also reveal several other transitions that are shown in the simplified level scheme in Fig. 6.18 that was the starting point of this work. The coincidences with the 191.8 and 85.0 keV transitions do not indicate the presence of any transitions decaying out of these levels. This is consistent with the systematics of a $1/2^-$ state in N=99 isotones; this assignment is discussed further in section 6.4. The coincidences with the 85.0 keV line are then placed on top of the level at 236.1 keV and the coincidences with the 191.8 keV gamma ray are placed on top of the level at 191.8 keV. Dashed lines are lines seen in the projection that may correspond to levels placed in the level scheme. No coincidence information is available for these transitions.

Once the ground state has been assigned, the rest of the levels can be placed relative to these levels. Shown in Fig. 6.19 are the spectra seen when gating on the four transitions placed highest

in the level scheme in Fig. 6.18. Several new high energy and low energy transitions can be seen and placed in the level scheme. Notice that there is not a 52.8 keV transition easily visible in either the 138.0 or 115.9 keV gates, though it is placed in the level scheme. However, the 481.4 keV transition is visible and the 52.8 keV transition should occur as electron conversion. If the 481.4 keV were not placed depopulating the level at 2297.9 keV, it would have the consequence of placing as many as 6 other levels "floating" like isomers above the ground state which does not seem to make sense systematically. There are also transitions at 76.1 and 2219 keV that are seen in both of the 138.0 and 115.9 keV gates, but are not placed in the level scheme because of subsequent gating. There is an inconsitency in these gates. If the 1713.7 and 1758.0 keV gates decay into the 236.1 and 191.8 keV levels respectively, the 85.0 and 191.8 gamma rays should be able to be seen in the low energy region of this spectrum. Yet, these gamma rays are not seen. Note that in the gates on 115.9 and 138.0 keV transitions the low energy region is over subtracted, so it is perhaps not surprising that these transitions are not seen in these gates.

There is a question of the competing transition probabilities for a ≈2 MeV and a <.1 MeV gamma ray. For example, the level at 1816.5 shows a competing gamma ray transition from a 45.2 keV transition which is surely several orders of magnitude lower in probability that the 1816.5 transition. The 45.2 transition is seen only very well in the gate on 531.0 keV, and is shown in Fig. 6.20. Very careful measurements of the intensities of the low energy transitions need to be done before this work can be published. This is dificult because most of these transitions are placed in several locations in the level scheme. In addition, there are large uncertainties in the efficiency in this region. The energy level spacing is similar to the energy spacing seen in high lying collective bands in other isotones and there may be collective enhancement of the matrix element for these transitions.

6.3.2 ^{165}Gd

A similar methodology to what was used in the mass 163 run (where some decays were known) was used in the search for ^{165}Gd (where no transitions were known). The magnet settings

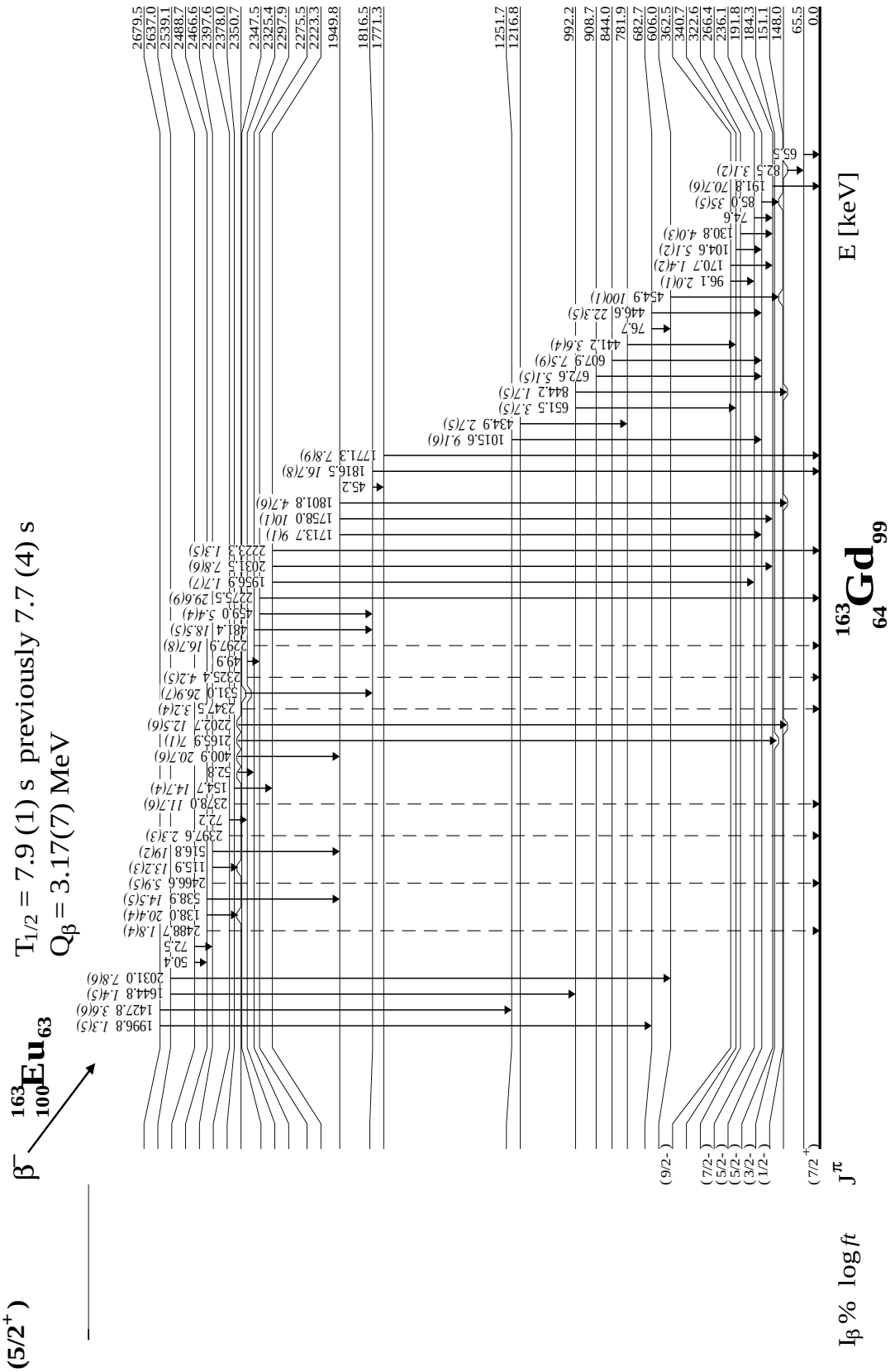

Figure 6.14: Low energy decays in the new level scheme of ^{163}Gd as seen in beta decay.

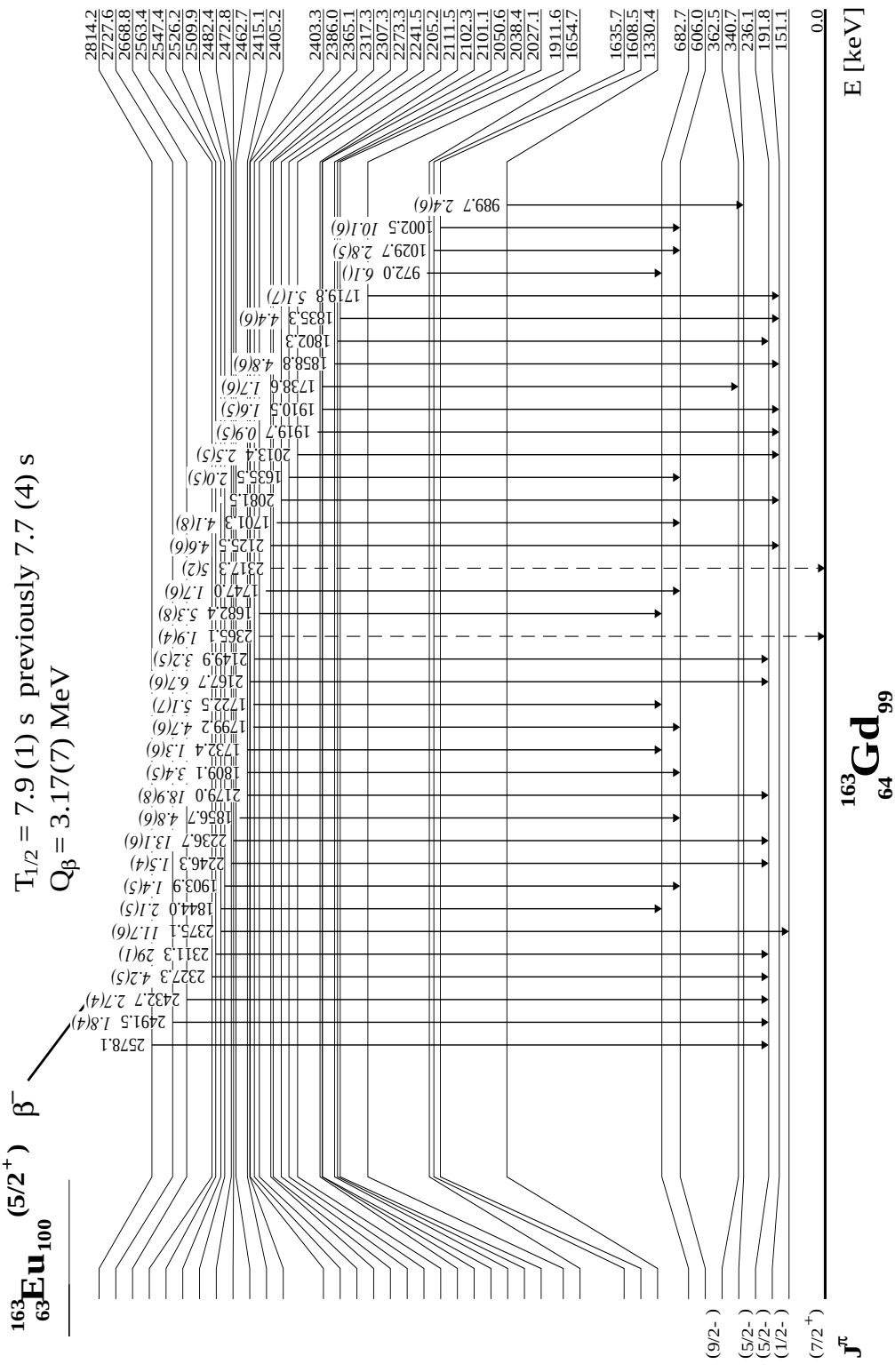

Figure 6.15: High energy decays in the new level scheme of ^{163}Gd as seen in beta decay

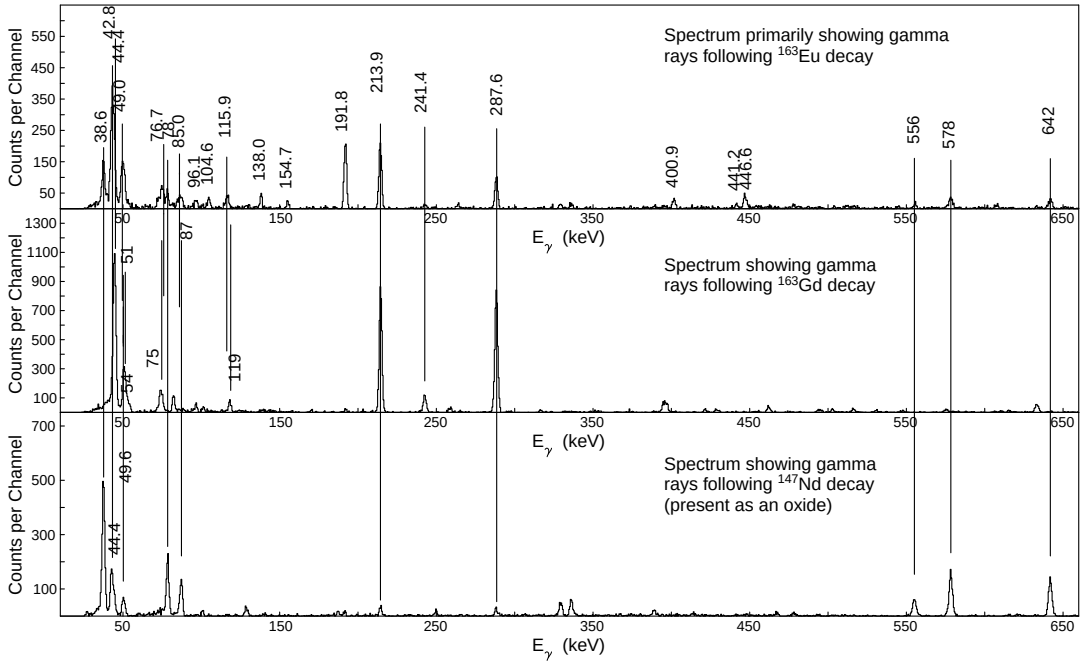

Figure 6.16: Gamma rays seen in the mass 163 run. The top spectrum shows gamma rays in ^{163}Gd identified by an X-ray gate. The middle spectrum shows gamma rays in ^{163}Tb identified by an X-ray gate. The bottom spectrum shows gamma rays in ^{147}Nd ($+^{16}$O) identified by an X-ray gate. Drop lines reveal the degenerate energies as distinguishable.

for moving to nearby masses are fairly accurate and the move from 163 to 165 is confimed by the NdO contaminates seen. Peaks are known in ^{149}Pm at 114.3 and 155.9 keV and are seen in this data and these confirm the mass settings (16+149=165). The top spectrum in Fig. 6.21 shows the tape cycle spectrum with the long lived activity subtracted, gates on the X-rays were used in the $\gamma-\gamma$ (middle) spectrum and the $\beta-\gamma-\gamma$ spectrum. The primary contamination in this run was from ^{149}Nd decay and gates on the X-ray are shown in blue on the bottom two spectra. Statistics were too low to measure a half life. All of these gates should enhance the visibility of gamma rays associated with ^{165}Gd. Because the previously measured half life was 1.7(3)s, the gamma rays that occur in the first 3-5s of the 7.5s decay curve and not in the last 2.5s may enhance Gd. This is seen through the observation of the 42.8 keV X-ray in this spectrum. The gate on this transition reveals a few peaks not in the gate on 38.6 keV and are seen in the time gated spectrum. Though the bottom spectrum only shows the 288.6 very well it is still seen with very few counts (20 or so) and it is understandable to not see the 195.5 keV transition in this spectrum because of the low

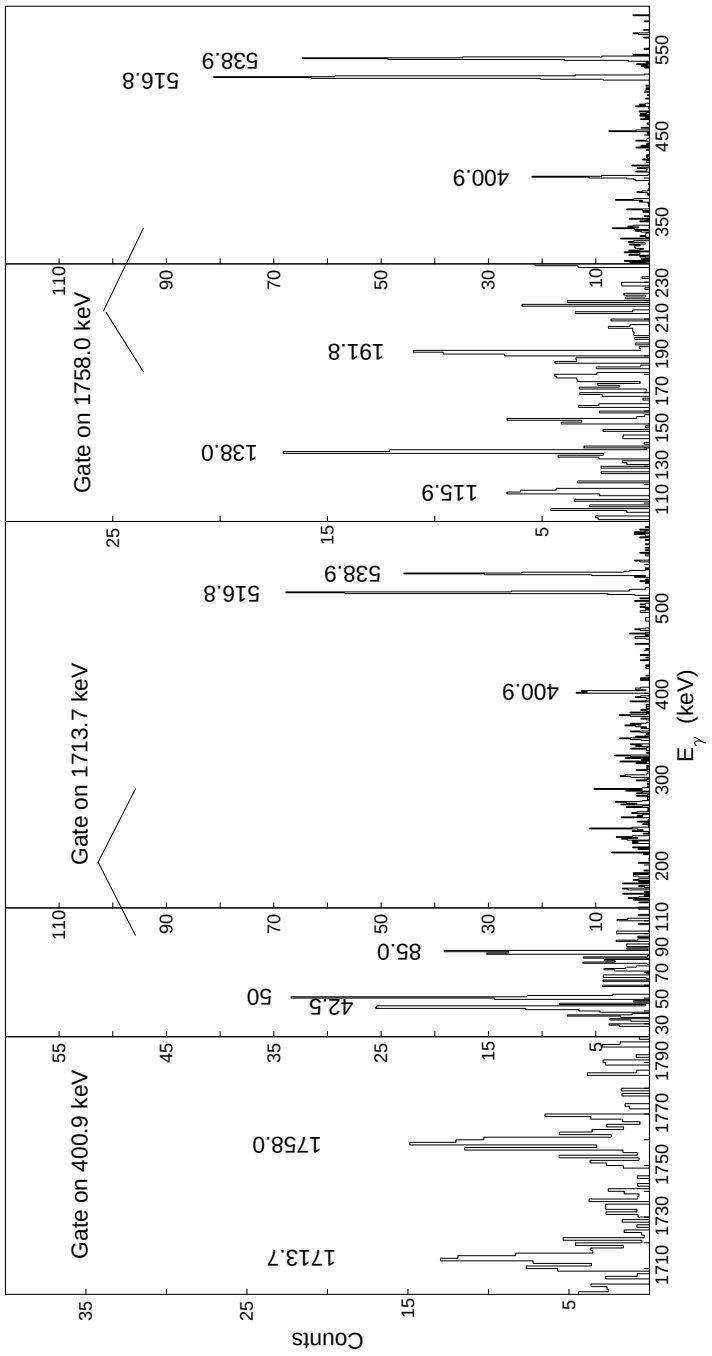

Figure 6.17: Spectra showing the evidence for the placement the 1713.7 and 1758.0 feeding levels at 191.8 and 236.1 levels respectively.

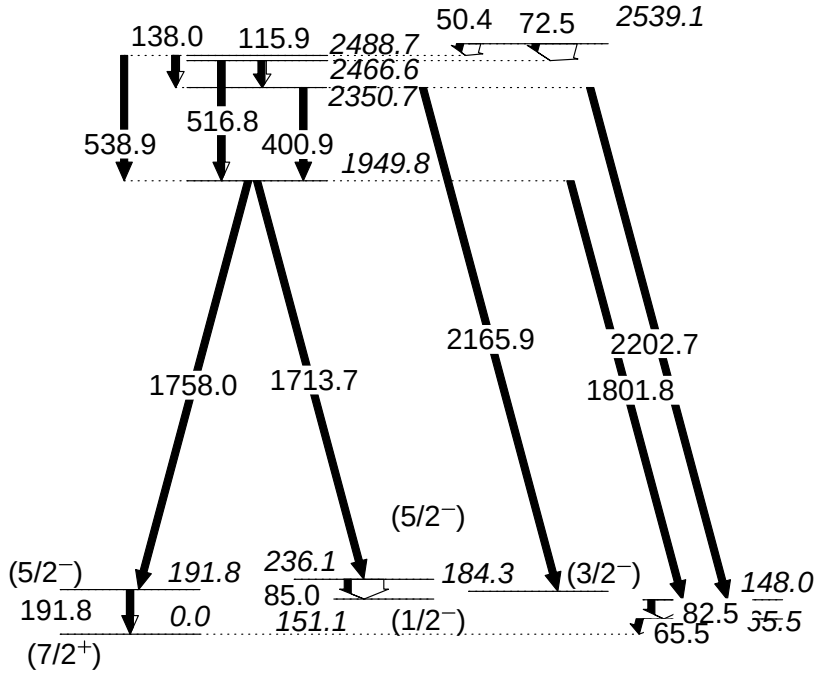

Figure 6.18: The simplified level scheme that was the starting point of this work.

efficiency of the beta detector. Therefore, the first measurement of gamma rays associated with ^{165}Gd are shown to be 288.6 and 195.5 keV.

6.4 Level Systematics and Quadrupole Deformation of Odd-A Gd

The summary of the systematics for low lying levels in the odd mass Gd are shown in Fig. 6.22. Based on these systematics it is most sensible to suggest a ground state spin and parity of $7/2^+$ consistent with N=99 isotones. The parent ground state level should be $5/2^+$ but is unmeasured, so it would feed lower spin states than a $9/2^+$. The ground state of ^{163}Gd may have been either the $1/2^-$ or $5/2^-$ states had these states continued to come lower in energy and become the new ground state. Had this been the case, a well defined band structure containing dipole and quadrupole transitions into the ground state should have been observed. However, no such band structure is seen. Had the $1/2^-$ state been the ground state, there should have been direct population to the 3/2, 5/2, and $7/2^-$ band members. Had the ground state been $5/2^-$ some low energy transitions should

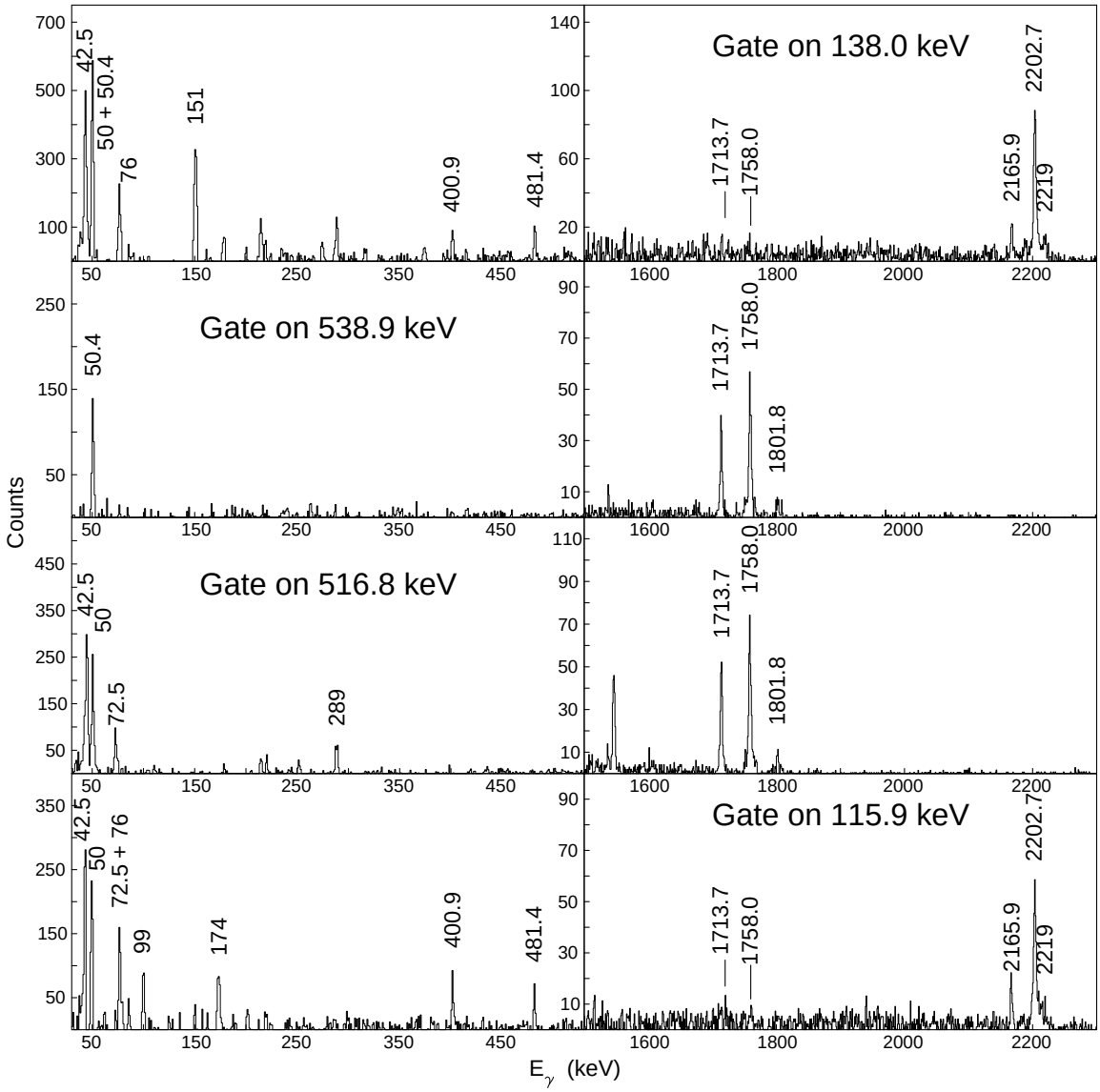

Figure 6.19: Spectra resulting from gates on 115.9, 516.8, 538.9, and 138.0 keV (bottom to top). There are some inconsistencies with what is shown (see text).

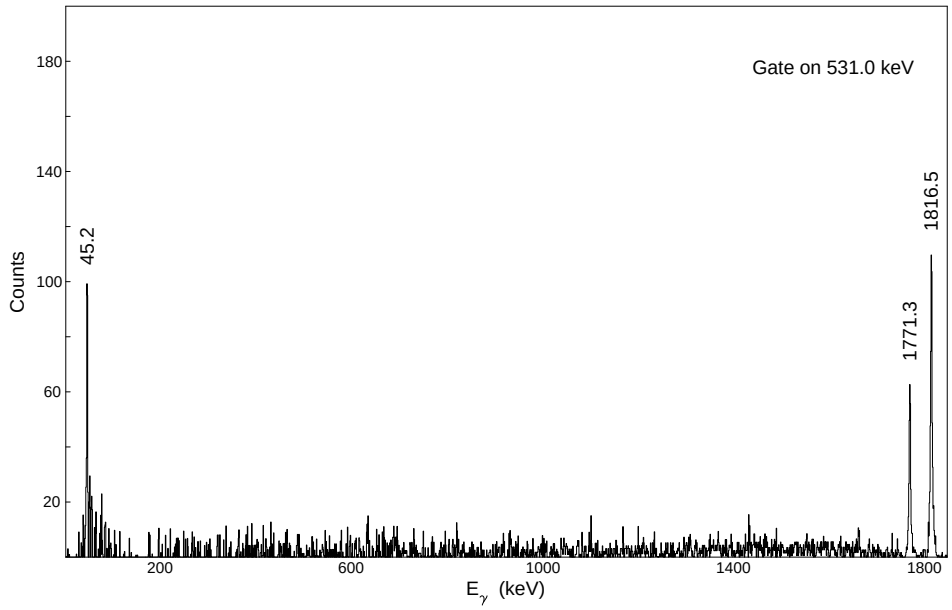

Figure 6.20: Gate on 531.0 keV (minus background from 535 keV) showing the competition between 45.2 and 1816.5 keV gamma rays.

have been observed with comparatively high intensity. There is a possibility that the 184.3 level is the $3/2^-$ member of the $1/2^-$ band, but the gammas that may have been seen are obscured, so the spin and parity suggestion is based solely on the level spacing.

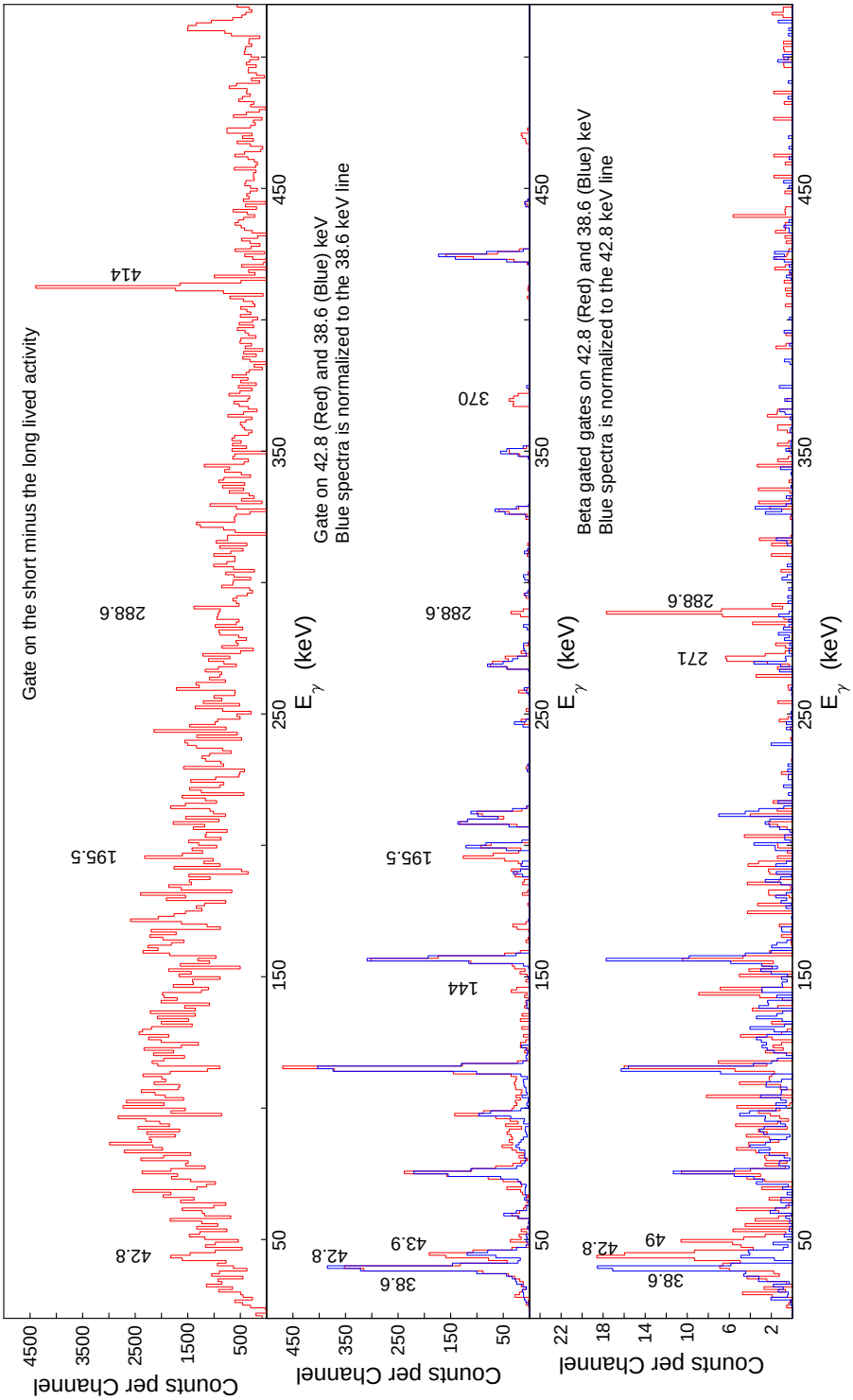

Figure 6.21: Spectra from mass 165 run comparing 3 different gating methods. First, a gate on short lived activity (first 120ms) with the long lived activity (140-200 ms) subtracted off. Second, the comparison of gates from the gamma-gamma matrix on 42.8 keV and 38.6 keV (the primary contaminant from ^{149}Nd+^{16}O decay). Shown third, are the same gates from the beta gated gamma-gamma matrix.

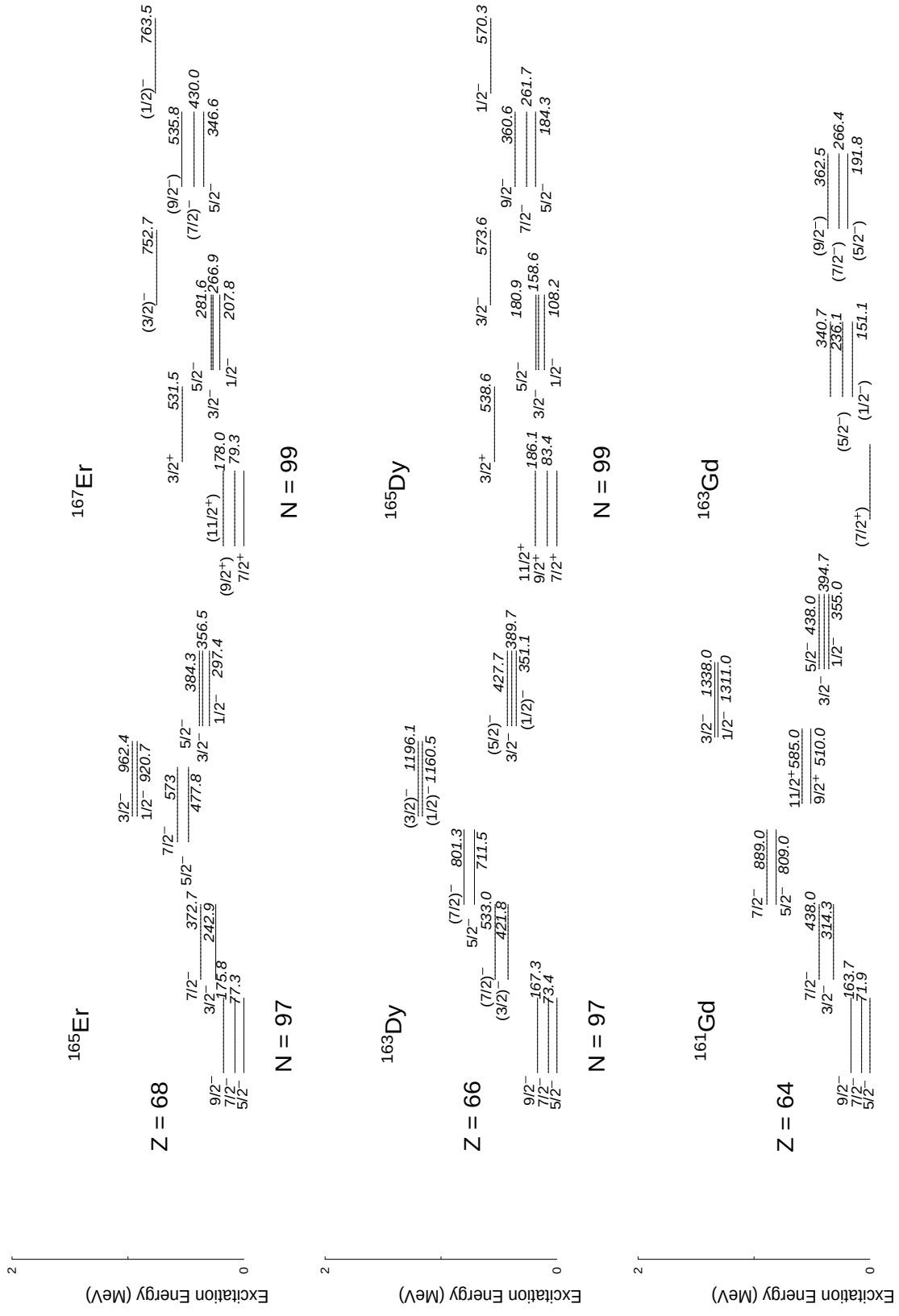

Figure 6.22: Systematic comparison of collective structures in even-odd nuclei near ^{162} Gd

CHAPTER 7

STRUCTURE OF NUCLEI NEAR Z=56, N=88

Octupole deformation has been extensively studied in this region [94–101]. However, until now firm assignments of spins and parities had not been given to members of both s= +1 and s= -1 bands in any even-even isotopes. These isotopes, as well as those in the Ra-Th region, as reviewed in [11], have been best described by a soft quadrupole-octupole shape in the ground state. It is more vibrational in nature at low spin and octupole deformation only becomes stabilized at higher angular momentum. There are important questions that need to be answered.

Both s= +i and s= -i bands have been clearly seen in nuclei with odd mass number [95, 96, 100]. While the s= +1 band is easily seen in even-A nuclei, the s= -1 band had only been seen in ^{148}Ce [102] with a measure of alternating parity, but not a measure of the spin of each level. Now I^{π}, spins and parities, for the levels in the s= -1 bands in ^{148}Ce as well as ^{144}Ba are determined through the use of angular correlation measurements. We show new values for the multipole mixing ratios of transitions in ^{145}Ba as an improvement over, but consistent with those in reference [95]. In addition, we find extensions of existing bands and in ^{146}Ba and ^{148}Ce and new bands built on previously known levels. We then carried out analyses in terms of a geometrical model [37, 41].

7.1 Results

The discussion begins with the new levels found in this work by showing in Table 7.1 the list of all new levels and transitions, previously known levels with newly measured properties, or those used in angular correlation measurements. Columns show the gamma ray energy-E_γ (keV), the intensity of the transition-I_γ, the level energy (keV) of the level that the transition depopulates-

E_i, and I^{π} if known or postulated. Uncertain assignments are shown with parentheses and new assignments and new transitions with their energy levels are shown with an asterisk. Spectra, level schemes and details regarding new assignments follow. In these figures the transitions that are not certain are shown with a dashed arrow and uncertain assignments are shown in parenthesis. Errors in the gamma ray energies are ≈ 0.5 keV, and errors in the intensities are estimated to range from 5 to 20%. If the intensity of a transition is less than 0.1%, the error in that number is high and the measured value carries little meaning. Though certainly seen, they are not listed with any greater detail. In order to ascertain that a given transition exists, many coincident gates are considered and intercompared to observe complete consistency. If a level was not seen with certainty it is listed in parenthesis.

Shown extensively in this section are spectra from the 4d coincidence hypercube that has been built. As was mentioned in Section 4.3.1, the 4d hypercube has been built to allow for the possibility of finding transitions that may have been hidden by contamination from other transition pathways in the data set with similar energies. Examples showing the advantages of using the 4d hypercube are shown.

7.1.1 ^{143}Ba

The levels in ^{143}Ba are shown in Fig. 7.1, with 7 new levels compared to earlier work [96], and the addition of linking E1 transitions up the bands. With the strong statistics found in our data, the level scheme of ^{143}Ba has been extended up to $(43/2^{+})$. We have added 7 new levels at 3123.6, 3699.1, 4403.7, 4588.7, 4788.9, 5432.9,and 5685.4 keV. No new angular correlations are measured for this isotope and values for spins and parities are reasonable extensions of the s= -i and +i bands, and no new band structures or transitions are seen. An example of how we know these new transitions exist is shown in figure 7.2. Since we know the 691.7 and 593.8 keV transitions, we gate on them and we see known transitions at 778.8, and 625.7 keV. This gate does not show the 727.3 keV line, which is depopulating the state at 2998.8 keV to feed another 691.7 keV line in the s= -i band depopulating the $25/2^{-}$ state at 2271.5 keV. This is evidence that the background

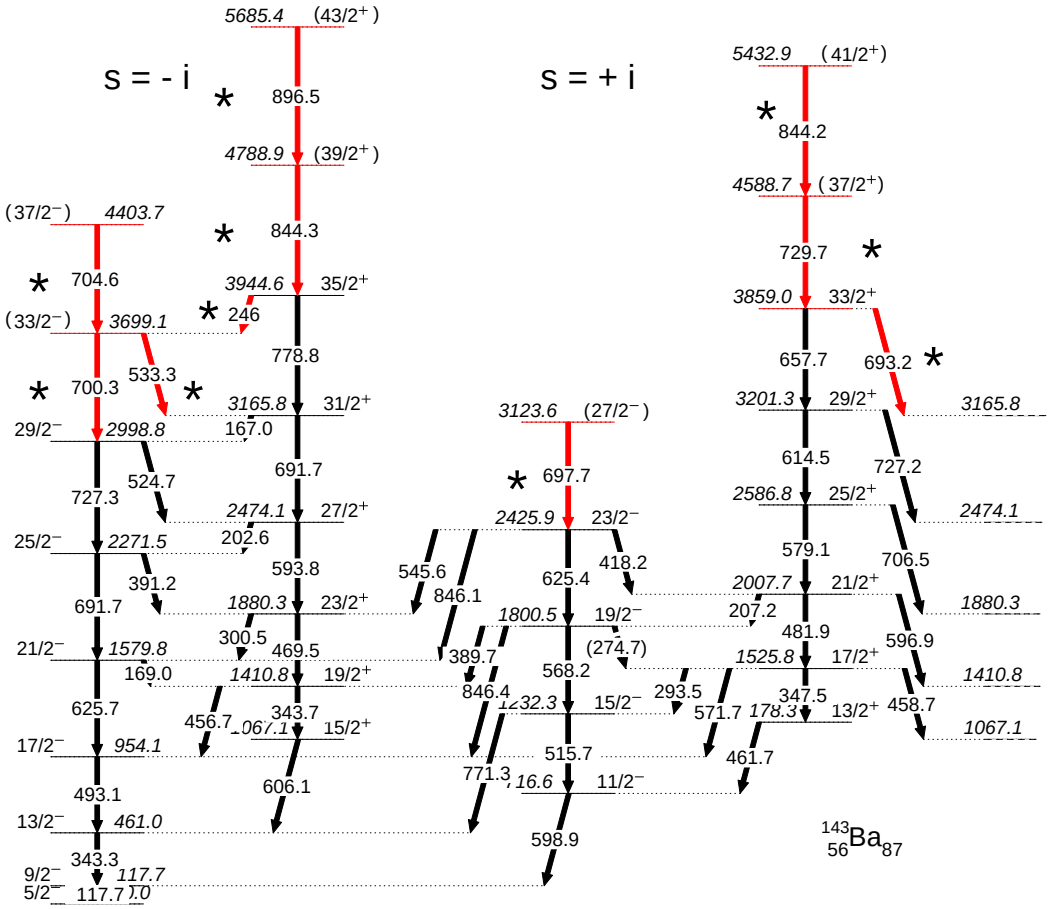

Figure 7.1: Level scheme showing new levels and transitions (marked with * and in red) in ^{143}Ba.

and contamination in this gate are low. We then see 4 new transitions (marked with an *), at 533.3, 704.6, 844.3 and 896.5 keV. A similar process is used throughout and many coincident gates are checked to confirm that a given transition exists.

7.1.2 ^{144}Ba

The level scheme of ^{144}Ba shown in Fig. 7.3 now goes up to (20^+) and (21^-) in the previously assigned s= +1 band [98]. Now, via angular correlations, very strong evidence has been found to support the s= -1 assignment for the side band found in [103]. It should be mentioned that the 5^+ level at 1882.0 keV was seen by [103] but not placed in the level scheme and band structure as it is now. The decay pattern and selection rules applied to these decays would make a different assignment of the spin and parity of these states unlikely, but with the measurement of

Table 7.1: Details of the new gamma ray data found in this work in $^{143-146}$Ba

E_γ	I_γ	E_i	J^π	E_γ	I_γ	E_i	J^π	E_γ	I_γ	E_i	J^π
^{143}Ba											
343.3	100	461.0	$\frac{13}{2}^-$	245.5*	0.1	3944.6	$\frac{35}{2}^+$	533.3*	1.0	3699.1*	$\frac{33}{2}^-$
693.2*	0.2	3859.0	$\frac{33}{2}^+$	697.7*	0.1	3123.6*	$\frac{27}{2}^-$	700.3*	0.5	3699.1*	$\frac{33}{2}^-$
704.6*	0.5	4403.7*	$\frac{37}{2}^-$	729.7*	0.2	4588.7*	$\frac{37}{2}^+$	844.3*	0.3	4788.9*	$\frac{39}{2}^+$
896.5*	0.1	5685.4*	$\frac{43}{2}^+$								
^{144}Ba											
110.7*	0.3	1992.7	6^-*	(113.0)	<0.4	1769.0*	(3^+)	213.7*	0.4	1992.7	6^-*
239.7*	<0.1	2904.9	10^-	331.0	100	530.5	4^+	341.8*	0.1	5029.1*	(19^-)
376.2*	0.1	3281.1*	11^+	384.7*	0.1	5413.8*	(20^+)	443.5*	0.1	4687.3*	(18^+)
472.6*	0.2	3993.0	(16^+)	590.1*	0.9	2364.0	8^-	615.9*	0.1	3281.1*	11^+
620.0*	0.3	2665.2	9^+	636.7*	1.2	1992.7	6^-*	655.5	2.3	3520.4	15^-*
688.9*	0.5	2160.4	7^+*	694.3*	0.5	4687.3*	(18^+)	726.5*	0.3	5413.8*	(20^+)
739.5*	0.7	1779.0*	(4^-)	785.3*	0.2	5029.1*	(19^-)	804.4*	0.3	2160.4	7^+*
833.6*	<0.1	5862.7*	(21^-)	891.3*	0.8	2665.2	9^+	930.4*	0.1	1769.0*	(3^+)
1030.7	0.7	1992.7	6^-*	1131.0*	0.4	2904.9	10^-	1193.7*	0.2	2665.2	9^+
1198.4	1.1	2160.4	7^+*	1235.9*	0.1	3281.1*	11^+	1238.5*	0.2	1769.0*	(3^+)
1351.5	2.1	1882.0	5^+*	1569.5*	0.5	1769.0*	(3^+)				
^{145}Ba											
112.9	100	112.9	$\frac{7}{2}^-$	155.0	29	618.3	$\frac{13}{2}^+$	164.7	28	277.6	$\frac{9}{2}^-$
185.7	24	463.3	$\frac{11}{2}^-$	277.6	7.9	277.6	$\frac{9}{2}^-$	292.1*	0.1	3922.7	$\frac{39}{2}^-$
316.2*	<0.1	386.4	$\frac{25}{2}^-$	350.4	18	463.3	$\frac{11}{2}^-$	364.2	12	641.8	$\frac{13}{2}^-$
395.5	10	508.4	$\frac{11}{2}^-$	539.7*	<0.1	3293.1*	$\frac{33}{2}^-$	546.7*	0.12	2753.4*	$\frac{29}{2}^-$
551.6*	0.1	3844.7*	$\frac{37}{2}^-$	584.2*	0.1	2474.7*	$\frac{27}{2}^+$	653.0*	<0.1	3127.7*	$\frac{31}{2}^+$
755.8*	0.2	4386.4*	$\frac{41}{2}^-$								
^{146}Ba											
164.5*	3.3	1968.3*	(6^-)	169.3*	0.5	2330.3*	(8^-)	185.0*	7.4	1968.3*	(6^-)
192.7*	0.3	2161.0*	(7^+)	213.9*	<0.1	3737.4	(16^+)	316.3*	0.1	3192.8	14^+
339.7*	0.1	2632.4	12^+	357.2*	2.8	2161.0*	(7^+)	362.0*	0.7	2330.3*	(8^-)
373.5*	6.6	2191.5	9^-	377.7*	4.1	2161.0*	(7^+)	386.5*	0.3	2161.0*	(7^+)
425.1*	0.1	1774.5*	(6^+)	465.1*	0.3	3176.7*	(13^-)	581.2*	1.0	4318.6*	(18^+)
585.2*	0.5	2530.2	(9^-)	618.9*	0.1	1968.3*	(6^-)	647.0*	0.5	3523.5*	(15^-)
678.2*	0.6	2161.0*	(7^+)	712.2*	1.0	2530.2	(9^-)	793.2*	0.3	1818.0*	(7^-)
811.6*	0.4	2161.0*	(7^+)	824.8*	6.7	1783.3*	(5^+)	845.3*	1.9	1803.8*	(5^+)
859.5*	3.9	1818.0*	(7^-)	948.7*	0.5	1973.5	(7^-)	1030.9*	1.3	1989.4*	(7^+)
1261.0*	0.8	1774.5*	(6^+)	1289.9*	0.4	1803.8*	(5^+)				

Table 7.2: Details of the new gamma ray data found in this work in ^{148}Ce

E_γ	I_γ	E_i	J^π	E_γ	I_γ	E_i	J^π	E_γ	I_γ	E_i	J^π
^{148}Ce											
109.5*	0.1	2205.3*	(9^+)	155.6*	0.2	1380.4*	(5^+)	158.7	100	158.7	2^+
167.1	9.0	1953.8	8^-*	183.2*	1.0	1024.7*	5^-	203.8*	4.0	1788.9	(7^+)
204.7*	0.6	1585.1	6^+*	282.2*	0.2	2487.5	(10^+)	290.4*	0.6	1380.4*	(5^+)
295.2	82	453.9	4^+	328.1*	6.5	1352.8	7^-	353.5	9.9	2307.3	10^-*
363.3	7.1	1786.7	7^+*	386.1	63	840.0	6^+	398.7*	2.4	1423.4	5^+*
408.5*	1.9	1788.9	(7^+)	416.4*	0.2	2205.3*	(9^+)	444.6	3.4	2751.9	12^-*
451.1	39	1291.1	8^+	463.5	3.5	1754.6	9^-*	497.8*	11.6	1788.9	(7^+)
552.7*	0.4	2307.3	10^-*	570.8*	3.4	1024.7*	5^-	601.0*	2.3	1953.8	8^-*
663.2	2.2	1117.1	3^+*	745.1	4.0	1585.1	6^+*	770.9	3.3	1224.8	4^+*
914.2*	0.3	2205.3*	(9^+)	926.5*	0.1	1380.4*	(5^+)	931.3*	0.4	1090.0*	(3^+)
958.4	9.1	1117.1	3^+*	969.5	7.3	1423.4	5^+*				

angular correlations these assignments are certain.

Four new levels extend the s= +1 band including four new linking E1 transitions with measurable intensity. Three of these new transitions can be seen in Fig. 7.6, which shows a great deal of clarity by using the 4d-hypercube.

In addition, many gammas have been found that confirm the previous assignment of levels based on selection rules. Furthermore, we propose a level at 1769.0 keV as the 3^+ level for the s= -1 band. In order to find a transition of 1569.5 keV to the 2^+ level, we looked at the spectra formed from a gate on 199.5 keV and its fission partners and subtracted by a gate on the 331.0 and 199.5. This gate, shown in figure 7.5 drastically reduces the level of the background and allows us to identify the peak at 1569.5 clearly and then gate on it along with several other transitions to identify it as a real peak. This same process, along with the peak shape being very narrow, allows us to identify the peak at 966 keV as background.

Evidence is also shown for placing the previously known level at 1882.0 keV into the band structure now assigned to be an s = -1 band. The spectrum shown in Fig. 7.6 is fdrom a triple gate on 199.5, 331.0, and 1351.5 keV shows a new transition at 110.7 keV and a known transition at 371.3 keV, which links this newly measured 5^+ state to the rest of this band structure very well.

In addition, angular correlation measurements listed in Table 7.3 now reveal levels consistent only with spin values of 5 at 1882.0 keV, 6 at 1992.7 keV, and 7 at 2160.4 keV and with mixing

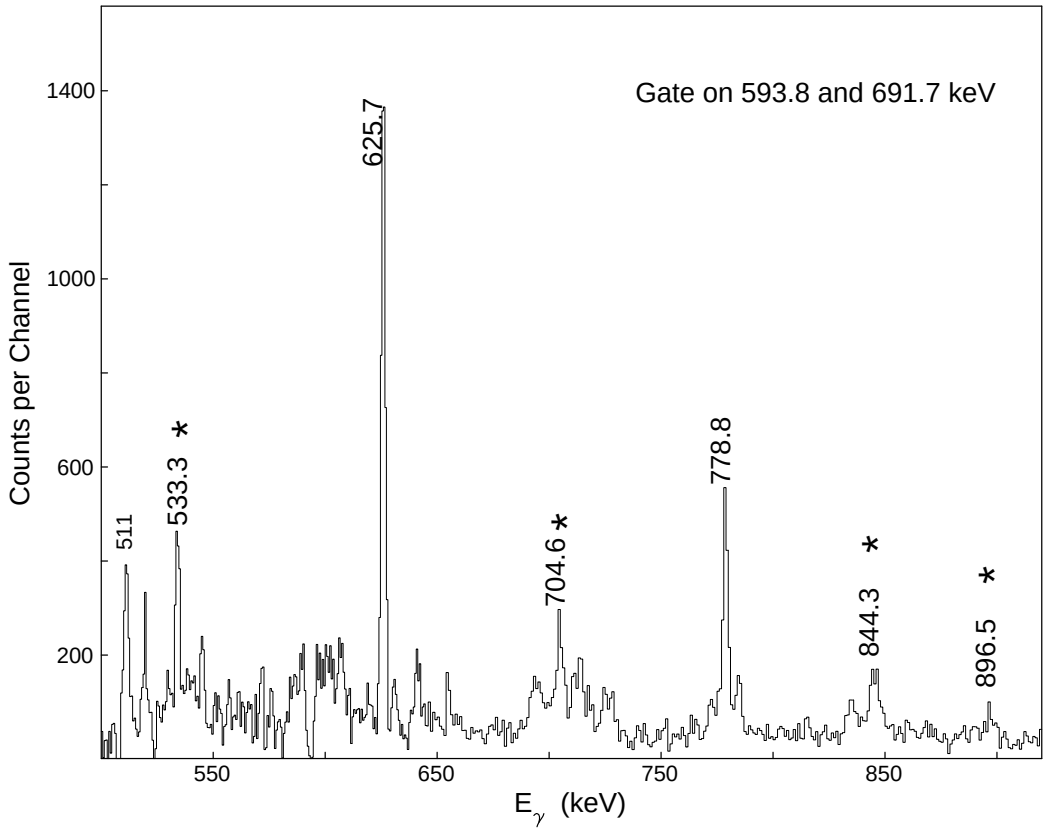

Figure 7.2: New transitions seen in a gate on the 593.8 and 691.7 keV γ rays in the s= -i band in ^{143}Ba. The 625.7 keV transition is seen because of the strong 300.5 keV transition that decays into it.

ratios only consistent with the alternating parity assignment of a 5^+,6^-,7^+. It can be seen in Fig. 7.7 that the shape of the correlation curve associated with the negative parity state is inverted compared to the positive parity states even though both are I→I-1 transitions. In addition, the transitions now seen within the s= -1 and connecting the s= -1 band to the s= +1 band are sufficient to assign the spins and parities of the 8^-, 9^+, 10^-, and 11^+ levels as well.

7.1.3 ^{145}Ba

In ^{145}Ba, we have extended both simplectic band structures over previous studies [95, 96]. The new level scheme is shown in figure 7.8. In total, we have found 6 new levels and 8 new gamma rays. The transitions from the positive parity members of the s= +i band to the negative parity members of the same band were expected but not observed. However, because of the level energy

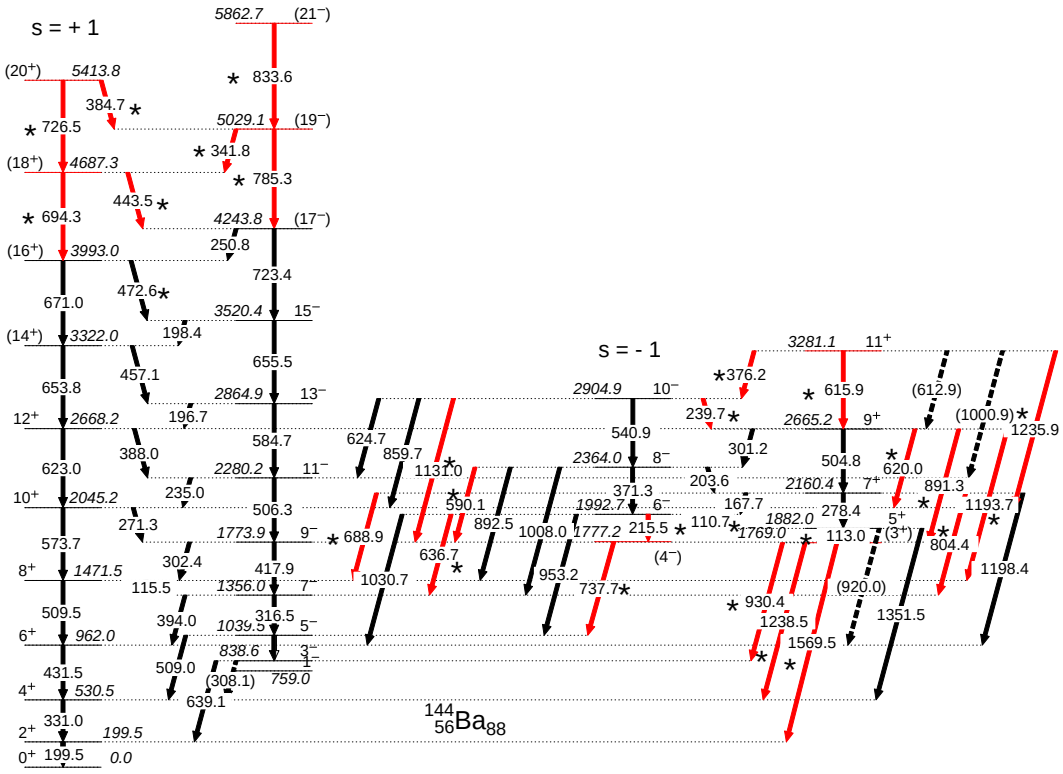

Figure 7.3: Level scheme showing new levels and transitions (marked with * and in red) in ^{144}Ba.

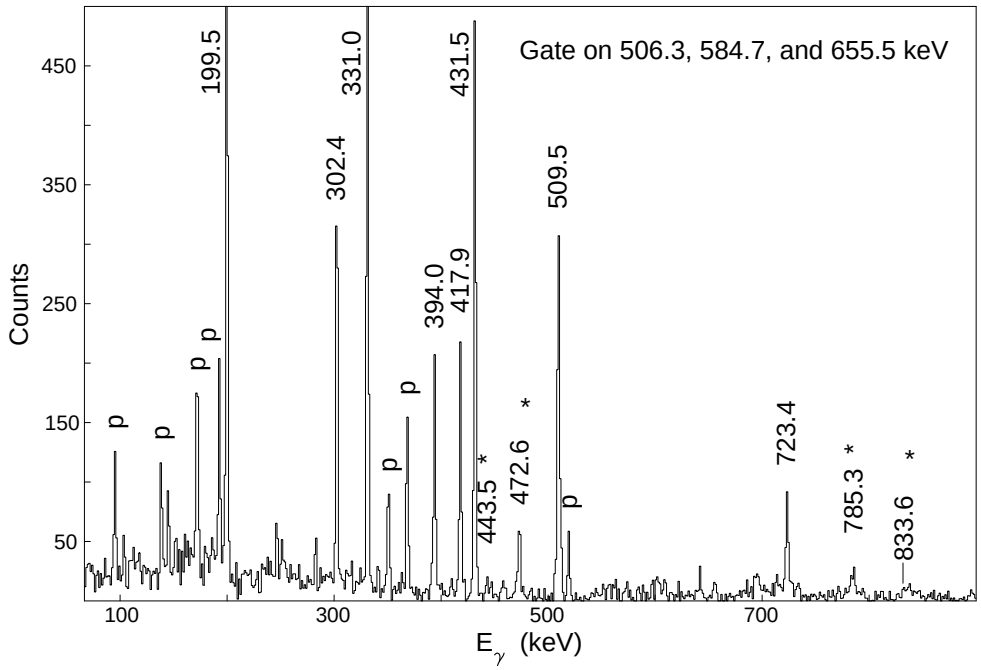

Figure 7.4: Spectrum showing the gate on 506.3, 584.7 and 655.5 keV found in ^{144}Ba. New transitions labeled with an asterisk(*), partner transitions are labeled with a p.

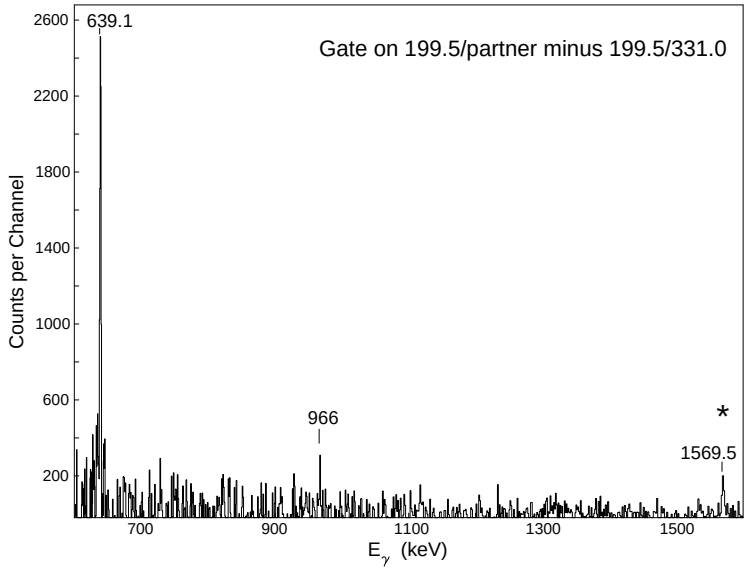

Figure 7.5: New ^{144}Ba transition seen in a gate on the 199.5 keV and Mo partner transitions minus the gate on the 199.5 and 331.0 keV transitions. The 1569.5 keV transition is new and the 966 is background.

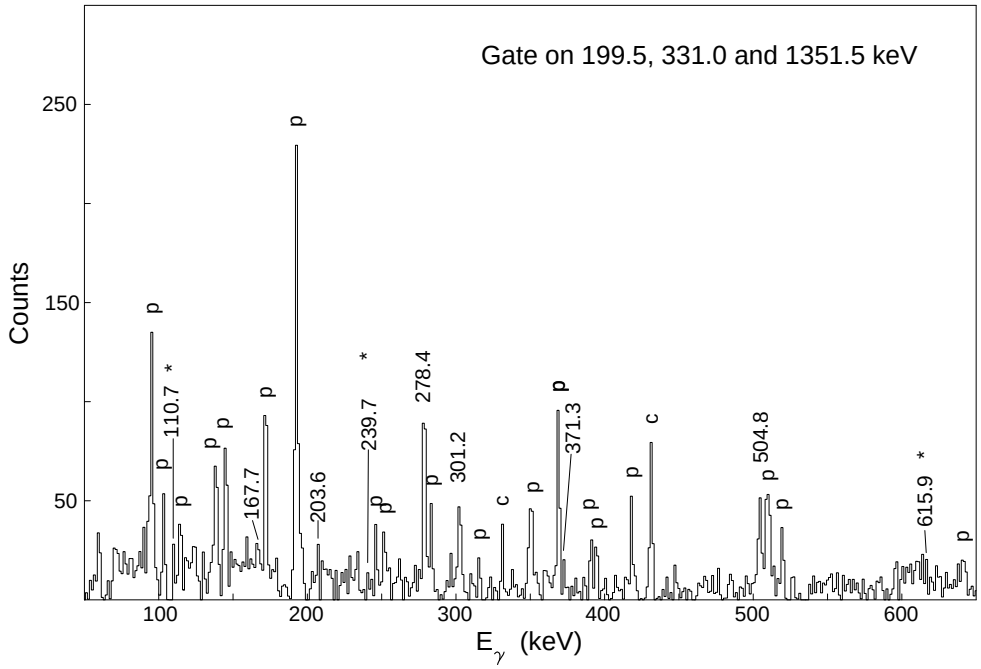

Figure 7.6: Spectrum showing the gate on 199.5, 331.0, and 1351.5 keV found in ^{144}Ba. New transitions labeled with an asterisk(*), partner transitions are labeled with a p.

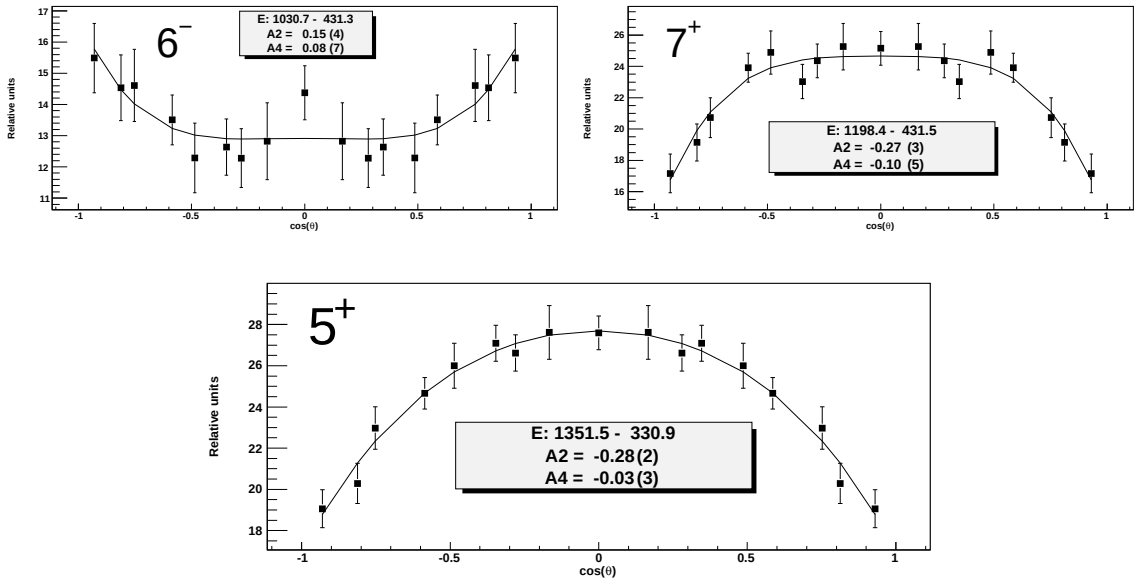

Figure 7.7: Angular correlations for the determination of spins and parities of levels in ^{144}Ba

spacing, the most likely observation could have been a transition from the $33/2^+$ level at 2924.0 keV to the $(31/2^-)$ level at 2726.1 keV and in the s= -i band the highest spin level depopulated by a tentative E1 transition is a $25/2^-$ level at 2206.7 keV. So, there may not be sufficient intensity at this energy in the s = +i band. It can be seen in figure 7.8, that the s= -i band fits well qualitatively with what one expects for a simplectic band. Starting at the $17/2^-$ level at 1098.6 keV we begin to see interlinking transitions in this band as well as the fact that the energy of the π=+ part of this band falls very near to halfway in between the π= - levels in this band. The evidence for the new transitions placed in this band is shown in Fig. 7.9. This spectrum shows the 546.7, 539.7, and 551.6 keV transitions placed on top of the clearly seen and previously known 566.3 keV transition in the s = -i band. The 584.2 keV transition in the proposed π=+ half of this band may also be seen via coincidence with a weak transition of 250.1 keV that is obscured by a partner transition from ^{103}Mo.

This study also differs from the previous report [96] with statistically poorer data where now the level at 1940.6 keV has been removed for lack of evidence for a 546.1 keV transition in the gate on the transitions at 527.5 and 248.2 keV. We have also performed angular correlations on the lower spin levels in this isotope to give better measures of the mixing ratios for these gamma

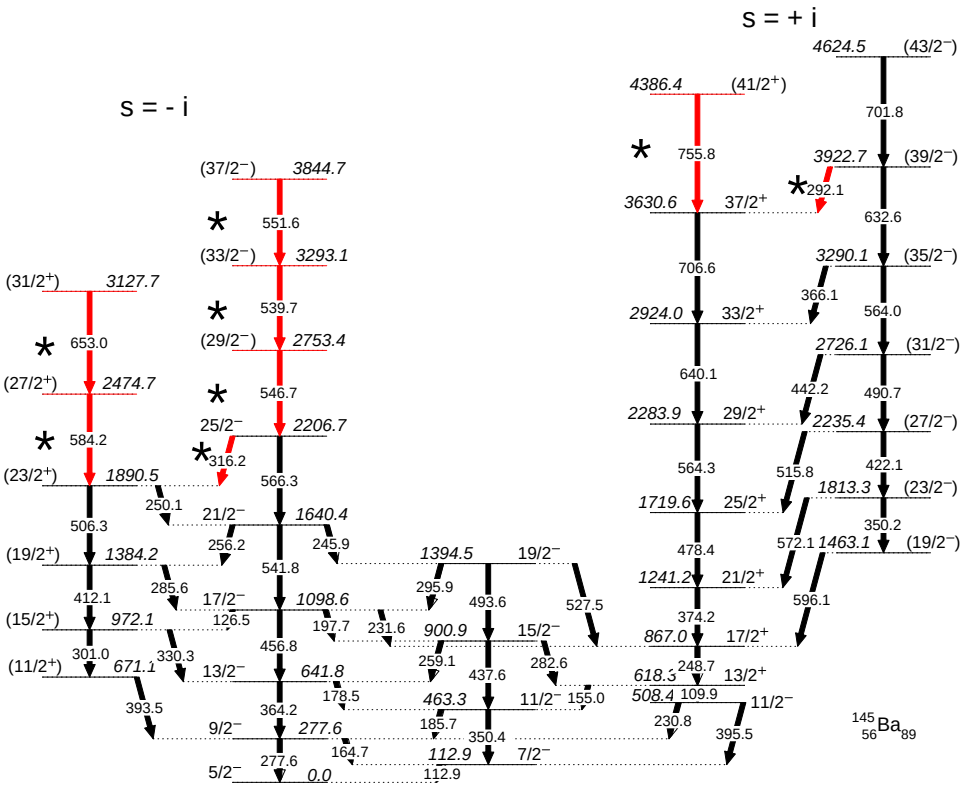

Figure 7.8: Level scheme showing new levels and transitions (marked with * and in red) in ^{145}Ba

rays [95]. Though attempted, because of contamination in the 330 keV line (which occurs strongly in several isotopes in this data set), no new spin parity assignments could be made.

7.1.4 ^{146}Ba

For ^{146}Ba, we show only a partial level scheme in figure 7.13 and report only those bands where there is something new to be shown, mostly over the work in ref. [103]. The s= +1 structure has been seen and extended in the π= + and - bands to (20^+) and (17^-) respectively. In addition, several transitions are seen in this band depopulating the π= + band members, however, the interlinking transitions from the π= - levels are obscured by contamination though there is some evidence for them. Shown in figure 7.10 is a comparison of a double gate (bottom spectrum) on 514.7 and 583.8 keV showing a great deal of contamination from transitions in ^{110}Ru, ^{138}Xe and also ^{102}Zr. This serves to bury the new peak at 667.2 keV, which is seen much more clearly from the triple gated spectrum shown in the top of the figure. Dramatic suppression of contaminant

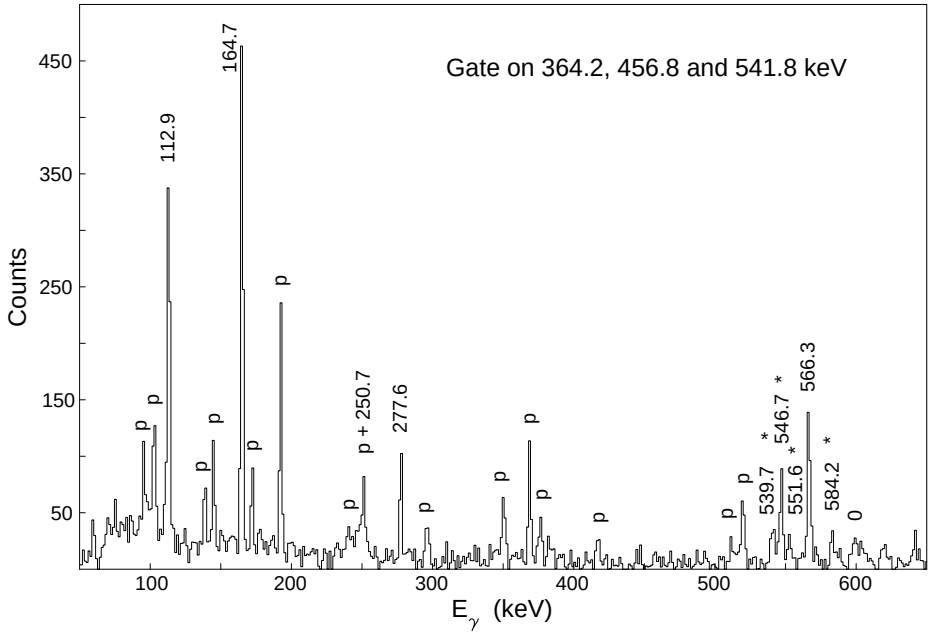

Figure 7.9: Spectrum showing some of the new transitions found in ^{145}Ba labeled with an asterisk(*). Partner transitions are labeled with a p.

peaks at 240.7, 459.0 and 151.8 keV can be easily seen.

Considering the side bands, it is interesting that much of the depopulation from different states occurs to the 6+ level in ^{146}Ba, and we have identified several more. Band (1) has been extended with a new level and two new transitions. We performed angular correlations in band (2) with the 607.7-524.4 keV gamma-rays (A2/A4= 0.14(3)/0.01(4)) and in band (3) with the 708.7-524.4 keV cascade (A2/A4= -0.07(3)/-0.01(4)). These correlations are most consistent (but not exclusively) with the previous assignments [103] made for these levels. The levels in band (2) have now been extended to (18^-). In band (4), three new transitions have been found. Since the previously known level at 2530.2 keV is now seen to decay to known 7^- and 9^- levels, a lower assignment of the spin of this level than the previous ($10,11^-$) is determined. Intensities of these three transitions are similar, therefore (8^+) is suggested. Because of the uncertainty of these suggestions for spins and parities, no structure is inferred for band 4.

There is still no clear s= -1 band in this nucleus, but a possible set of levels in band (5) all

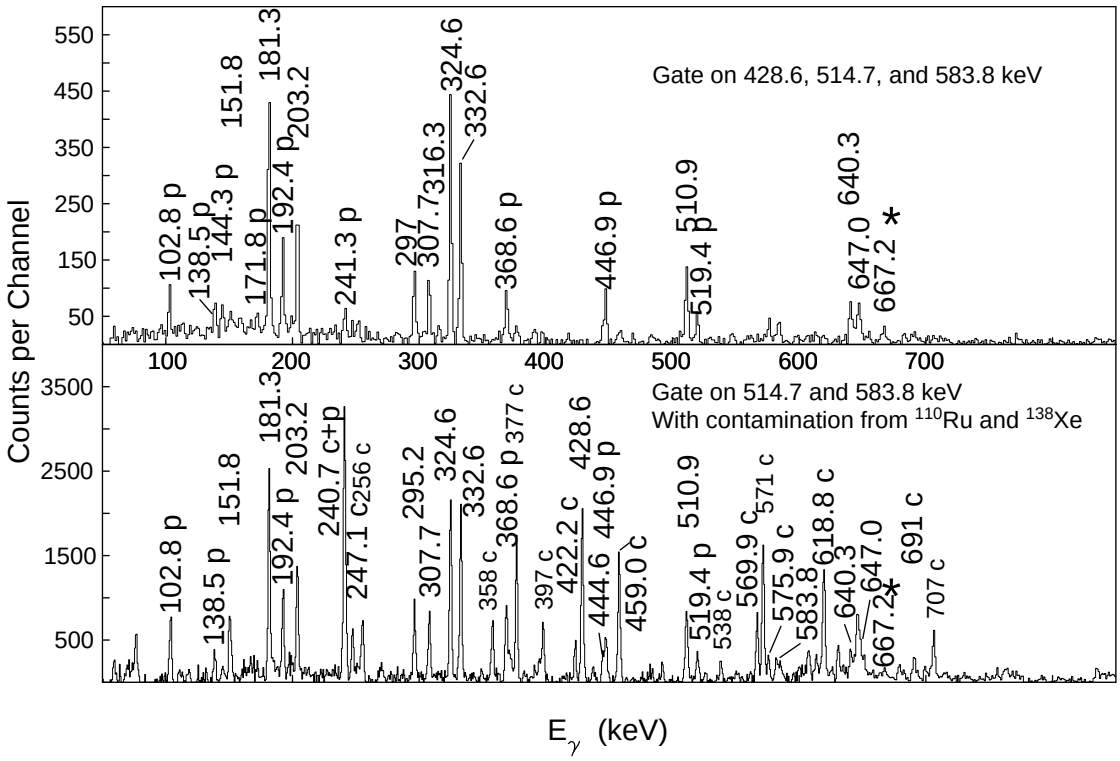

Figure 7.10: Spectra showing the improved peak to background and purity of a triple gate compared to a double gate used to identify a new peak in the s= +1,π=- band in ^{146}Ba. Here the partner peaks from Mo are labeled with a 'p' and known contaminants with a 'c'.

of which are new would fit that picture if spin and parity assignments could be made there. The decay pattern is consistent with an alternating parity band. However, there is only some qualitative description of low energy interlinking transitions that can be given at this time. The evidence for the placement of these new levels is shown in Figs. 7.11 and 7.12. The spectrum in Fig. 7.11 shows clear evidence for new transitions at 824.8 and 845.3. Gates on these transitions in Fig. 7.12 show the relative counts of low energy transitions at 164.5 and 185.0 keV compared to 357.2 and 377.7 keV respectively. The relative intensities are 1.2 for the 164.5/357.2 ratio and 1.8 for the 185.0/377.7 ratio. These values could potentially effect the value of the dipole moment of ^{146}Ba if spin and parity assignments could be made for the levels that they depopulate.

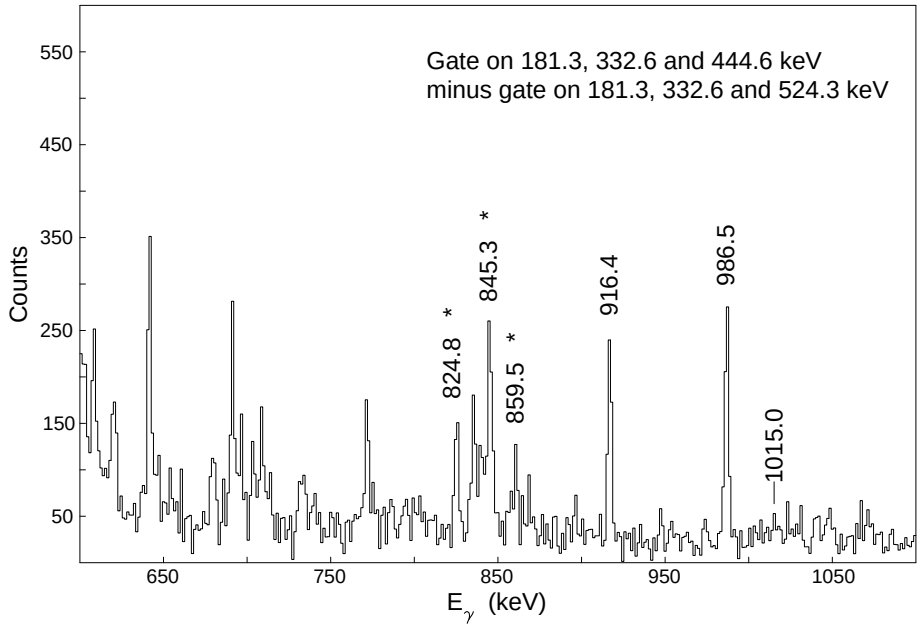

Figure 7.11: Triple gate on the lowest three yrast gamma rays minus a triple gate on the next highest yrast transition. This makes side band feeding more visible. New transitions are marked with an *.

7.1.5 ^{148}Ce

The new level scheme of ^{148}Ce over previous work [102] has 7 new levels, 22 new gamma rays and 9 new angular correlation measurements. The new levels and transitions are shown is shown in figure 7.14. In figure 7.15, the triple gated spectrum showing a peak at 574.9 keV is presented. This peak is not easily seen in double gates because of the 576.4 keV gamma ray in the yrast band. The higher fold coincidence has allowed us to resolve this doublet structure.

New transitions related to the s= -1 band are shown in Fig. 7.16. The 648.4 keV transition extends this band to (18^-). The 601.0 keV transition is one of several new transitions that links this band to the s= +1 band, and which are consistent with what one would expect for the assignments of spins and parities for these states.

A gamma vibrational band is now assigned where a beta vibrational band was thought to occur [97]. It was thought that this state at 936.2 keV, was part of a beta vibrational band because

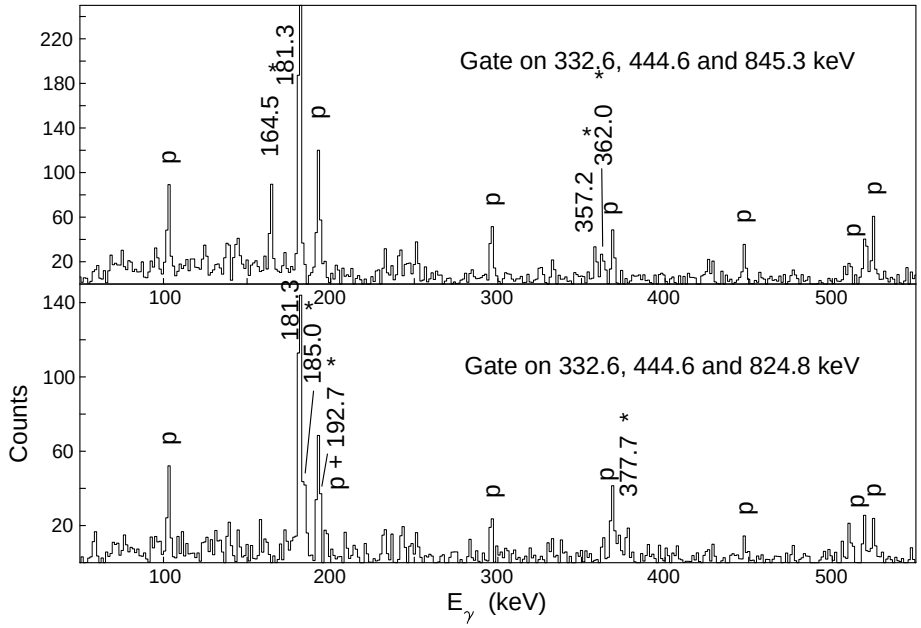

Figure 7.12: Triple gates on yrast gammas with 845.3 and 824.8 keV showing the significant enhancement of low energy transitions (164.5 and 185.0 keV) compared to high energy transitions (357.2 and 377.7 keV).

of a systematic observation that other N=90 isotopes such as those in Nd had an assigned beta vibrational band where the I→I-2 transitions were not observed. There is no known physical reason that this should be the case. According to the collective model selection rules, there should be no difference for the transistion strength between the gamma or beta band 2^+ level and the ground state band. The new interpretation of these levels being part of a gamma vibrational band is based on the existence of interlinking gamma rays up to the (9^+) level. It is still an open question as to why the I→I-2 transitions from the even spin members of this band to the yrast band are not observed. Yet, it seems that the gamma vibrational band assignment is the one that is most consistent.

Angular correlations have been measured in order to assign spins and parities for the states at 1224.8 keV and 1585.1 keV to be 4^+ and 6^+ respectively. The values for all correlations are given in Table 7.3 and the correlation curve for the 295.2-770.9 cascade is shown in Fig. 7.17. Additionally, we have been able to extend the s= +1 to high spin (22^+) and the correlation between the 463.5

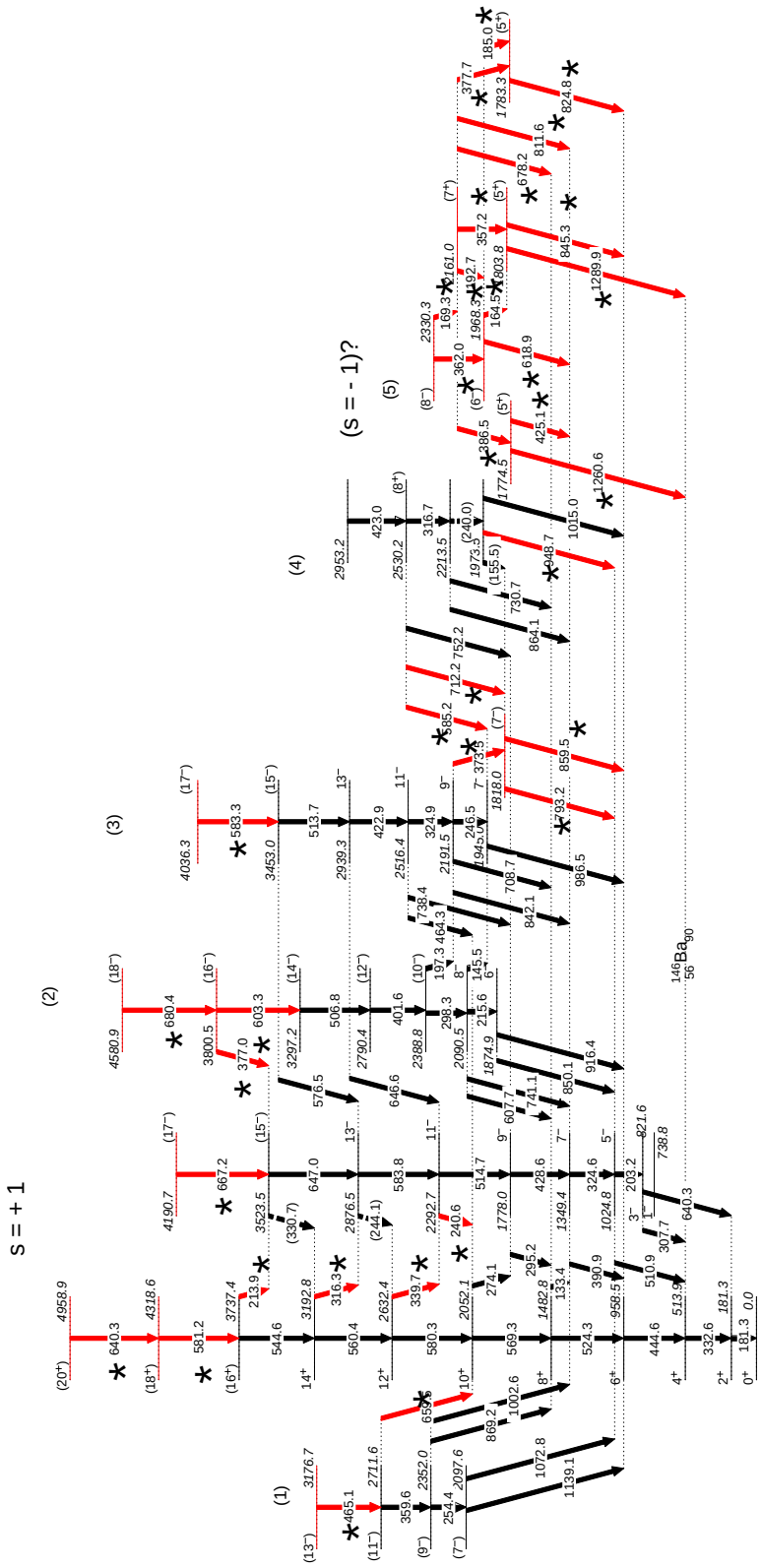

Figure 7.13: Partial level scheme showing new levels and transitions (marked with * and in red) in ^{146}Ba

Table 7.3: Angular Correlation values for ^{144,145}Ba, and ^{148}Ce

Gate (mixing D,Q,O)	A2 / A4 Coefficients	mixing ratio δ
^{144}Ba		
655.5/584.7 (Q,O→Q)	0.11 (1) / 0.04 (2)	0.02(3)
1198.4/431.5 (D,Q→Q)	- 0.27 (3) / - 0.10 (5)	-3.5 (7)
1351.5/331.0 (D,Q→Q)	- 0.27 (2) / - 0.03 (3)	-4.4 (7)
1030.7/431.5 (D,Q→Q)	0.15 (6) / 0.08 (7)	0.13 (16)
^{145}Ba		
350.0/112.9 (Q→D,Q)	- 0.11 (1) / 0.01 (2)	0.11 (4)
185.7/277.0 (D,Q→Q)	- 0.21 (2) / 0.00 (2)	0.20 (4)
364.0/165.0 (Q→D,Q)	- 0.15 (2) / - 0.02 (2)	-0.18 (4)
^{148}Ce		
295.4/663.0 (Q→D,Q)	0.05 (5) / - 0.24 (8)	10 (6)
969.9/295.4 (D,Q→Q)	- 0.06 (1) / - 0.09 (2)	9.6 (14)
363.7/969.5 (Q→D,Q)	0.03 (2) / - 0.02 (3)	*unk*
167.1/363.5 (D,Q→Q)	- 0.04 (2) / - 0.04 (4)	0.04 (4)
353.0/167.0 (Q→D,Q)	- 0.07 (3) / - 0.01 (4)	0.00 (6)
353.5/444.6 (Q→Q,O)	0.16 (3) / 0.03 (5)	0.14 (8)
295.2/770.9 (Q→D,Q)	- 0.02 (2) / 0.16 (4)	3.8 (9)
386.3/745.1 (Q→D,Q)	- 0.07 (2) / 0.13 (4)	4.5 (18)
450.7/463.3 (Q→D,Q)	- 0.06 (2) / - 0.01 (2)	0.01 (3)

and 451.1 keV gamma rays yields a δ of 0.01(3) in the 463.5 keV gamma ray depopulating a spin 9 level at 1754.6 keV. The gamma ray is therefore assigned to be of an E1 character and the level it depopulates is assigned to be 9^-. We also show that for the s= -1 band, two angular correlations firmly assign the spin parity values to the 3^+ and 5^+ levels, while two other cascades, the 353.0-167.0 keV and the 167.0-363.5 keV cascades both show that there is no dipole-quadrupole mixing in the 167.0 keV transition. This gamma is therefore a pure E1 and there is a parity shift between the states as was previously reported from conversion coefficient measurement [102]. This, with what has been seen in ^{144}Ba, confirms what was first proposed [37], that even-even isotopes would have two simplex characterized rotational bands. Until now, these spins and parities had not been firmly assigned. The results from all angular correlations are summarized in Table 7.3.

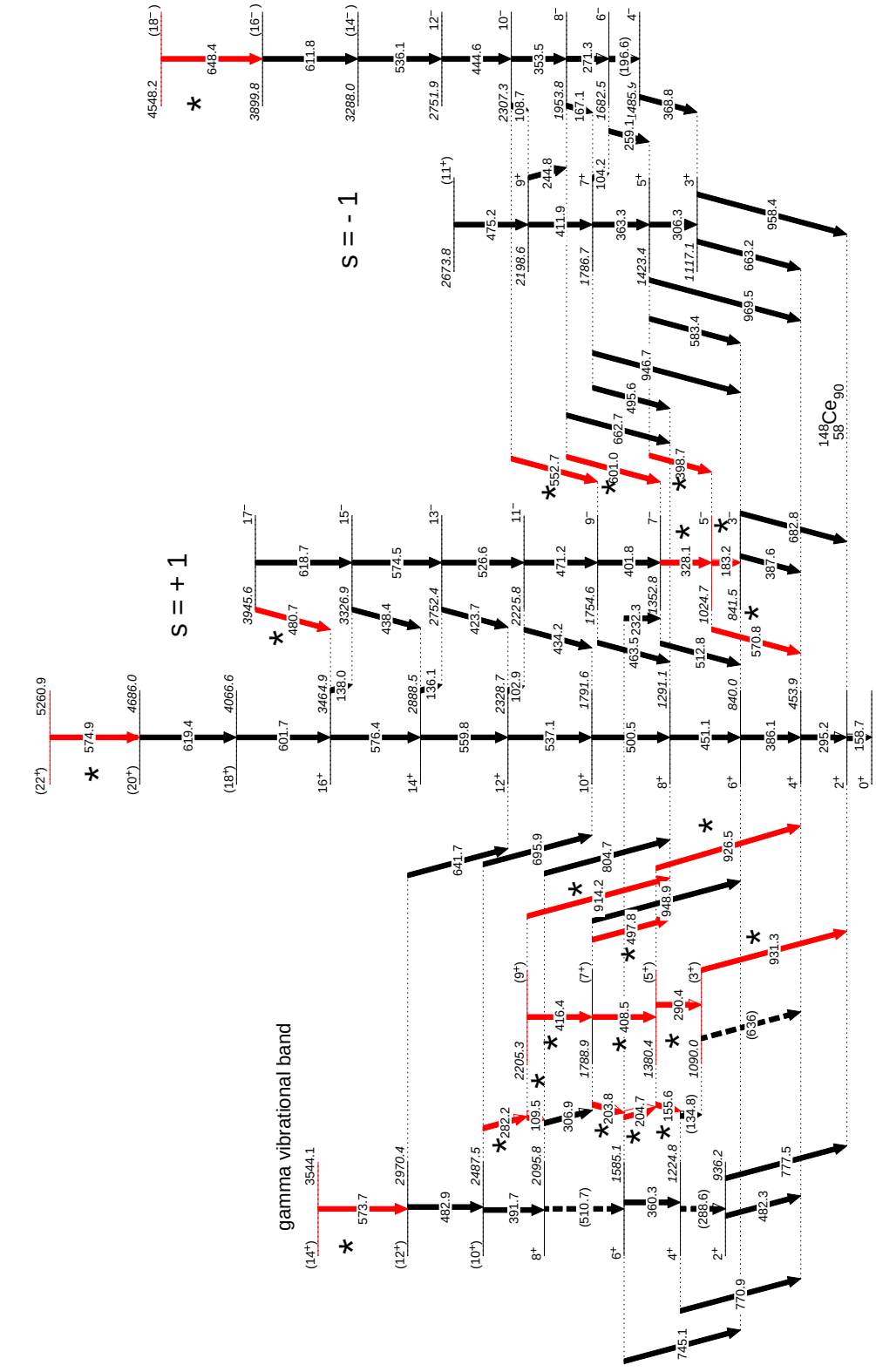

Figure 7.14: Levels scheme showing new levels and transitions (marked with * and in red) in ^{148}Ce

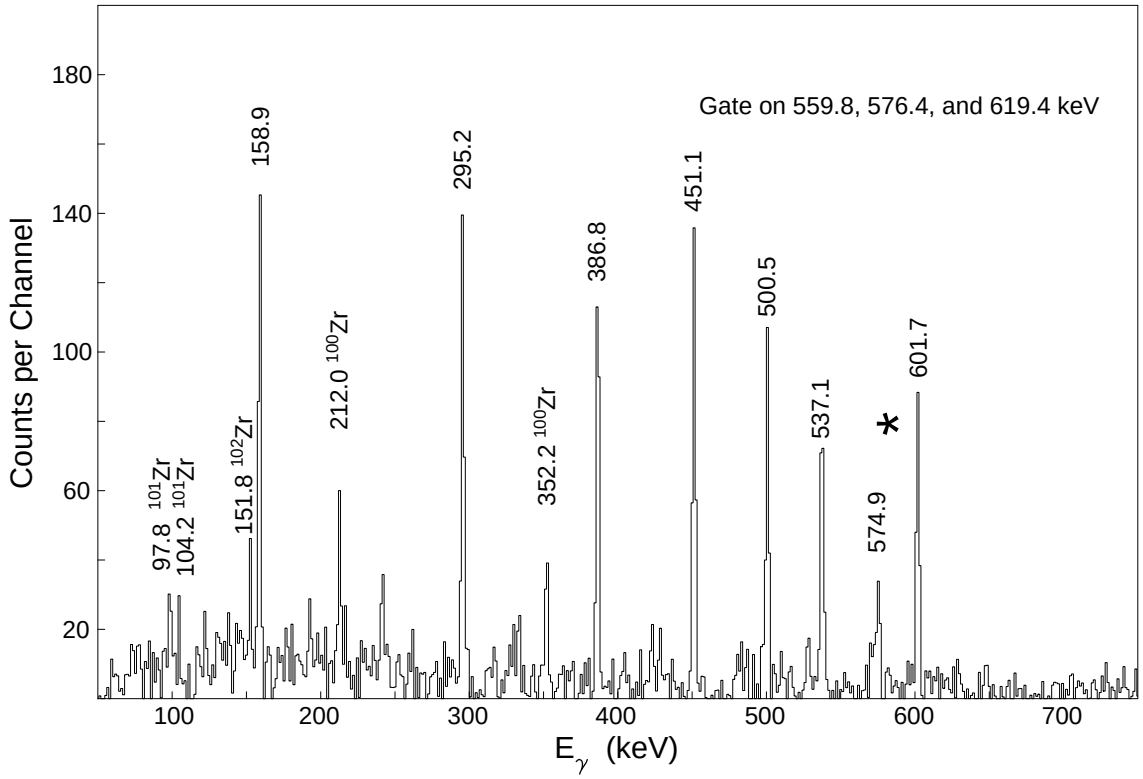

Figure 7.15: Triple gate showing a new 574.9 keV transition depopulating a (22^+) level in ^{148}Ce

7.2 Discussion

The geometric model [37] provides helpful analysis of new states and trends in these nuclei. We show the analyses in Fig. 7.18 They are found in three formulae. It is well established that these nuclei have mixed rotational/vibrational character closer to the ground state. We give the extension of these formulae to analyze new higher spin states. It should be noted, however, that band (5) in ^{146}Ba is not included in these analyses. Rotation should stabilize the vibrational mode and these formulae reveal the qualitative balance between these degrees of freedom.

$$\delta E(I) = E(I)^- - \frac{(E(I+1)^+ - E(I-1)^+)}{2}$$

The energy displacement formula is a way to quantify deviations from an asymmetric rigid rotor, where negative parity levels would lie halfway between the positive parity levels. Therefore, $\delta E \approx 0$ is an indication of the stabilization of octupole deformation.

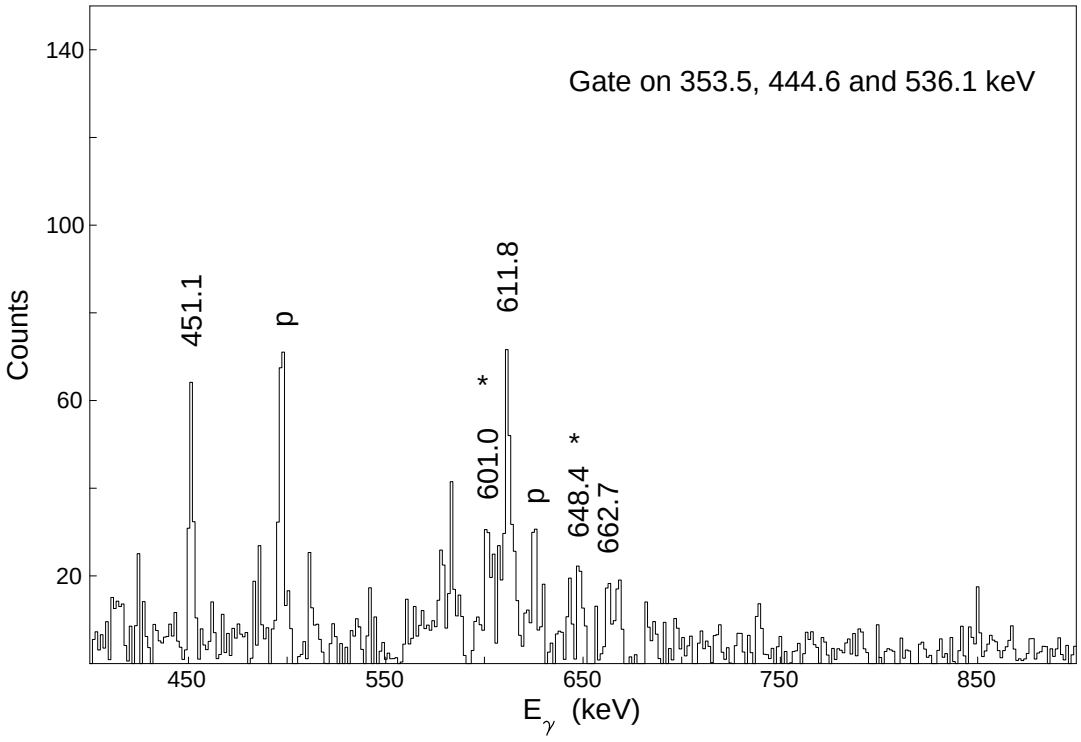

Figure 7.16: Triple gate on known gamma rays in the s =-1 band in ^{148}Ce

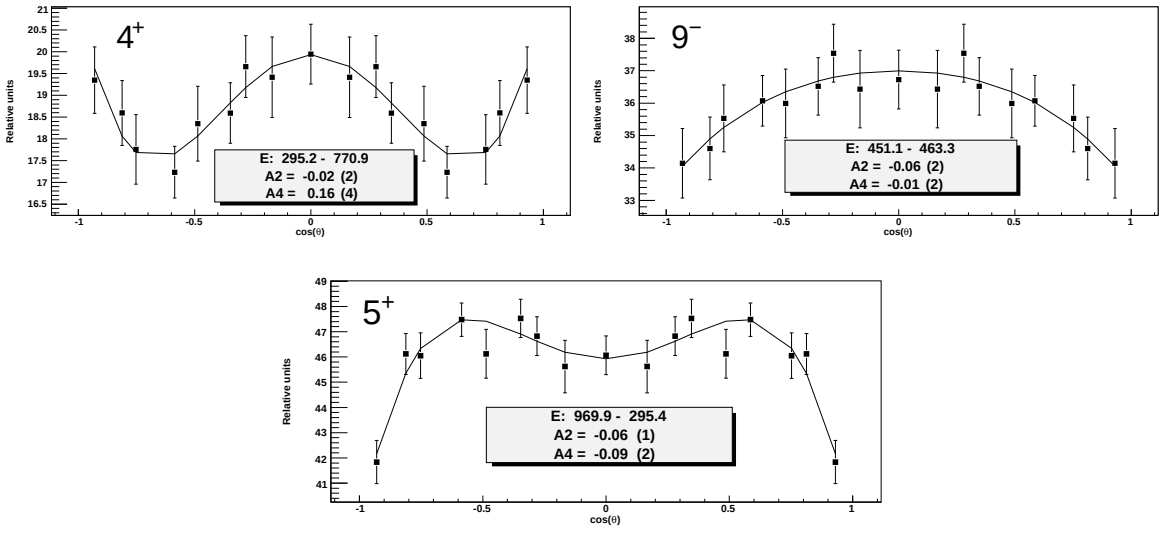

Figure 7.17: New angular correlations uniquely determine the spins and parities of 4^+,9^-, and 5^+ levels in ^{148}Ce.

The rotational frequency ratio is a collective model measure, which assumes pure rotational levels and that each gamma depopulating a level has an energy of $\hbar\omega$. The ratio of the positive parity states to the negative parity states is then expressed in terms of the level energies.

$$\frac{\omega(I)^-}{\omega(I)^+} = \frac{2[E(I+1)^- - E(I-1)^-]}{[E(I+2)^+ - E(I-2)^+]}$$

The limits we expect to see are, $\frac{\omega(I)^-}{\omega(I)^+} = 1$ for angular momentum stabilized octupole deformation and the limit we expect to see for a rotational level built off an octupole phonon is, $\frac{\omega(I)^-}{\omega(I)^+} = \frac{2I-5}{2I+1}$, called the vibrational limit. Furthermore, the intrinsic dipole moment [41] is expressed as:

$$D_0 = \sqrt{\frac{5B(E1)}{16B(E2)}}\ Q_0$$

It is a way to analyze deformation as well as other effects that may be present in the nucleus [37, 41]. $\frac{B(E1)}{B(E2)}$ ratios are found from relative intensity measurements. However, the aforementioned E1 transitions and their strengths give strong evidence that a band is rotational rather than mixed rotational/vibrational in nature. However, this is stated cautiously because octupole deformation is not the only thing that can cause a non-zero dipole moment [11, 37, 41]. The interpretation of the drop in D_0 in ^{146}Ba is that there are several cancellation effects in the shell correction contribution as well as the macroscopic contribution to D_0. This theoretical approach, from reflection asymmetric mean field theory, as well as others are reviewed in [11].

Energy displacement $\approx$0 indicates likely spin states where the nuclear angular momentum stabilizes the deformation of the nucleus. The results from the current study are shown in Fig. 7.18 part a. The low spin states, which tend to have higher values, likely have a vibrational component. In all cases we see values, at medium to high spin, near to δE=0. For ^{143}Ba we now see the s= -i band begin to turn back closer to 0, however the s= +i continues to increase. The s= +1 band in ^{144}Ba continues to stay very near -100 keV. For the first time we present the values of these variables in this isotope for the s= -1 and we note that these values are all less than 100 keV below δE=0. We see the values for the s= -i band in ^{145}Ba are all very close to 0, but only the last two in

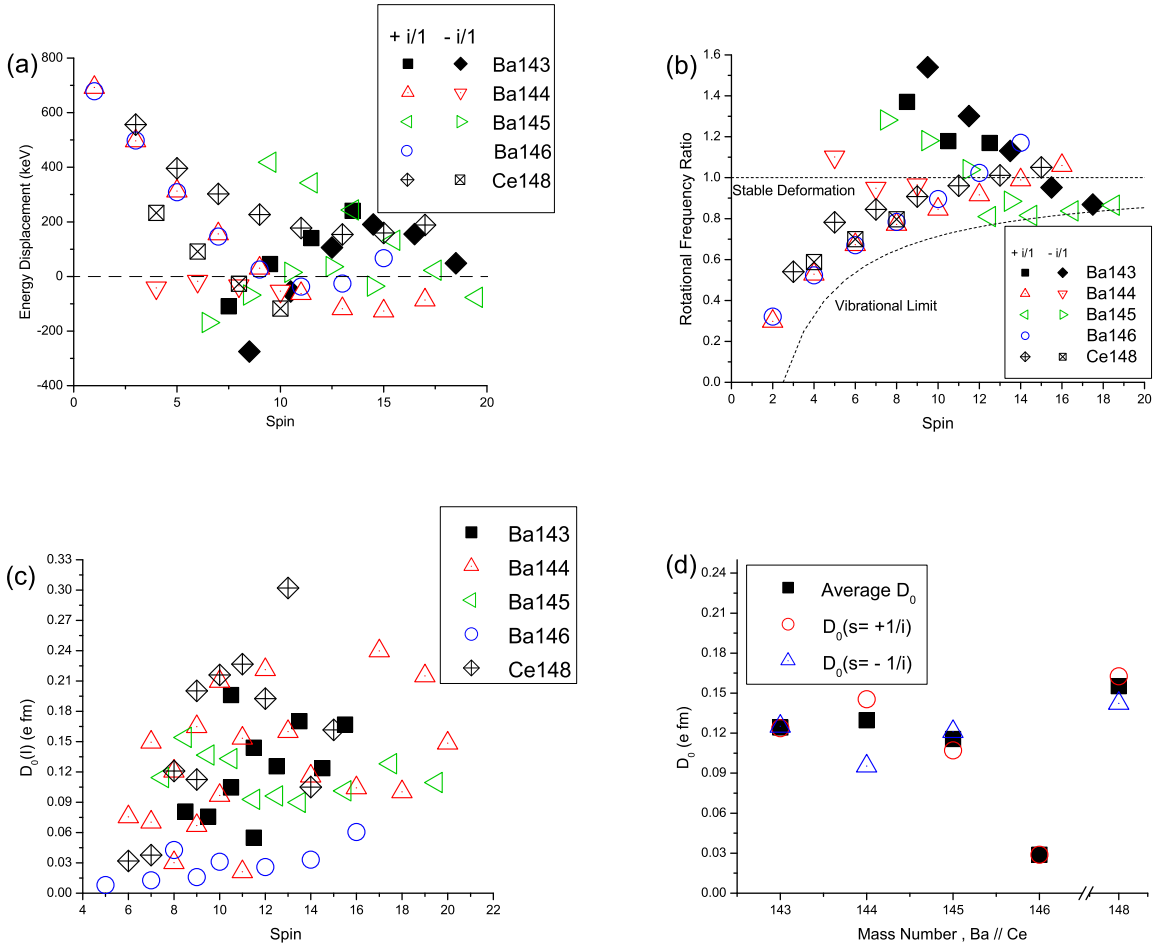

Figure 7.18: Plots of δE, $\frac{\omega(I)^-}{\omega(I)^+}$, D_0, and $D_0(I)$.

the s= +i band are near 0. We also note that curve for ^{148}Ce continues to be higher at high spin and does not reach δE=0 in the s= +1 band. Yet there is convincing evidence in its s= -1 band as well for near zero values. This supports our argument that these are simplectic bands, because in ^{144}Ba and ^{148}Ce the π=- and π=+ members show similar rotation properties.

The rotational frequency ratio is plotted in figure 7.18 part (b). The conclusion drawn from these curves is similar to the δE plots with regard to stable octupole deformation. The curves for ^{144,146}Ba and ^{148}Ce all trend, at higher spin values, toward one, the stable octupole deformation limit. In addition, the three new values in the s= -1 band of ^{144}Ba are all very nearly one. However, the curves for ^{143,145}Ba seem to trend toward the vibrational limit at high spin. This could mean one of two things: either the band is vibrational in nature at high spin, or because these limits are closer together at high spin, it goes beyond the ability of this simple model to explain these trends in detail. It is curious that δE(I) and $\frac{\omega(I)^-}{\omega(I)^+}$ curves look very similar for ^{148}Ce,^{144}Ba and ^{146}Ba, yet as of now no s= -1 structure has been definitively identified in ^{146}Ba. This qualitative assessment suggests that we should observe a s= -1 band, since this structure is in the other two.

In part c of figure 7.18, we show D_0, the intrinsic dipole moment and how the components of this variable in each simplectic band compare to the average. If we separate the average of the intrinsic dipole moment into simplectic components, it is shown that there are very different moments in each band only in ^{144}Ba, and this may guide the theoretical interpretation of these band structures. In part d, we show D_0(I), how this value varies with spin. Notice that mean values for D_0(I) in these nuclei vary greatly with spin except for ^{145,146}Ba. This constancy is indicative of stability in rotational properties and possibly deformation.

CHAPTER 8

CONCLUSION

This dissertation has presented, progress that has been made in the understanding of the structure of neutron rich nuclei. It has been shown that there are several techniques that can be used to produce these isotopes from fission reactions, though other techniques as well may be employed. These fission sources have produced nuclei in the neutron rich region of the table of isotopes. These isotopes have provided a new context in which to examine theories that were developed for low-spin states and isotopes near the valley of stability.

The near-spherical cadmium isotopes have been examined with very high count rates as the intruder states are pushed higher in energy. Instead of a more consistent picture with the anharmonic harmonic vibrator model, the nuclei seem to become less consistent with that picture. In ^{122}Cd, a great deal has been added to the level scheme including several states which could be grouped into something like a gamma vibrational band. New thoughts have been proposed for the assignment of spins and parities for the states and lifetimes in the parent silver isotope. New alternative explanations have also been suggested for the negative and positive parity structures seen.

In the study of gadolinium isotopes, many structures and lifetimes have been measured. In the decay of ^{162}Eu, the lifetime of the parent states and associated lifetimes have been re-evaluated. The non-yrast levels and gamma rays have been seen in both experimental setups, where only level energies had been known previously for non-yrast states. The gamma and (4^+) band structures have been seen along with a curious (5^-) state. There is a possibility of a band structure seen in the work done on ^{164}Gd. Many other non-yrast levels and gamma rays have been observed in ^{164}Gd and some previously observed but unplaced gamma rays have now been placed in the level

scheme. The first level scheme of ^{163}Gd is now proposed along with a measurement of the lifetime of ^{163}Eu and a determination of the ground state. In ^{165}Gd the first gamma rays associated with this isotope have been observed. In all of these cases systematics of quadrupole deformation can be analyzed.

In the barium-cerium region, simplectic bands associated with an quadrupole-octupole shape in the intrinsic frame have been observed. These bands labeled s= +1 and -1 have been seen in two even-A isotopes near Z=56, N=88. The assignment of these levels as simplex band structures has been confirmed through the measurement of their spins and assignment of their parities via the angular correlation method. Remarkable consistency with simplectic band structures and the geometrical model for observables δE, $\frac{\omega(I)^-}{\omega(I)^+}$ and D_0 are seen, which may be surprising for isotopes that are so neutron rich. Importantly this has revealed that there may exist alternative explanations for these structures. The data collected in this work show some of the the best evidence to date of the rotational consequences of octupole deformation in even-even isotopes. Trends for these bands in nuclei provide an important testing ground for models of exotic deformations. It will be interesting to see if the deformation properties might still be more pronounced in ^{148,150}Ba, as is predicted by theory [39, 40].

This work contained in this thesis has contributed to the leading edge of research in theory and experiment. These studies involve three very important isotopic regions where near-spherical shapes, well deformed quadrupole shapes and mixed quadrupole octupole shapes had been reported to occur. This work has contributed to an experimental basis for testing and challenging these models. This thesis serves as a basis for attempting to understand the physics of neutron-rich matter and the cumbersome nuclear many-body problem.

This work can specifically inform and motivate future experiments. It is known that research groups at Liverpool[104] and at Argonne National Lab[105] are pursuing quantitative measurements, via Coulomb Excitation, of the octupole moment of barium isotopes. These experiments will be very important for the understanding of the octupole moment of these nuclei, especially if they can observe trends in the octupole moment with increasing spin. The use of

GRETA/GRETINA would significantly enhance the possibility of this measurement. It has also been presented that researchers at RIKEN desire to pursue measurements of short lived isomers across the nuclear landscape including those in Ag and Eu. There is also much work left to be done to complete the picture of the Cd isotopes by pursuing measurements out to ^{130}Cd to understand the development of shell structure and its influence on these isotopes and to push higher in energy the intruder levels in order to seek after an isolated picture. At the same time, it will be important to pursue quantitative measurements of ground state properties in cadmium isotopes and not just the spectroscopic information. Further measurements of the lifetimes of excited states in the rare earth region should also be pursued for the role they play in r-process abundance calculculations.

BIBLIOGRAPHY

[1] Jones, K. L. and Nazarewicz, W. *The Physics Teacher* **48**(6), 381–385 (2010).

[2] Ilyushkin, S. V., Winger, J. A., Gross, C. J., Rykaczewski, K. P., Batchelder, J. C., Cartegni, L., Darby, I. G., Goodin, C., Grzywacz, R., Hamilton, J. H., et al. *Physical Review C* **80**(5), 054304 (2009).

[3] Madurga, M., Surman, R., Borzov, I. N., Grzywacz, R., Rykaczewski, K. P., Gross, C. J., Miller, D., Stracener, D. W., Batchelder, J. C., Brewer, N. T., et al. *Physical Review Letters* **109**(11), 112501 (2012).

[4] Ilyushkin, S. V., Winger, J. A., Rykaczewski, K. P., Gross, C. J., Batchelder, J. C., Cartegni, L., Darby, I. G., Grzywacz, R., Hamilton, J. H., Korgul, A., et al. *Physical Review C* **83**(1), 014322 (2011).

[5] Padgett, S., Madurga, M., Grzywacz, R., Darby, I. G., Liddick, S. N., Paulauskas, S. V., Cartegni, L., Bingham, C. R., Gross, C. J., Rykaczewski, K., et al. *Physical Review C* **82**(6), 064314 (2010).

[6] Winger, J. A., Rykaczewski, K. P., Gross, C. J., Grzywacz, R., Batchelder, J. C., Goodin, C., Hamilton, J. H., Ilyushkin, S. V., Korgul, A., Królas, W., et al. *Physical Review C* **81**(4), 044303 (2010).

[7] Winger, J. A., Ilyushkin, S. V., Rykaczewski, K. P., Gross, C. J., Batchelder, J. C., Goodin, C., Grzywacz, R., Hamilton, J. H., Korgul, A., Królas, W., et al. *Physical review letters* **102**(14), 142502 (2009).

[8] Beene, J. R., Bardayan, D. W., Uribarri, A. G., Gross, C. J., Jones, K. L., Liang, J. F.,

Nazarewicz, W., Stracener, D. W., Tatum, B. A., and Varner, R. L. *Journal of Physics G: Nuclear and Particle Physics* **38**(2), 024002 (2011).

[9] Wolinska-Cichocka, M., Rykaczewski, K., Karny, M., Kuzniak, A., Grzywacz, R., Rasco, C., Miller, D., Gross, C. J., and Johnson, J. *Bulletin of the American Physical Society* **56** (2011).

[10] Gross, C. J., Rykaczewski, K. P., Stracener, D. W., Wolinska-Cichocka, M., Varner, R. L., Miller, D., Jost, C. U., Karny, M., Korgul, A., Liu, S., and Madurga, M. *Phys. Rev. C* **85**, 024319 Feb (2012).

[11] Butler, P. A. and Nazarewicz, W. *Reviews of Modern Physics* **68**(2), 349 (1996).

[12] Engel, J., Friar, J. L., and Hayes, A. C. *Physical Review C* **61**(3), 035502 (2000).

[13] King, J. P., Li, Y., Meriles, C. A., and Reimer, J. A. *Nature Communications* **3**, 918 (2012).

[14] Ismail, M., Seif, W. M., and Botros, M. M. *Nuclear Physics A* **828**(3-4), 333–347 (2009).

[15] Umar, A. S., Oberacker, V. E., Maruhn, J. A., and Reinhard, P. G. *Physical Review C* **81**(6), 064607 (2010).

[16] Wang, N., Li, J., and Zhao, E. *Physical Review C* **78**(5), 054607 (2008).

[17] NNDC. Chart of Nuclides, http://www. nndc. bnl. gov/chart/ (2012).

[18] Yang, F. and Hamilton, J. H. *Modern Atomic and Nuclear Physics*. World Scientific, (2010).

[19] Krane, K. S. and Halliday, D. *Introductory nuclear physics*. Wiley, (1987).

[20] Ring, P. and Schuck, P. *The nuclear many-body problem*. Springer-Verlag, (1980).

[21] Jackson, J. D. *Classical Electrodynamics*. John Wiley & Sons, (1998).

[22] Maxwell, J. C. *A treatise on electricity and magnetism*, volume 1. Clarendon Press, (1881).

[23] Senn, P. *Journal of chemical education* **69**(10), 819 (1992).

[24] Ramayya, A. V., Hwang, J. K., Hamilton, J. H., Sandulescu, A., Florescu, A., Ter-Akopian, G. M., Daniel, A. V., Oganessian, Y. T., Popeko, G. S., Greiner, W., et al. *Physical review letters* **81**(5), 947–950 (1998).

[25] Hwang, J. K., Ramayya, A. V., Hamilton, J. H., Beyer, C. J., Kormicki, J., Zhang, X. Q., Rodin, A., Formichev, A., Kliman, J., Krupa, L., et al. In *APS Division of Nuclear Physics Meeting Abstracts*, volume 1, (2000).

[26] Hamilton, J. H., Ramayya, A. V., Hwang, J. K., Ter-Akopian, G. M., Daniel, A. V., Rasmussen, J. O., Wu, S. C., Donangelo, R., Beyer, C. J., Kormicki, J., et al. *Physics of Atomic Nuclei* **65**(4), 645–652 (2002).

[27] Blatt, J. M. and Weisskopf, V. F. *Theoretical nuclear physics*. Wiley, (1952).

[28] Singh, B., Rodriguez, J. L., Wong, S. S. M., and Tuli, J. K. *Nuclear Data Sheets* **84**(3), 487–563 (1998).

[29] Hinke, C. B., Böhmer, M., Boutachkov, P., Faestermann, T., Geissel, H., Gerl, J., Gernhäuser, R., Górska, M., Gottardo, A., Grawe, H., et al. *Nature* **486**(7403), 341–345 (2012).

[30] Mayer, M. G. and Jensen, J. H. D. *Elementary theory of nuclear shell structure*. Wiley New York, (1955).

[31] Bohr, A. and Mottelson, B. R. *Nuclear Structure*. Number v. 1,2 in Nuclear Structure. (1969).

[32] Firestone, R. B. and Shirley, V. S. **1,2** (1998).

[33] Nilsson, S. G. *Kgl. Danske Videnskab. Selskab. , Mat. -fys Medd.* **29** (1955).

[34] Iachello, F. and Arima, A. *The interacting boson model*. Cambridge University Press, (1987).

[35] Garrett, P. E., Green, K. L., and Wood, J. L. *Physical Review C* **78**(4), 044307 (2008).

[36] Leander, G. A., Nazarewicz, W., Olanders, P., Ragnarsson, I., and Dudek, J. *Physics Letters B* **152**(5), 284–290 (1985).

[37] Nazarewicz, W. and Olanders, P. *Nuclear Physics A* **441**(3), 420–444 (1985).

[38] Rudolph, D., Baktash, C., Gross, C. J., Satula, W., Wyss, R., Birriel, I., Devlin, M., Jin, H. Q., LaFosse, D. R., Lerma, F., et al. *Physical Review C* **56**(1), 98 (1997).

[39] Robledo, L. M., Baldo, M., Schuck, P., and Viñas, X. *Physical Review C* **81**(3), 034315 (2010).

[40] Wei, Z., Zhi-Pan, L., and Shuang-Quan, Z. *Chinese Physics C* **34**, 1094 (2010).

[41] Butler, P. A. and Nazarewicz, W. *Nuclear Physics A* **533**(2), 249 – 268 (1991).

[42] Furnstahl, R. *Nuclear Physics News* **21**(2), 18–24 (2011).

[43] Oberacker, V. http://www. vanderbilt. edu/AnS/physics/volker/p365 (2011).

[44] Long, W., Meng, J., Van Giai, N., and Zhou, S. G. *Physical Review C* **69**(3), 034319 (2004).

[45] Nazarewicz, W. and Tabor, S. *Physical Review C* **45**(5), 2226 (1992).

[46] Garrote, E., Egido, J., and Robledo, L. *Physical review letters* **80**(20), 4398–4401 (1998).

[47] http://www. phys. utk. edu/expnuclear/LeRIBSS. html (2012).

[48] Batchelder, J. C., Wood, J. L., Garrett, P. E., Green, K. L., Rykaczewski, K. P., Bilheux, J. C., Bingham, C. R., Carter, H. K., Fong, D., Grzywacz, R., et al. *Physical Review C* **80**(5), 054318 (2009).

[49] Batchelder, J. C., Brewer, N. T., Goans, R. E., Grzywacz, R., Griffith, B. O., Jost, C., Korgul, A., Liu, S. H., Paulauskas, S. V., Spejewski, E. H., and Stracener, D. W. *Physical Review C* **86**(6), 064311 (2012).

[50] Korgul, A., Rykaczewski, K. P., Winger, J. A., Ilyushkin, S. V., Gross, C. J., Batchelder, J. C., Bingham, C. R., Borzov, I. N., Goodin, C., Grzywacz, R., et al. *Physical Review C* **86**(2), 024307 (2012).

[51] Gross, C. J., Rykaczewski, K. P., Shapira, D., Winger, J. A., Batchelder, J. C., Bingham, C. R., Grzywacz, R. K., Hausladen, P. A., Krolas, W., Mazzocchi, C., et al. In *The 4th International Conference on Exotic Nuclei and Atomic Masses*, 115–116. Springer, (2005).

[52] Grzywacz, R. *Nucl. Inst. and Meth. B* **204**, 649–659 (2003).

[53] Batchelder, J. C., Bilheux, J. C., Bingham, C. R., Carter, H. K., Cole, J. D., Fong, D., Garrett, P. E., Grzywacz, R., Hamilton, J. H., Hartley, D. J., et al. *Nucl. Inst. and Meth. B* **204**, 625–628 (2003).

[54] Hamilton, J. H., Ramayya, A. V., Zhu, S. J., Ter-Akopian, G. M., Oganessian, Y. T., Cole, J. D., Rasmussen, J. O., and Stoyer, M. A. *Progress in Particle and Nuclear Physics* **35**, 635–704 (1995).

[55] Daniel, A. V., Goodin, C., Li, K., Ramayya, A. V., Stone, N. J., Hwang, J. K., Hamilton, J. H., Stone, J. R., Luo, Y. X., Rasmussen, J. O., et al. *Nucl. Inst. and Meth. B* **262**(2), 399–406 (2007).

[56] Radford, D. C. *Nucl. Inst. and Meth. A* **361**(1), 297–305 (1995).

[57] Radford, D. C. *Nucl. Inst. and Meth. A* **361**(1), 306–316 (1995).

[58] Radford, D. C. http://radware.phy.ornl.gov/.

[59] Kibédi, T., Burrows, T. W., Trzhaskovskaya, M. B., Davidson, P. M., and Nestor, C. W. *Nucl. Inst. and Meth. A* **589**(2), 202–229 (2008).

[60] http://root.cern.ch/drupal/ (2012).

[61] Taylor, H. W., Singh, B., Prato, F. S., and McPherson, R. *Nuclear Data Tables, Vol. A9, p. 1* **9**, 1 (1971).

[62] Haustein, P., Taylor, H., McPherson, R., and Fairchild, R. *Atomic Data and Nuclear Data Tables* **10**, 321–467 (1972).

[63] Fedoseyev, V. N., Jading, Y., Jonsson, O. C., Kirchner, R., Kratz, K. L., Krieg, M., Kugler, E., Lettry, J., Mehren, T., Mishin, V. I., et al. *Zeitschrift für Physik A Hadrons and Nuclei* **353**(1), 9–10 (1995).

[64] Kratz, K. L., Pfeiffer, B., Thielemann, F. K., and Walters, W. B. *Hyperfine Interactions* **129**(1), 185–221 (2000).

[65] Luo, Y. X., Rasmussen, J. O., Nelson, C. S., Hamilton, J. H., Ramayya, A. V., Hwang, J. K., Liu, S. H., Goodin, C., Stone, N. J., Zhu, S. J., et al. *Nuclear Physics A* (2011).

[66] Zamfir, N. V., Gill, R. L., Brenner, D. S., Casten, R. F., and Wolf, A. *Physical Review C* **51**, 98–102 (1995).

[67] Shih, L. L., Hill, J. C., and Williams, S. A. *Physical Review C* **17**(3), 1163 (1978).

[68] Smith, D. L., Mach, H., Penttilä, H., Bradley, H., Äystö, J., Elomaa, V.-V., Eronen, T., et al. *Phys. Rev. C* **77**, 014309 Jan (2008).

[69] Breitenfeldt, M., Borgmann, C., Audi, G., Baruah, S., Beck, D., Blaum, K., Böhm, C., Cakirli, R., Casten, R., Delahaye, P., et al. *Physical Review C* **81**(3), 034313 (2010).

[70] Fogelberg, B., Bäcklin, A., and Nagarajan, T. *Physics Letters B* **36**(4), 334–336 (1971).

[71] Montes, F., Estrade, A., Hosmer, P. T., Liddick, S. N., Mantica, P. F., Morton, A. C., Mueller, W. F., Ouellette, M., Pellegrini, E., Santi, P., et al. *Physical Review C* **73**(3), 035801 (2006).

[72] Audi, G., Wapstra, A., and Thibault, C. *Nuclear Physics A* **729**(1), 337 – 676 (2003).

[73] Schreckenbach, K., Mheemeed, A., Barreau, G., von Egidy, T., Faust, H. R., Börner, H. G., Brissot, R., Stelts, M. L., Heyde, K., van Isacker, P., Waroquier, M., and Wenes, G. *Physics Letters B* **110**(5), 364 – 368 (1982).

[74] Zhu, S. J. et al. *In preparation* .

[75] Aprahamian, A., Wu, X., Lesher, S., Warner, D., Gelletly, W., Börner, H., Hoyler, F., Schreckenbach, K., Casten, R., Shi, Z., et al. *Nuclear Physics A* **764**, 42–78 (2006).

[76] Dodder, R., Jones, E., Hamilton, J., Ramayya, A., Gore, P., Beyer, C., De Lima, A., Hwang, J., Zhang, X., Zhu, S., et al. *Il Nuovo Cimento A (1971-1996)* **110**(9), 949–954 (1997).

[77] Hamilton, J., Ramayya, A., Hwang, J., Luo, X., Rasmussen, J., Jones, E., Zhang, X., Zhu, S., Gore, P., Ginter, T., et al. *The European Physical Journal A-Hadrons and Nuclei* **15**(1), 175–179 (2002).

[78] Jones, E., Gore, P., Hamilton, J., Ramayya, A., De Lima, A., Dodder, R., Kormicki, J., Hwang, J., Beyer, C., Zhang, X., et al. *Physics of Atomic Nuclei* **64**(7), 1157–1164 (2001).

[79] Jones, E., Gore, P., Hamilton, J., Ramayya, A., Lima, A., Dodder, R., Kormicki, J., Hwang, J., Beyer, C., Zhang, X., et al. *Nuclear Physics A* **682**, 1–4 (2001).

[80] Jones, E., Hamilton, J., Gore, P., Ramayya, A., Hwang, J., Zhu, S., Luo, Y., Beyer, C., Kormicki, J., Zhang, X., et al. *Journal of Physics G: Nuclear and Particle Physics* **30**(12), L43 (2004).

[81] Lovhoiden, G., Thorsteinsen, T. F., and Burke, D. G. *Phys.Scr.* **34**, 691 (1986).

[82] Gerçeklioglu, M. *Annalen der Physik* **14**(5), 312–323 (2005).

[83] Osa, A., Ichikawa, S., Matsuda, M., Sato, T. K., and Jeong, S. C. *Nucl. Inst. and Meth. B* **266**(19), 4394–4397 (2008).

[84] Anderl, R. A. and Greenwood, R. C. *J.Radioanal.Nucl.Chem.* **142**, 203 (1990).

[85] Gehrke, R. J., Greenwood, R. C., Baker, J. D., and Meikrantz, D. H. *Radiochim.Acta* **31**, 1 (1982).

[86] Greenwood, R. C., Lee, M. A., and Anderl, R. A. *Radiochim.Acta* **43**, 129 (1988).

[87] Ichikawa, S., Tsukada, K., Nishinaka, I., Hatsukawa, Y., Iimura, H., Hata, K., Nagame, Y., Osa, A., Asai, M., Kojima, Y., Hirose, T., Shibata, M., Kawade, K., and Oura, Y. *Phys. Rev. C* **58**, 1329–1332 Aug (1998).

[88] Morcos, N. A., James, W. D., Adams, D. E., and Kuroda, P. K. *Journal of Inorganic and Nuclear Chemistry* **35**(11), 3659 – 3668 (1973).

[89] Simpson, G. S., Urban, W., Genevey, J., Orlandi, R., Pinston, J. A., Scherillo, A., Smith, A. G., Smith, J. F., Ahmad, I., and Greene, J. P. *Physical Review C* **80**(2), 024304 (2009).

[90] Hwang, J., Ramayya, A., Hamilton, J., Luo, Y., Daniel, A., Ter-Akopian, G., Cole, J., and Zhu, S. *Physical Review C* **73**(4), 044316 (2006).

[91] Govor, L. I., Demidov, A. M., Kurkin, V. A., and Mikhailov, I. V. *Physics of Atomic Nuclei* **72**(11), 1799–1811 (2009).

[92] Sato, T. K., Osa, A., Tsukada, K., Asai, M., Hayashi, H., Kojima, Y., Shibata, M., and Ichikawa, S. (JAEA-Review 2006-029,P31) (2006).

[93] Hayashi, H., Akita, Y., Suematsu, O., Shibata, M., Asai, M., Sato, T., Ichikawa, S., Nishinaka, I., Nagame, Y., Osa, A., et al. *The European Physical Journal A-Hadrons and Nuclei* **34**(4), 363–370 (2007).

[94] Zhu, S. J., Lu, Q. H., Hamilton, J. H., Ramayya, A. V., Peker, L. K., Wang, M. G., Ma, W. C., Babu, B. R. S., Ginter, T. N., Kormicki, J., et al. *Physics Letters B* **357**(3), 273–280 (1995).

[95] Jones, M. A., Urban, W., Durell, J. L., Leddy, M., Phillips, W. R., Smith, A. G., Varley, B. J., Ahmad, I., Morss, L. R., Bentaleb, M., et al. *Nuclear Physics A* **605**(2), 133–159 (1996).

[96] Zhu, S. J., Hamilton, J. H., Ramayya, A. V., Jones, E. F., Hwang, J. K., Wang, M. G., Zhang, X. Q., Gore, P. M., Peker, L. K., Drafta, G., et al. *Physical Review C* **60**(5), 051304 (1999).

[97] Gill, R. L., Shmid, M., Chrien, R. E., Chu, Y. Y., Wolf, A., Brenner, D. S., Sistemich, K., Wohn, F. K., Yamamoto, H., Chung, C., et al. *Physical Review C* **27**(4), 1732 (1983).

[98] Phillips, W. R., Ahmad, I., Emling, H., Holzmann, R., Janssens, R. V. F., Khoo, T. L., and Drigert, M. W. *Phys. Rev. Lett.* **57**, 3257–3260 Dec (1986).

[99] Zhu, S. J., Sakhaee, M., Hamilton, J. H., Ramayya, A. V., Brewer, N. T., Hwang, J. K., Liu, S. H., Yeoh, E. Y., Xiao, Z. G., Xu, Q., et al. *Phys. Rev. C* **85**, 014330 Jan (2012).

[100] Luo, Y. X., Rasmussen, J. O., Hamilton, J. H., Ramayya, A. V., Hwang, J. K., Beyer, C. J., Zhu, S. J., Kormicki, J., Zhang, X. Q., Jones, E. F., et al. *Phys. Rev. C* **66**, 014305 Jul (2002).

[101] Sakhaee, M., Zhu, S. J., Hamilton, J. H., Ramayya, A. V., Hwang, J. K., Zhang, X. Q., Yang, L. M., Zhu, L. Y., Gan, C. Y., Jones, E. F., et al. *Phys. Rev. C* **60**, 067303 Nov (1999).

[102] Chen, Y. J., Zhu, S. J., Hamilton, J. H., Ramayya, A. V., Hwang, J. K., Sakhaee, M., Luo, Y. X., Rasmussen, J. O., Li, K., Lee, I. Y., Che, X. L., Ding, H. B., and Li, M. L. *Phys. Rev. C* **73**, 054316 May (2006).

[103] Urban, W., Jones, M. A., Durell, J. L., Leddy, M., Phillips, W. R., Smith, A. G., Varley, B. J., Ahmad, I., Morss, L. R., Bentaleb, M., Lubkiewicz, E., and Schulz, N. *Nuclear Physics A* **613**(1-2), 107 – 131 (1997).

[104] Butler, P. *NS2012 conference* (2012).

[105] Zhu, S. *NS2012 conference* (2012).